Passive Low Frequency RFID for Non-Destructive Evaluation and Monitoring

A doctoral thesis submitted for the degree of Doctor of Philosophy

G.A.M Ali Imam Sunny

Intelligent, Sensing and Communications Research Group (ISC),

School of Engineering, Newcastle University

October 2017

CERTIFICATE OF ORIGINALITY

This is to certify that all the works submitted in this thesis are my own works except as specified in acknowledgements. Neither the work nor the thesis has been submitted to any other institution for another degree. I am responsible for all the works in this thesis.

..... (Signed)

..... (Candidate)

I dedicate this thesis to my loving parents and siblings

Table of Contents

List of Figures

List of Tables

List of Publications

A. I. Sunny, G.Y. Tian, J. Zhang and M. Pal, "*Low frequency (LF) RFID sensors and selective transient feature extraction for corrosion characterisation*" Sens. Actuators A: Phys., 241, 2016, 34–43

A. I. Sunny, G. Y. Tian and M. Alamin, "*RFID Sensor System for Detecting Corrosion Progression Using Transient Responses*". In: British Institute of Non-Destructive Testing (BINDT), Manchester, UK, 2014

A. I. Sunny and G. Y. Tian "*Enhanced Sensitivity of Low Frequency (LF) RFID Sensor Signal for Structural Health Monitoring (SHM) in High Temperature Environment''*, World Conference of NDT, Munich, Germany, 2016

A. I. Sunny, J. Zhang, and G. Y. Tian, "Temperature independent defect detection using smart RFID sensing system*'',* IEEE Transactions on Industrial Electronics, 2017 (under review)

J. Zhang, A. I. Sunny and G. Y. Tian, "*Feature Extraction and Fusion for Robust Defect Monitoring Using Passive Sweep-Frequency RFID Wireless Sensors'',* IEEE Transactions on Industrial Electronics, 2017 (under review)

M. Fan, B. Cao, A. I. Sunny, W. Li, G. Y. Tian and B. Ye, *"Pulsed eddy current thickness measurement using phase features immune to liftoff effect'',* NDT & E International, Volume 86, March 2017, Pages 123-131

J. Zhang, G.Y. Tian, A. M. J. Marindra, A. I. Sunny and A. B. Zhao, *"Review of passive RFID tag antenna based sensors and systems"* Sensors 2017, *17*, 265

C. Tang, H. F. Rashvand, G. Y. Tian, P. Hu, A. I. Sunny and H. Wang . Structural Health Monitoring with WSNs: Space, Underwater, Underground and Industrial. In: Habib F. Rashvand and Ali Abedi *Wireless Sensor Systems for Extreme Environments: Space, Underwater, Underground, and Industrial*. London: Wiley. August 2017. P383-409.

Abbreviations

ACFM	Alternating Current Field Measurement
CUI	Corrosion under Insulation
ECPT	Eddy current pulsed thermography
ECT	Eddy Current Technique
EIS	Electrochemical impedance spectroscopy
EMAT	Electromagnetic Acoustic Transducer
EPSRC	Engineering and Physical Sciences Research Council
FEA	Finite Element Analysis
FET	Field Effect Transistor
FFT	Fast Fourier Transform
FSM	Field Signature Method
HF	High Frequency
LF	Low-Frequency
LOI	Lift-off Point of Intersection
LPG	Liquefied Petroleum Gas
MFL	Magnetic flux leakage
NDT&E	Non-Destructive Testing and Evaluation
OCR	Optical Character recognition
PCA	Principal Component Analysis
PEC	Pulsed Eddy Current Technique
PC	Protective Coatings
PMP	Permanent Magnetic Perturbation
PMFL	Pulsed magnetic Flux Leakage
PPA	Polyphthalamide
PTFE	Poly-tetra-fluoro-ethyulene
RC	Reinforced Concrete
SAW	Surface Acoustic Wave
SCC	Stress Corrosion Cracking
SCMR	Strongly Coupled Magnetic Resonance
SHM	Structural Health Monitoring
STFT	Short-Term Fourier Transform
UHF	Ultra-High Frequency
UT	Ultrasonic testing
UWB	Ultra-Wide Band
VNA	Vector Network Analyser
WPT	Wireless Power Transfer

"If anyone travels on a road in search of knowledge, Allah will cause him to travel on one of the roads of Paradise. The superiority of the learned man over the devout is like that of the moon, on the night when it is full, over the rest of the stars. " - reported to have been said by the Prophet Muhammad ﷺ

All the praise is due to the Almighty Allah, Who guides us in the darkness and helps in the difficulties.

Acknowledgements

My deepest gratitude and appreciation to my respected supervisor, Professor Gui Yun Tian, Professor of Sensor Technologies in Newcastle University. He has been a constant support since the days I began working as a postgraduate researcher. His devoted time towards his students shows how much he cares about each and every single one of the students in the group. He has always allowed me to explore and learn which eventually helped me boost my research career. He was always available for any discussion and without his constant motivation and guidance, the completion of this degree would not have been possible. It is my great privilege and honour to have been one of his research students.

My sincere thanks also goes to Mr Jeffrey Neasham, Dr Rishad Shafik and especially my mentor as I count, Dr Jun Zhang, who have not only taught me about research but have guided me towards becoming a contributor to science. I would also like to thank my fellow research mates and friends, Mr. Ruslee Sutthaweekul, Mr. Buhari Dahiru, Mr. Chaoqing Tang, Mr. Aobo Zhao, Mr. Chen Xiaotian, Dr Kongjing Li, Ms. Safaa Nash'At Awny, Dr Nabeel Ahmed, Mr Abdul Rehman and Ms. Ana Carolina, for stimulating discussions and all the mirthful moments. I would also like to thank the staffs and technicians of Newcastle University who has always helped me in everything that I needed. Thanks to Engineering and Physical Sciences Research Council (EPSRC) CASE for funding the project in collaboration with the National Nuclear Laboratory (NNL).

A special thanks to my friend, Dr. Waqas Rafiq, who has been more like a brother to me, who was always there throughout the phases of melancholy and contentment. Thanks to the lovely people that I met here, Barrister Jalal Uddin, Mrs Lata Kazi and their lovely children, thanks for making me feel home at all times.

Lastly, but most importantly, I am beholden to my family. The incentive behind all my success. Their constant support and prayers throughout my educational career are worth more than I can express on paper in words. My father, Dr Shah Alam and mother Mrs Gulshan Ara Shabnam, who raised me and cared for me and always put me before themselves in many circumstances so that I always get the best. Their unconditional love, countless sacrifices, positive involvement and approbation are the most overwhelming keys to my success. My icon, my brother, Capt. Ali Reza, who is an exceptionally intelligent human being, has always been a strength for me and a constant source of encouragement. Love and prayers of my sister and sister-in-law and the excitement of seeing me in both my niece's eyes, are what that has given me the strength and inspired me each day. These are the most important people in my life.

Abstract

Despite of immense research over the years, defect monitoring in harsh environmental conditions still presents notable challenges for Non-Destructive Testing and Evaluation (NDT&E) and Structural Health Monitoring (SHM). One of the substantial challenges is the inaccessibility to the metal surface due to the large stand-off distance caused by the insulation layer. The hidden nature of corrosion and defect under thick insulation in harsh environmental conditions may result in it being not noticed and ultimately leading to failures. Generally electromagnetic NDT&E techniques which are used in pipeline industries require the removal of the insulation layer or high powered expensive equipment. Along with these, other limitations in the existing techniques create opportunities for novel systems to solve the challenges caused by Corrosion under Insulation (CUI).

Extending from Pulsed Eddy Current (PEC), this research proposes the development and use of passive Low Frequency (LF) RFID hardware system for the detection and monitoring of corrosion and cracks on both ferrous and non-ferrous materials at varying high temperature conditions. The passive, low cost essence of RFID makes it an enchanting technique for long term condition monitoring.

The contribution of the research work can be summarised as follows: (1) implementation of novel LF RFID sensor systems and the rig platform, experimental studies validating the detection capabilities of corrosion progression samples using transient feature analysis with respect to permeability and electrical conductivity changes along with enhanced sensitivity demonstration using ferrite sheet attached to the tag; (2) defect detection using swept frequency method to study the multiple frequency behaviour and further temperature suppression using feature fusion technique; (3) inhomogeneity study on ferrous materials at varying temperature and demonstration of the potential of the RFID system; (4) use of RFID tag with ceramic filled Poly-tetra-fluoro-ethyulene (PTFE) substrate for larger applicability of the sensing system in the industry; (5) lift-off independent defect monitoring using passive sweep frequency RFID sensors and feature extraction and fusion for robustness improvement.

This research concludes that passive LF RFID system can be used to detect corrosion and crack on both ferrous and non-ferrous materials and then the system can be used to compensate for temperature variation making it useful for a wider range of applications. However, significant challenges such as permanent deployment of the tags for long term monitoring at higher temperatures and much higher standoff distance, still require improvement for real-world applicability.

Chapter 1. Introduction

This chapter gives a brief introduction to RFID sensing system for non-destructive testing related under harsh environmental condition (high temperature) and an overview of the work that is carried out throughout the project. A summary of the objectives of the research work is provided and the research scope is discussed. Highlights of the major research achievements are outlines and finally the thesis layout is structured.

1.1 Research Background

Non-destructive testing and evaluation (NDT&E) refers to the implementation of the material damages detection techniques without affecting the serviceability of the material. Corrosion is a major problem faced by numerous industries, mainly the chemical and the petrochemical industries where majority of the pipes are made from steel and steel alloys. One of the reasons for it being the interaction of the metallic structures with moisture. In the absence of moisture, many contaminants would have little or almost no corrosive effect. Sulphuric acid exposed from the industrial atmosphere provides an aggressive electrolyte for the promotion of corrosion. Temperature plays another important role in atmospheric corrosion. These two major factors acts as stimulants which are often combined in the aforementioned industries. Due to temperature effect there is a normal increase in the corrosion activity which is theoretically thought to be doubled each ten-degree increase in temperature. Also another little recognized factor is the temperature lag of metallic objects due to their heat capacity. During the evening, the ambient temperature drops, metallic structures tend to stay warmer than the surrounding air and until the dew points are reached, the materials do not begin to collect condensation. As soon as the temperature begins to rise in the surrounding air, the lagging temperature of the metallic structures will produce a film of moisture on them.

Due to the relative low cost, mechanical strength and the ease of manufacturing, mild steel is a preferred metal for many applications. However, one of the major limitations of mild steel is that they tend to corrode easily unless they are well protected and tested periodically thus ultimately losing its strength which then leads to catastrophic failure. Similarly, for the petrochemical industries corrosion and pit holes lead to oil spills, gas leaks and these come along with the major environmental problems which lead to significant revenue losses, severe disruption of operations and threat to marine life and the ecosystem. For corrosion resistance, usually these steel are coated with insulation layer or galvanized.

A large number of sectors are affected due to lack of proper inspection for corrosion and defects developing in steel structures. In 2009, there has been a bridge collapse which caused a freight

train to derail in Ayrshire, Scotland. It was reported that corrosion had significantly weakened the girders that they were no longer able to carry loading from the trains. On 22nd November 2013, an explosion occurred in Qingdao, China, killing 55 people. Reportedly there was leakage of oil from the pipelines due to corrosion. Recently on July 26th 2017, in Ohio State Fair, a Fire Ball ride collapsed killing and injuring people and it was reported that excessive corrosion on the interior of the support beam badly reduced the beam's wall thickness. An estimated 30,900 injuries associated with amusement attractions had been filed in 2016, in the US itself. These are depicted in Figure 1.1.

(a)

(b)

(c)

Figure 1.1: Catastrophic failures due to corrosion (a) Bridge collapse in Scotland in 2009 [1], (b) The 2013 pipeline explosion in Qingdao damaging cars and roads in Shandong province and killing 55 people [2], and (c) Fun fair accident in Ohio state in 2017 [3]

Corrosion under insulation (CUI) and other damages are amongst the other major problems in oil and gas industries. Not only restricted to petrochemical industries, this is a major problem related to any steel pipelines which are fitted under thick insulation such as in power and manufacturing industries. As mentioned earlier, when the steel comes in contact with moisture and oxygen at a particular temperature variation, it leads to corrosion. Not only petroleum spill is an economic concern, it also acidifies the soil and thus starve the roots of the plants from receiving vital oxygen. This ultimately destroys the crops. In agricultural communities, often a

year's supply of food is destroyed instantaneously. The ingress of water inside insulation materials results in the water and air gaining access in metal surface. This is mainly due to poorly designed and installed protective coating finish. CUI is an excessively costly issue for industries as well as commercial sectors worldwide and causes significant impact on the global economy. Inspection of corrosion or defects under insulation is a costly method and often insulation layer requires to be removed in order to gain access to the metallic surface. Worthy of mentioning that there are number of NDT&E techniques adopted to detect corrosion and defects under insulation without removing the insulation layer or even removing small sections of insulation layer to gain access to the pipe surface [4-7] and each one these techniques have different capabilities. However, there are constrains related as well since some of these methods require critical equipment to carry out measurement which makes it even more complex and the process requires shutting down of operations.

Accurate defect detection and characterisation due to corrosion is a major challenge by itself. There are a number of factors that contribute to this, amongst which the most notable are the inhomogeneity of the materials under inspection, lift-off or coupling variation effect and larger stand-off distance due to coating or insulation layer. The immediate effect of larger standoff distance is the reduction in spatial resolution and thus reducing sensitivity to small changes in corrosion layer. This is one of the major problems for traditional electromagnetic NDT techniques such as EC and MFL which are mainly surface or near surface inspection techniques. Though there exists commercial PEC based techniques that can inspect defects through thick layer of insulation, they also require immense amount of currents and are generally bulky systems. In addition, any variation in insulation or coating thickness will result in variation of the lift-off which will lead to erroneous detection of corrosion and defects.

In order to address these aforementioned problems, this work provides a study of how passive low frequency RFID sensing system can be applied for the inspection of corrosion and cracks under coating and in high temperature environmental conditions. RFID is a wireless tagging and identification system which simply consists of two parts, a reader and a tag. One of the limitations of RFID based sensing is that the reading distance between the tag and the reader is significantly reduced in the metal environment and the sensing area is dependent on the size of the coil. Keeping these concerns in mind, the following research objectives have been outlined for this research.

1.2 Research Aim and Objectives

The overall aim of the project is to design and develop a new generation non-destructive testing and evaluation technique for structural health monitoring that is cost effective and passive in nature.

The research objectives are summarised as follows:

- Design and implementation of passive low frequency RFID sensing system for monitoring corrosion.
- Further investigation is carried out to explore the potentials of time feature extraction from RFID signal response. Further to improve the sensing sensitivity using ferrite sheet which increases the magnetic flux density and thereby enhancing the signal response of the RFID system.
- To investigate the potential of the RFID sensing system to detect and characterise different non-ferrous material crack depth at high temperature conditions.
- Fusion of features from the resonant frequency curve is extracted in order to supress the temperature variation for robust defect detection.
- Experimental demonstration of the RFID system for defect monitoring at varying lift-off distances which is suppressed using feature fusion technique for improved sensitivity of the system.

1.3 Scope of the Research

In this research, an experimental approach is undertaken to assess the RFID sensing system extended from the previous Pulsed Eddy Current (PEC) system, with carefully selected samples with known electromagnetic properties, defect geometry and further signal processing techniques along with feature extraction techniques are exploited to determine the repeatability of the RFID sensing system.

Samples are designed in order to emulate real world conditions. Corrosion is built on mild steel samples via exposure to the atmosphere for varying time periods. Also samples used in this study include amongst others surface machined slot (to stimulate metal loss) thus to emulate real world defects.

Initially, feasibility tests are carried out with surface prepared samples with different surface conditions and corrosion levels in order to understand whether it is even possible to distinguish between varying surface conditions. Based on the results and previous works, it was inferred

from the monotonic behaviour of the signal response that RFID sensing system could perform well to determine varying degree of permeability and conductivity changes in the material.

Following the feasibility study, improvements on the robustness of the signal sensitivity has been carried out with the attachment of ferrite sheet on the tag. The response showed further improved results in comparison to the aforementioned responses. Following this, an experimental study was carried out to investigate the influence of temperature with varying frequency responses on non-ferrous crack samples. This experiment was carried out in conjunction with mild steel corrosion materials in order to understand the inherent characteristics difference between the two materials and their defect structures with varying temperature.

Further simulation was carried out on ceramic filled PTFE substrate on RFID tags for its performance on temperature compensation and validated with experimental studies that the substrate had a lower thermal conductivity and thus improved the compensation further by 40% in comparison to the aforementioned test without ceramic.

Application and validation of the significance of the lift-off invariant RFID defect detection has been carried out on the machined slot cracks. The lift-off variation have been compensated using the feature fusion technique. In addition, this research work also details the behaviour of the lift-off variation with respect to sensor configuration and sample material.

1.4 Main achievements

An expansion to the EPSRC NEWTON project in conjunction with industries, the novelty of the contributions of this project is supported by the following achievements in international journals and conference papers.

- A thorough research of magnetic and electromagnetic NDT&E techniques for detection and characterisation of defects in petrochemical structures has been carried out. This is followed by a literature review on the passive RFID based sensing. Major benefits and the limitations of the techniques and the potential of the RFID based sensing system has been assessed.
- Since the commercially available RFID reader units are not built for metal interaction as their performance degrades in metal proximity. Therefore, a custom built reader unit was designed and implemented that could perform at a sweeping frequency range and experimental works have carried out to validate its performance.

- Experimental validation of the proposed system, demonstrating the defect detection ability and distinguishing between different surface conditions and corrosion levels which relate to variation in permeability and conductivity on mild steel samples have been carried out.
- Transient feature analysis have been emphasised on for corrosion characterisation based on its wide spectral coverage of the response for higher accuracy along with ferrite sheet for generating higher magnetic flux density for improved sensitivity has been achieved. The features account for the greater variance in the measured data.
- Temperature independent defect detection and characterisation has been carried out using sweeping frequency analysis and feature fusion technique. Furthermore, inhomogeneity study is carried out to prove the potential of the RFID sensing system on both ferrous and non-ferrous materials at high temperature conditions and the effectiveness of the new feature extraction for temperature suppression.
- Finally lift-off independent defect detection and characterisation is shown based on the sweeping frequency analysis. Also defects under thick calcium silicate insulation layer has been obtained.
- Publication of research in peer reviewed journal [8] and presentation of work in leading conferences of NDT&E [9, 10].

1.5 Thesis layout

Chapter 2 presents the literature survey of operational defects in steel pipelines specifically focussing on different types of corrosion. Next, is the review of electromagnetic techniques used for corrosion monitoring. Both their advantages and disadvantages are discussed. Research challenges and problems in the area of NDT&E and SHM are identified. Finally the RFID as a NDT based sensing system has been reviewed for sensing applications.

Chapter 3 presents the theoretical background of passive LF RFID sensing system, followed by explanation of operational principle of RFID as a corrosion and crack based sensing element. The geometric topologies along with hardware design is explained thoroughly. Lastly, research methodology is set out in the rest of the chapters.

Chapter 4 elaborates the experimental case studies. The chapter begins with integration of RFID principle with Wireless Power Transfer (WPT) methods followed by an introduction to the samples and how they were prepared and this is followed by an initial feasibility study. Feature extraction and the selection method is outlined which is followed by the experimental setup of

the RFID system for corrosion characterisation. Experimental results and validation are outlined along with simulation results for the enhanced sensitivity using ferrite sheet.

Chapter 5 demonstrates the temperature independent defect monitoring beginning with the methods and measurement principles for crack monitoring with varying temperature. RFID readout instrumentation with swept frequency measurement is outlined followed by feature extraction techniques and then experimental validations. A subsection of the chapter also describes the inhomogeneity study using steel corrosion progression samples. Finally the thermal reduction and system robustness improvement is validated with both simulation and experimental works using ceramic substrate.

Chapter 6 outlines lift-off independent defect monitoring using passive sweep frequency RFID sensors and feature extraction and fusion for robust output. The chapter begins by outlining the effect of lift-off variation and the related sensing principle is explained followed by feature extraction techniques. Furthermore, work focused on conducting a more realistic experimental study where a pipeline with artificial defects have been monitored under 50mm thick insulation layer at harsh environmental condition.

Chapter 7 summarises the research work, derives conclusions and outlines further work based on the current findings.

1.6 Chapter summary

This chapter outlines a brief introduction to the research work. The achievements and challenges associated in the previous research are generalised and explained in the background on the current study. This is followed by the aims and research objectives. The current contributions for the research work are presented. Lastly, the thesis layout and the contents of each chapter are summarised.

Chapter 2. Literature Review

Following on from an extensive introduction to the thesis in the previous chapter, this chapter presents a literature review on the different types of defects and electromagnetic NDT techniques used in the detection and quantification process of them defects. First, different corrosion types and operational defects such as cracking; its causes and the issues and challenges related with it are studied. Next, the most commonly used NDT&E methods applicable for detection and quantification of such defects are analysed. A table summarising the pros and the cons of the methods are presented towards the end of the section. Next, a study into the modalities of passive LF RFID sensors specifically focusing on corrosion sensing followed by viability in high temperature environment is carried out. And finally, the problem synopsis is presented mentioning the need for a passive RFID based sensing for long term monitoring of defects and its viability in extreme conditions.

2.1 Operational defects in steel pipes

There are different types of defects that may be found in the steel pipelines and the pipeline coatings. They can be categorised in various types such as manufacturing defects which usually occur during the manufacturing process, construction defects which occur during the construction process, cathode protection defects which usually creates the condition where external corrosion can develop and operational defects which grow from the commissioning of the pipelines [11]. Amongst these types of defects, operational defects are of interest and this section will consider exploring a few of them in the following subsections. In general, corrosion of steel reinforcement is a universal issue that leads to failure of the reinforced concrete (RC) structures, liquefied petroleum gas (LPG) tanks and destruction caused by steel deterioration requires correct inspection followed by maintenance in order to save billions of pounds which are spent behind it [12-15]. This cost vary depending on the material structure, including the reason for damage, level of damage and the effect of the damage on the structural behaviour [16]. Atmospheric corrosion of steel is a term for an arrangement of iron oxides (hematite Fe_2O_3 and magnetite Fe_3O_4) and hydroxides (ferrous hydroxide Fe (OH) and ferric hydroxide Fe (OH) $_3$). Mostly in marine climates rusts are developed, which is a ferromagnetic mineral. Over time, only the parts of the corrosion constituents have changes with little effect on the composition [17]. This is because density of pure steel is more than that of the iron oxides and hydroxides. During the initial phases of corrosion, the thickness of it will increase but in the long-term corrosion it tends to decrease due to metal loss.

Usually the pipes are made of steel alloys which are used within the petrochemical industries to transport wide variety of chemicals which are often operated at high temperatures. Under these circumstances the steel pipe is subjected to stress which in conjunction with temperature leads to corrosion and cracking [18]. Also, corrosion is caused by the moisture ingress where water can enter the coating or insulation during rain, flood or earth embankments causing corrosion. Moisture can also appear due to the atmospheric condensation. Operation of the pipes in repeated cycle of condensation and evaporation will result in hostile form of corrosion [19]. Based on the morphology of the damage, corrosion is classified into the following modes of attacks:

2.1.1 General corrosion

General corrosion is the outcome of chemical and electrochemical reactions which form over the entire exposed surface at an equal rate. Presence of this corrosion causes metal to be thinner changing the shape of the surface. General corrosion is resulted in failure through lowering the mechanical strength of components or reduced wall thicknesses which eventually leads to leaking. General corrosion can also be thought to be caused due to different soil contamination underground [20].

Figure 2.1: General corrosion patterns with major corrosion (left) to minor corrosion throughout the pipe surface (right) [20]

2.1.2 Crevice corrosion

Crevice corrosion is caused due to metal exposure to environment. There are certain regions where the environment does not freely blend with the bulk environment thus causing a significant difference in the concentration of some chemical constituents within the material in those occlude regions and eventually leading to crevice corrosion [21]. This kind of corrosion can range from being slightly localised to pitting and the rate of corrosion is uneven on the material surface due to heterogeneities in the metal.

Figure 2.2: Crevice pipe at saddle clamp [21]

2.1.3 Pitting corrosion

Another form of crevice corrosion where a small impact or defect or even impurity can initialise the corrosion process is known as the pitting corrosion. Any highly localized attack in specific area results in small put which penetrates into the metal and leads to a hole. They commonly occur at flaws in coatings and ineffective cathodic protection. The increment of pitting depend on temperature variation and the environmental conditions containing halide ions [22-24].

Figure 2.3: General pitting corrosion where smaller pits interconnecting to form larger pits [20]

2.1.4 Stress corrosion cracking (SCC)

SCC is formed from the combined interaction of the stress on the material, cracking environment and temperature variation causing corrosion to develop in steel pipes. The stress involved in the formation of SCC are either from the use of components in service or the residual stresses formed during manufacturing. This sort of corrosion is different from usual cracking and corrosion because, SCC corrosion mechanism involves combination of a material with a certain environment such as high strength steels with Hydrogen [25]. Typical SCC failures can be found in pressure vessels, pipework, and highly stressed components and in systems where there is a change in the operational or environmental conditions. Metals and

environment that we commonly associate with SCC are; carbon steel which combines with Hydroxide at a higher concentration and high temperature, Nitrates and Carbonate at a moderate temperature and concentration. Also strong steels, copper alloys, aluminium alloys and titanium alloys combine with environment to cause SCC [26].

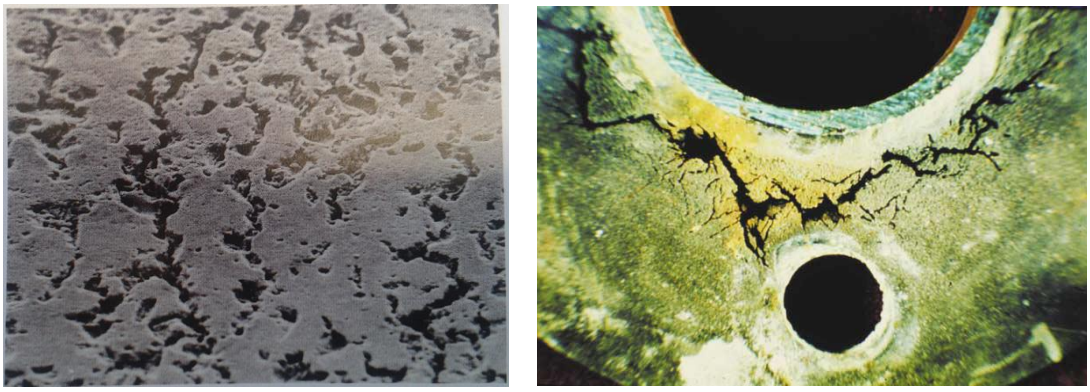

Figure 2.4: Stress corrosion cracking in steel pipeline [20, 27]

2.1.5 Galvanic Corrosion

Galvanic corrosion develop when two metals with different chemical activities are joined together. The difference between the two metal types creates a potential difference. The noble metals act as the cathode whereas the active metals act as the anode. Presence of any moisture will create a conduction path and a current will flow from the anode to the cathode and thereby developing corrosion in between the joints. This corrosion is known as the galvanic corrosion. It is also known as the bimetallic or dissimilar metal corrosion [28].

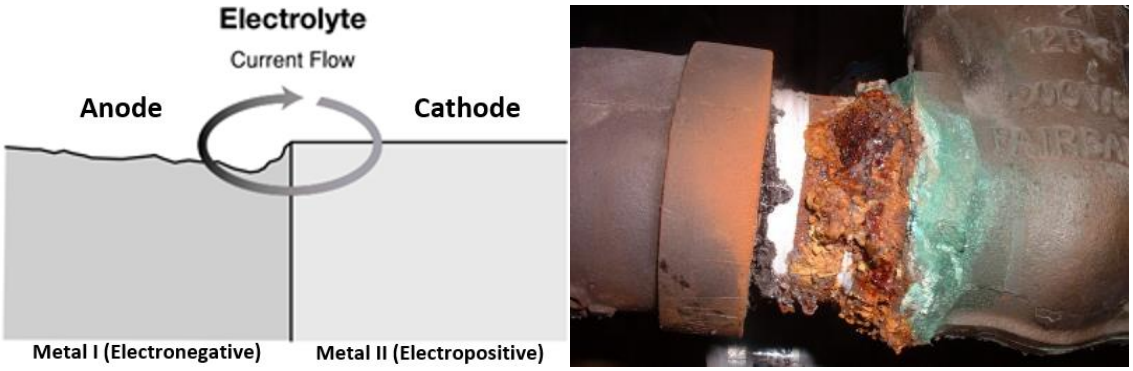

Figure 2.5: Galvanic corrosion process (left), galvanic corrosion in a pipe joint [28, 29]

2.1.6 Erosion Corrosion

When sand particles flow with the product that is being transported in a pipeline, it will cause a high level of turbulence. This turbulence damages the protective layer or films of the pipe to

allow erosion or corrosion to develop. So, an increase in the rate of corrosion, as a result of motion of the environment is known as erosion corrosion [28].

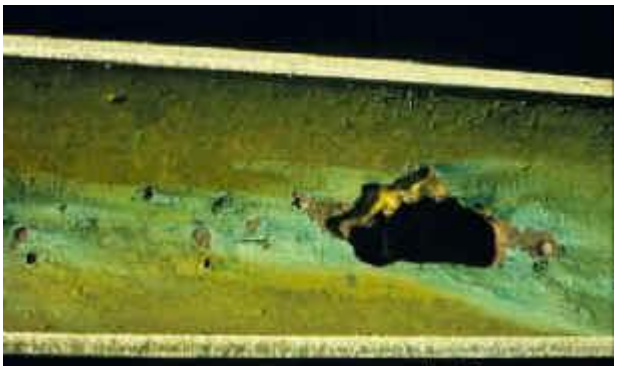

Figure 2.6: Erosion corrosion [20]

2.2 Corrosion prevention and associated challenges

One of the most potent techniques to slow down and in certain cases even avert corrosion from developing is to apply protective coatings (PC) onto the metals. These coatings are paints that are specifically designed for resisting corrosion development and contain highly resilient anti-corrosive properties. One of the many reasons for using PCs is to act as a barrier between the metal and moisture [29]. Operating temperatures and the environmental factors confirms which type of coating to be used on a pipeline. Most common type of high temperature coating is the siloxane or epoxy based coatings which can operate up to as high as 230°C and for higher temperatures up to ~500°C, thin aluminium film coatings can be used on pipelines [30]. However, these panacea are costly, therefore certain amount of increase in the efficiencies, longer lifetimes or reduction in the emission are essential [31]. Also, in order for the coatings to be effectively applied on the pipelines or any other material, it requires some kind of surface preparation and cleaning. The thickness of the coatings can vary from tens to hundreds of micrometres depending on the application.

Even though coatings render a high amount of protection from corrosion, they are also susceptible to damage and failure. Immense temperature variations, moisture evaporation/condensation cycles and salt contaminants can reduce the effectiveness of insulation properties and leading to damage. Fluctuation in temperature continuously causes the metal and coating to expand and contract [30]. This irregular expansion and contraction rate between the metal and the coating reduces the adhesion between them. This also releases stresses which may ultimately detach the coating from the metal causing it to interact with moisture. Therefore, flexibility of coating is a vital issue, as repeated stress and varying temperature can cause coatings to become brittle and malleable. Corrosion are also permeable

to water and may take place under the coating. Such corrosion can cause disastrous failures if not spotted and alleviated at an earlier stage [32].

Since, corrosion under an insulation layer or coating layer is not easily detected, hence, an effective monitoring method is needed to detect any corrosion while still in the earlier stages, in order to eliminate or control corrosion under coating. In most cases, pipelines are insulated and the most effective method of inspecting corrosion under insulation (CUI) is the removal of that insulation [33]. This can be done by cutting a small section of insulation and gain access to the metallic surface of the pipe. Once there is access to the metallic surface, different techniques can be used such as visual inspection and other electrochemical methods in order to determine the condition of the metal and the extremity of the corrosion.

The lift-off distance between the RFID sensor and the metal surface caused by the insulation layer, is one of the major challenges of CUI along with challenges of precise detection and quantification of corrosion. Immediate consequences of this increased lift-off distance is the reduction in sensitivity and spatial resolution of the sensing signal towards the trivial changes in the corrosion level such as metal loss.

2.3 Review of NDT&E technique for corrosion monitoring

NDT&E techniques are extensively used in the industries and for academic purposes as well in order to evaluate the structural rectitude and properties without causing any destruction to them. Previous section identified a number of defects and this section will give a summary to some of the most commonly used NDT techniques for corrosion monitoring and detection. The aim is to provide a review of each technique, the merits and demerits of the technique and their current applications. It should be known, that no one inspection method is suitable for detecting and evaluating all kinds of defects and corrosion. Often a fusion of technique is required in order to detect them. Therefore, a comparison between each of the NDT techniques is provided to evaluate their appropriateness to corrosion and crack detection and characterisation. This is depicted in Figure 2.7.

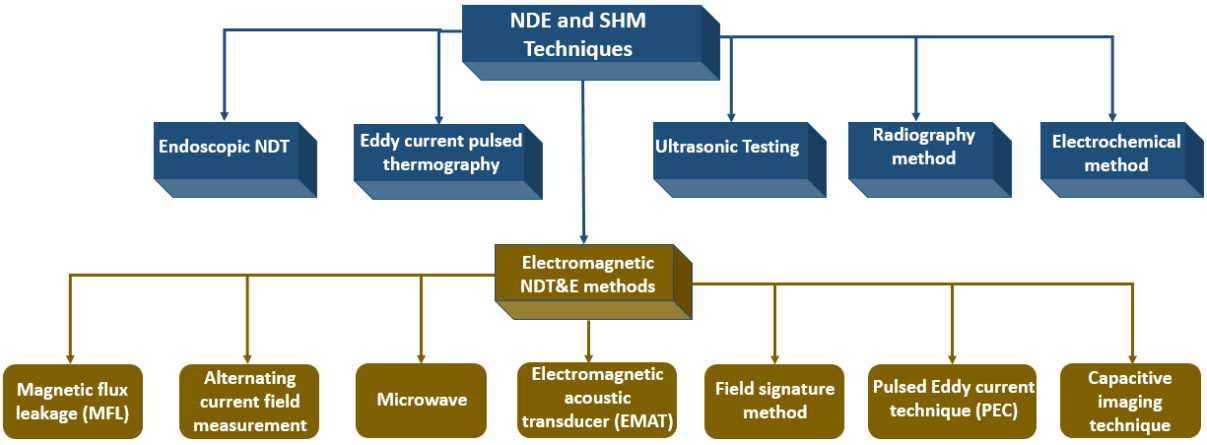

Figure 2.7: Bridging NDT&E and SHM techniques

2.3.1 Visual inspection/Endoscopic NDT

Visual inspection is known to be one of the most commonly used NDT methods. This is a regular inspection method that is used for assessing corrosion damage on the concrete structure surface. Though the inspection is very effective for surface structures and can be done with simple tools such as flashlights, but for the enclosed system the method is ineffective and it is strongly dependent on the experience of the inspector [32, 33]. In addition to this, visual inspection is also restricted from detecting surface roughness due to steel corrosion and crevice corrosions in difficult places [34]. Below in Figure 2.8 shows the structure for the electronic endoscope. It is a fibre optic cable with a small camera placed on the end of it which enables the operator to inspect limited areas. This is most beneficial side of this technique compared to visual inspection. These two techniques can be used to detect corrosion and other physical damages [35].

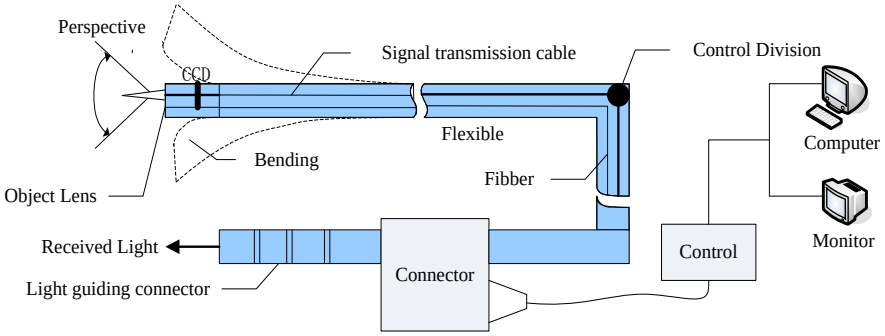

Figure 2.8: Structure of electronic endoscope [35]

2.3.2 Radiography methods

Radiographic method is another commonly used NDT&E technique which is based on the differences in the attenuation of penetrating radiation in the materials based on the radiation energy such as x-rays, gamma rays and neutrons. The attenuation coefficient relies on the

different thickness and the types of the material and any presence of damages or corrosion will vary the transmitted radiation intensity. This technique reportedly offers the best resolution of all the techniques with reported detection of corrosion defects as small as 6mm in diameter with 1.2mm depth [36] and also for sensing defects in carbon fibre composite materials [37]. In many of the cases any discontinuities in the insulated pipes are easily detected. Even though this technique offers more information about the characteristics of the pipeline, there are still some major limitations of using this technique. Firstly, usage of ionising radiation increases health and safety risks. Though recent developments in the radiography technique eliminated the use of film in order to reduce cost, but the fact that it requires highly trained technicians to safely operate this technique makes it an even more costly technique. Also the equipment used for the radiography method are usually large and bulky.

2.3.3 Eddy current pulsed thermography (ECPT)

Eddy current pulsed thermography includes the usage of a high frequency EM wave at a higher current on the material which is to be inspected for a time typically of about 20 ms to 1 s [38, 39]. Induced eddy current are focused on the discontinuity of the material under inspection which leads to increase or decrease in the eddy current density within the area. The areas with higher eddy current density will encounter higher level of heating and thus identifying any presence of damages from the IR image sequences during the phase of the heating and cooling.

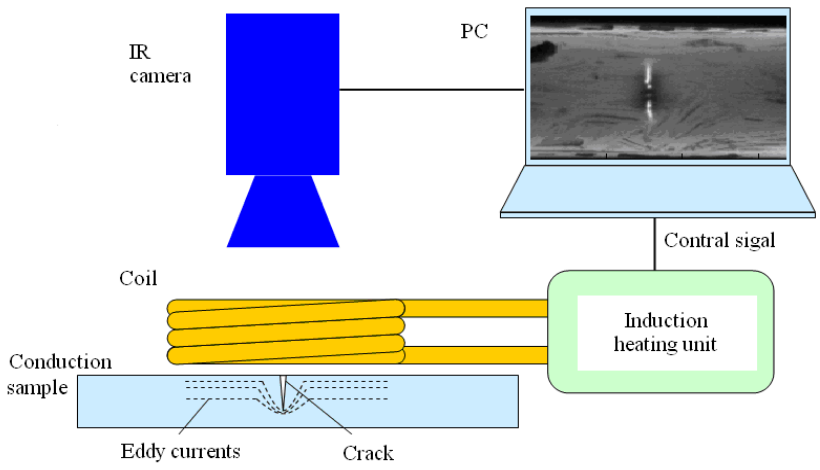

Figure 2.9: Basic diagram of eddy current pulsed thermography system [39]

The system shown In Figure 2.9 includes an induction heating system that is used to induce eddy currents on the sample under inspection where the heat produced on the surface of the sample is captured by the IR camera which is then displayed on the PC.

He et al [40] investigated corrosion blisters in mild steel under insulation using ECPT. Different damages were used to study the eddy current density distribution and heat conduction.

Xu et al [41] detected surface cracks on the tungsten carbide matrix of polycrystalline diamond compact bit using ECPT. To improve the sensitivity of the detection, he used principal component analysis (PCA) for the processing of the IR image sequences. Also recently, surface condition on freeform-surfaces have be measured and evaluated using thermal pattern reconstruction of ECPT system in [42].

Also early stage when fatigue crack has been detected by Peng et al [43]. He has used different feature extraction techniques to quantify the fatigue crack using ECPT. The proposed method showed an enhancement in the crack detection capability for railway.

However, one of the major drawbacks of the ECPT system is that it can only detect well conductive materials and also the equipment required for carrying out the experimental work is quite bulky.

2.3.4 Electrochemical Methods

Electrochemical methods are considered to be the most suitable methods for corrosion monitoring in NDT. They can provide reliable information on the corrosion probability, rate of corrosion on steel re-bars and the concrete structure's resistivity [44-46]. Electrochemical methods can be defined as the combination of the electrical and the chemical effects. Electrochemical impedance spectroscopy (EIS) is an electrochemical method that applies sinusoidal AC current of varying frequencies to the sample and then measures its response. Chemical reactions such as presence of corrosion can dominate at certain frequencies and this therefore can differentiate the insulation layers along with the corrosion layer and compare with the reference sample information provided by the company to investigate parameters such as the corrosion rate and reaction kinetics.

There has been numerous studies carried out based on the EIS method for various applications. Liu et al [47] studied the corrosion behaviour of zinc exposed in the coastal industrial atmospheric environment where as Sun et al [48] studied the formation of long-term atmospheric corrosion of pure Aluminium. One of the major reasons for using EIS method for these studies is because they provide dynamic measurements of corrosion rates and can be performed quickly. Though the drawback of EIS is that, higher technical expertise is required to carry out the data processing and also the equipment used are very costly [49] which makes them unsuitable for in-situ detection of corrosion and identification under insulation.

2.3.5 Ultrasonic testing method (UT)

Ultrasonic testing methods use the vibration of the sound waves that can penetrate through materials such as steel, alloys and with lower resolution through composites like concrete, wood, etc. Very short ultrasonic pulse waves with centre frequency ranging from 0.1MHz to as large as 50MHz are applied to the specimen under test [50]. This is one of the most commonly used techniques to determine the thickness variation in steel pipes due to corrosion [51]. Typically UT system consists of a number of functional units which are transducers, transceivers and the display units [52]. The UT can be divided into short and long ranges. Short range ultrasonic inspection is used to measure localised defects using time of flight technique. For better resolution of imaging, transducers arrays are also employed [36]. On the other hand, long range ultrasonic technique which is also known as guided waves or Lamb waves are used for pipeline inspection which travels along the surface of the pipe without spreading, however, the depth of penetration is limited but this gives the guided waves the advantage of travelling a longer distance of over 20m [53].

The transducer is usually segregated from the specimen using couplant or water. The ultrasound waveform can be obtained in two mode, i.e. reflection mode and the attenuation mode. In reflection mode, the transducer consists of an actuator which generates high voltage electrical pulses, which the produces high frequency ultrasound. This sound energy is instigated and propagated into the specimen in the wave form. If there is any discontinuity in the specimen, this will give rise to discontinuity in the propagated wave path and some of the sound energy will be reflected back. This reflected wave signal is then converted into the electrical signal by the transducer and is displayed onto the screen. Then a plot is drawn of the reflected signal strength versus the time interval between when the signal was generated and the echo was received [54]. From the obtained signal, information about the size and the location of the defect can be found.

On the contrary, in the attenuation mode, the transmitter sends ultrasonic waves through the surface which then travels through a medium and is received by a separate receiver. Any availability of flaws or discontinuity reduces the amount of ultrasonic wave received thus showing the presence of defect in the specimen [55]. Although UT has the capability to detect corrosion, but it is highly affected by any surface anomaly which then makes it difficult to differ between corrosion and other faults, therefore it requires a clean and regular surface [36]. Another limitation is that, ultrasonic waves do not travel well through the air and hence require a coupling agent such as water or gel to transfer the acoustic waves from the transducer to the material.

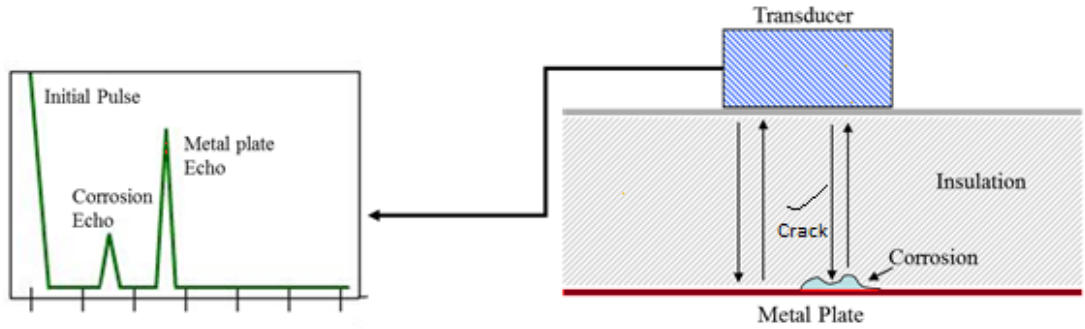

(a)

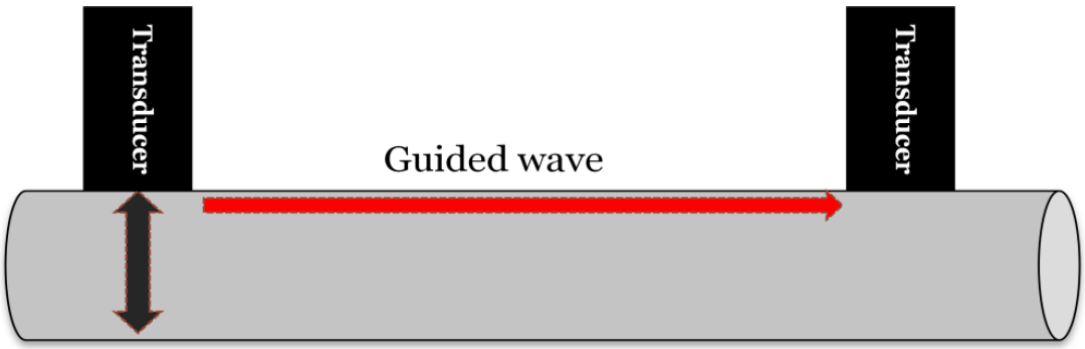

(b)

Figure 2.10: Ultrasonic NDT&E (a) Conventional ultrasonic testing (UT), (b) long range guided wave testing

Recent advances has proved to come up with better techniques such as laser ultrasonic technique where the lasers are used to detect the ultrasonic waves [56]. This system simply consist of a laser ultrasonic generator and an interferometric sensor. This non-contact technique can be used to measure material loss or any presence of flaw. Laser UT was used by Park et al [57] used laser ultrasonic technique for localization of any delamination in wind turbine blades based on the time-of-flight analysis. Also Francisco et al [58] employed laser UT for localising and detecting stress corrosion cracking (SCC) in stainless pipes. Similarly, here in this method, the laser is set to generate ultrasonic waves which in association with defects, changes the generated wave-modes which are examined using the time-frequency analysis methods. However, the limitation of this method is that the access to the surface of the specimen under test is needed, therefore, if pipelines with insulation are to be tested then the insulation must be removed. Also this technique is also sensitive to surface cracks and thus it limits further scope.

2.3.6 Electromagnetic NDT&E techniques

2.3.6.1 Magnetic flux leakage (MFL)

This method is another commonly used techniques for NDT&E [59] and it is most commonly used because of its simplicity. This system simply consists of a magnet yoke, which magnetises the pipe wall to near saturation flux density. Presence of flaws will give rise to varying permeability. Change in the permeability of the sample due to presence of defects will lead to an increased reluctance which causes the flux to take different routes. Saturated routes will 'leak' flux into the air which are then detected using magnetic sensors [60]. The characteristics of the field will depend on the permeability and the geometry of the material under inspection. Figure 2.11 below gives a graphical illustration of the principle.

One of the major challenges of traditional MFL technique was the difficulty in sizing and discriminating between internal and external defects. An extension to the MFL is the pulsed magnetic flux leakage (PMFL) which uses a square wave excitation to the magnetising coils. The square wave contains multiple frequency components which allows transient analysis to be carried out for depth information estimation and improved differentiation between internal and external defects [61, 62].

MFL is known as a famous method for testing ferrous materials such as steel pipes. The method is most suited for uniform wall loss and locating pitting corrosion [63, 64]. However, one of the other weaknesses of MFL is that cracks which are in the same lie as the fields produced, are not easily detected due to the defects dimension being not orthogonal to the axially orientated excitation flux [65]. This is illustrated in the Figure 2.11. They are also not suitable for the insulated pipes due their limitation in the smaller stand off-distance. Though there are works being carried out for flaw detection under thicker insulation and higher stand-off distances [66, 67], but more research is required to enhance the sensitivity of this system which is thought to be achieved by developing optimised MFL sensors and this is attempted by Lijian et al. [68]. In their work they have used a differential coil to minimise noise. One of the coil is placed near the sample surface while the other coil is placed isolated from the surface. The signals are then subtracted from one another in order to eliminate the noise. Generally the coil winding of one of these coils are clockwise and the other is anticlockwise.

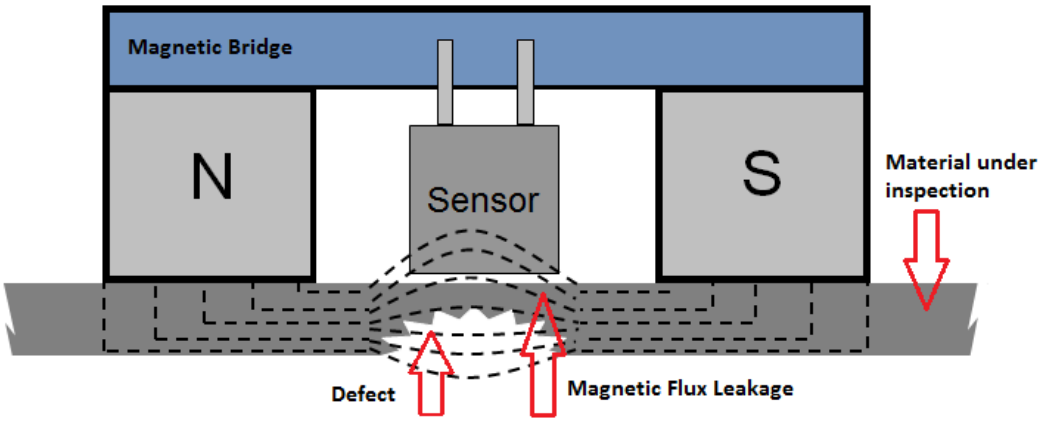

(a)

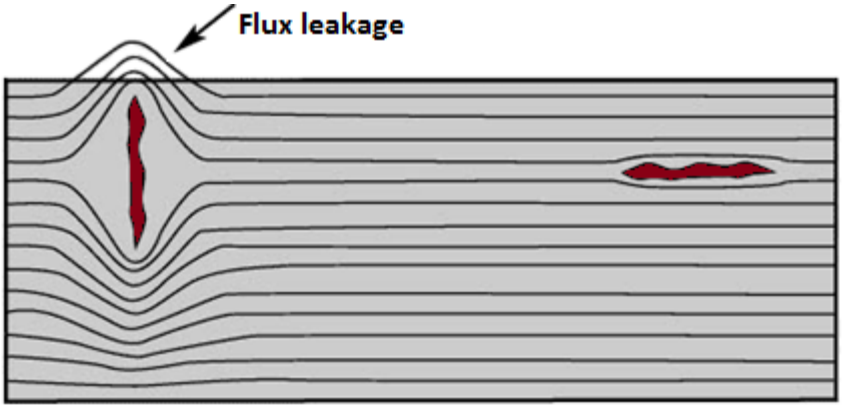

(b)

Figure 2.11: (a) MFL Inspection with magnetic bridge, (b) Defect alignment issue on the flux path [65]

Despite the attempt of MFL sensor optimisation, there are other issues such as the weight and volume of the sensor due to the requirement of the magnetic circuitry and the equipment, pipe end effects and magnetic compression effects. To this end, Sun et al [69] have proposed permanent magnetic perturbation (PMP) sensors which overcomes all the aforementioned deficiencies where the magnetic perturbation initiating by the discontinuities is directly captured. PMP sensors can also detect Omni-directional defects including those defects that are parallel to the magnetisation direction.

2.3.6.2 Alternating Current Field Measurement (ACFM)

This technique is an EM NDT technique that can detect breaking of the surface or near surface defects for both ferromagnetic and non-ferromagnetic materials [70]. In this technique, a solenoid is used induce uniform alternating current in the targeted sample. In presence of defects, the uniform alternating current distribution is interrupted making it to flow around and

beneath the flaw rather than producing uniform magnetic field. This non-uniform distribution is then measured using the ACFM probe. As can be seen in Figure 2.12, ACFM system measures two field components, i.e. Bz and Bx which gives the information about the length and the depth respectively.

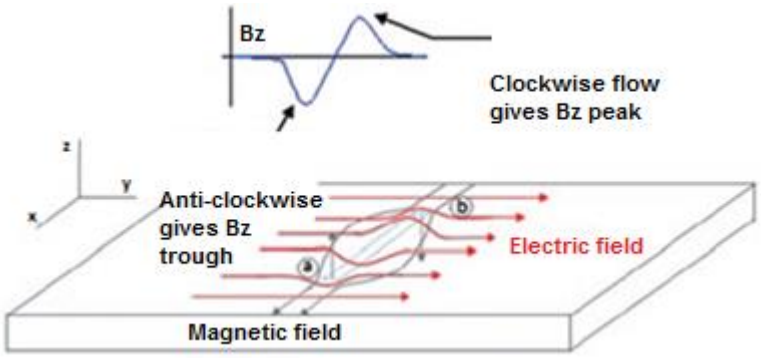

Figure 2.12: Current and Magnetic field distribution in ACFM [72]

ACFM technique has been used for various applications now even though at an earlier time it was developed for underwater weld inspection. Some of the useful applications of this technique involve inspection of pipes and vessels, railway track inspection [70] and stress measurement [71]. One of the major advantages of this technique is having little adverse probe lift-off effect which makes it attractive for rough surfaces [72]. Also it requires almost no surface preparation and since its insensitive to the electromagnetic property changes, which makes it even more suitable for ferrous and non-ferrous metals, ideally for weld inspection [73].

However, the limitation of this technique is that, it uses larger coils for induction which reduces the sensitivity for shallow defect detection. This can be improved using smaller coils and higher frequencies but that will then give rise to noise [74]. Also bogus signals may arise from unusual geometries, edges and defect arrays [73]. This system not portable and requires higher level of operational training which means even higher cost.

2.3.6.3 Microwave NDT&E

Microwaves, are high frequency radio waves that have recently found its application in NDT of corrosion. Their usual operational frequency is between 1 GHz – 100 GHz and frequencies over this range is known as millimetre waves [75]. A rising interest in the use of microwave based NDT&E techniques can be noticed since the last decades. Various studies have been conducted to utilize this method including radar sensors [76], open ended waveguides [77] and coaxial probes [78]. The condition of the target sample is determined from the magnitude and the phase of the reflected signal. The higher frequencies of the microwave makes it useful for

image reconstruction of defects because higher frequencies mean higher spatial resolution. Higher spatial resolution makes it easier to identify smaller pitting corrosion.

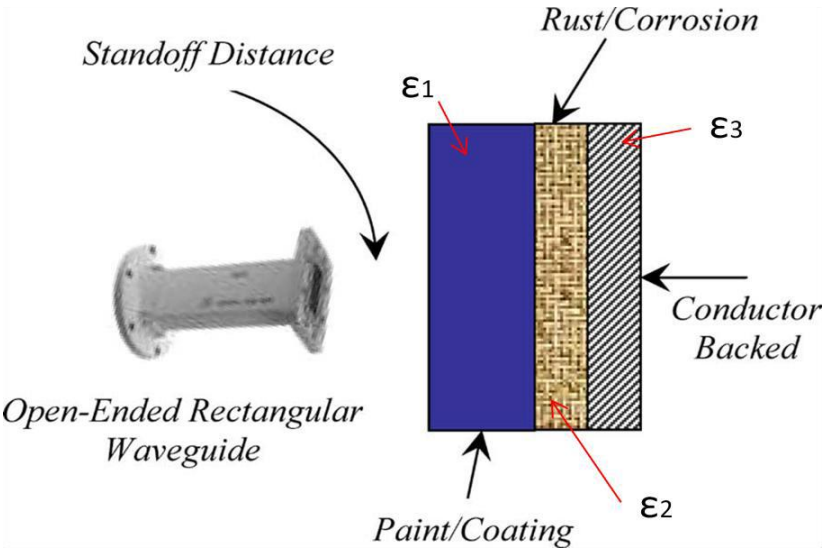

Figure 2.13: Typical microwave test setup showing an open-ended rectangular waveguide with multi-layers defected sample [78]

Yeh and Zoughi proposed and developed an NDT&E technique for microwave using open-ended waveguide to detect and quantify surface damages [79]. Also a wider range of applications have been discussed in the overview given by Kharkovsky and Zoughi [75] on microwave and millimetre wave based NDT&E technique which included corrosion detection and pitting in steels. Microwaves are also useful in terms of penetration through dielectric materials such as paint or non-conducting layered structures [80] and hence it gives microwave technique a supremacy compared to other electromagnetic NDT techniques. Ongoing research at Imperial College London, shows that microwave has the potential to detect moisture in the insulation which is considered the precursor to corrosion.

However one of the major limitations of the microwave is that, it cannot efficiently penetrate through conductive materials, which makes it difficult to detect subsurface damages and also it requires expensive detection instrumentations such as network analysers which will limit it the usage of this technique in various applications.

2.3.6.4 Electromagnetic Acoustic Transducer (EMAT)

EMAT is an emerging NDT&E technique which is beneficial for its non couplant requirement. Advantages of this technique also include non-contact operation, ability to use the shear horizontal (SH) waves, Rayleigh waves, lamb waves and its wide applicability in the high temperature environment [81-83]. Recently, techniques such as laser induced ultrasonic and air

coupled techniques have been introduced as an alternative to overcome the coupling problems [84-86], but the principle of EMAT which generates ultrasounds in a conducting material using eddy currents (as shown in Figure. 2.14), makes it a potential technique for detecting flaw in metallic materials.

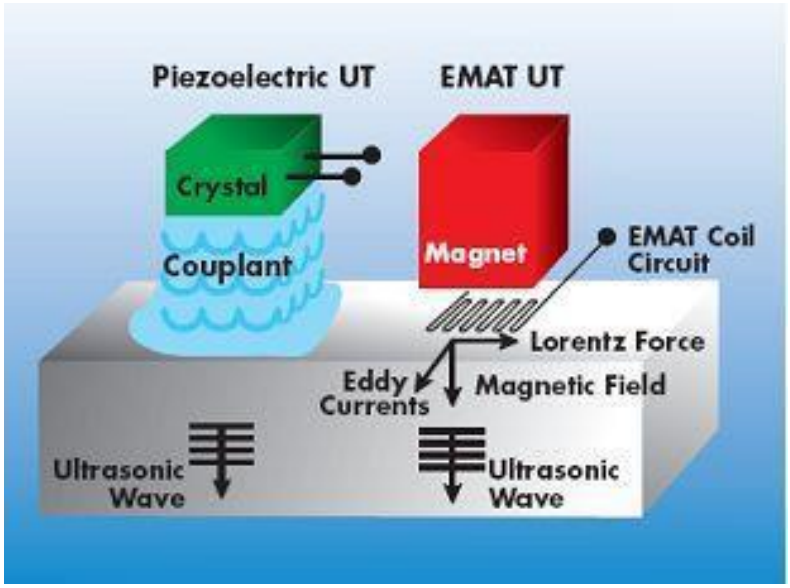

Figure 2.14: EMAT Testing [87]

In this, a coil which has a high frequency AC current will induce eddy current on the surface of the material. The electrons present in the surface of the material experiences a Lorentz force due to the magnetic field produced from the permanent magnet and thereby generating ultrasound. One of the drawbacks of the EMAT is the limitation of the material selection that means, they are only limited to conducting materials. Usually, the EMAT signal consists of backscattering noise (fault echo) or electronic noise (caused by electronic circuitry), which embeds the required echo from the flaws and therefore, making it difficult to obtain the correct flaw signal [88]. There are also non-contact probes produced such as dual EMAT and PEC non-contact probes [89] which enhances the sensing ability to defect and size the defects with higher accuracy.

Also laser EMAT have been efficiently used to generate shear waveforms at generator up to the Curie point of ferromagnetic material [90] and later Idris et al [91] developed and experimented a water-cooled EMAT which can obtain a temperature range of 1000°C. Generally, the developed high temperature EMATs can only operator at high temperature level for a short period of time which even though makes it suitable for detection but its not the solution for long term SHM [92].

However, one of the major disadvantages of EMAT is the presence of low coupling efficiency which means any presence of delamination might cause small lift-offs which might notably drop the power transferred to the metallic sample.

2.3.6.5 Field signature method

Field signature method depends on the measurement of changes in the potential difference of the sample under test once a current has been sent through it. A number of measuring probes are attached on the surface of the material to be inspected in a structure to form a measurement matrix. The space between two probes is known as a cube and this is also known to be a register. Therefore any changes the material caused by corrosion or any other forms of defect will alter the resistance between the probes and thus changing the electric field pattern [93, 94]. This system is depicted in Figure. 15:

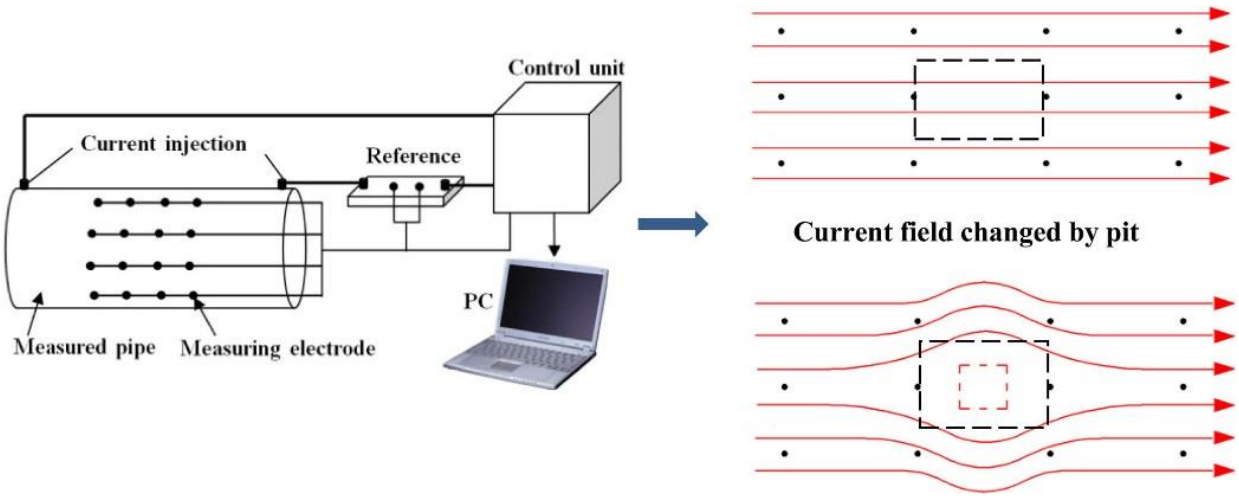

Figure 2.15: Current field distribution of field signature method [94]

Many researchers have adopted this technique due to its advantage that no measurement components are directly revealed to the harsh environmental conditions such as temperature (can work up to 350°C) or pressure [95, 96]. Also since there are no consumables so the lifetime of the system is longer and as it doesn't require for the protective layer on the pipe to be removed for measurement, this makes it a suitable online monitoring NDT method.

Gan et al proposed methods to assess pitting corrosion using finite element analysis which was later improved depending on the investigation of current redistribution caused by localised corrosion [97]. Further work was carried out in the understanding of the different causes for the accuracy of the pit corrosion detection and it was found that different corrosion pits had different sizes and depths, were highly influenced by the nearby probe pairs. Hence, subdivided network of resistors have been proposed as a new technique to examine the pit corrosion and

verified in [94]. The application of FSM was expanded from offshore industries and pipelines to refineries [36].

2.3.6.6 Pulsed Eddy Current Technique (PEC)

PEC has a long history of approximately going back to five-decades. Despite this, it is still considered as an emerging eddy current NDT&E technique. The reason for this arising attention towards PEC is potential benefits that it provides. Major benefit of using PEC is that, compared to single frequency eddy current technique (ECT), PEC has multiple frequencies [98] which is beneficial in terms of skin effect and even compared to the multi-frequency ECT, PEC can be applied in shorter times for depth inspection. PEC also doesn't require any surface preparation as compared to other ECT techniques which enhances inspection time. This can be shown in Figure 2.16:

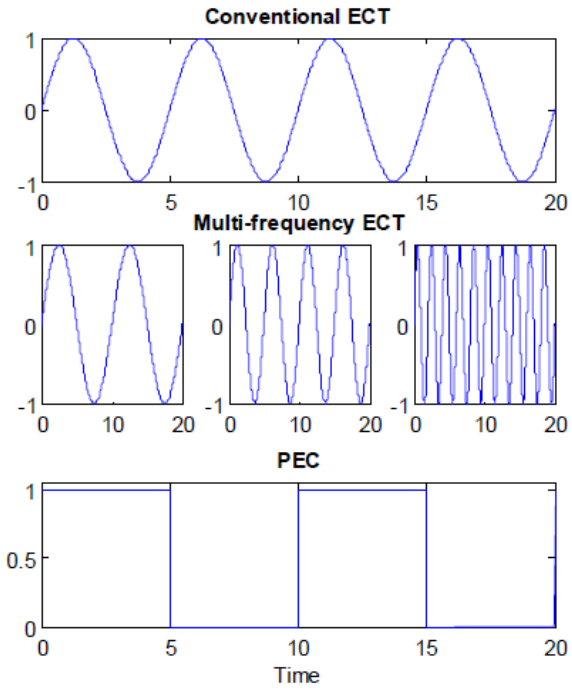

Figure 2.16: Different waveform excitation of ECT techniques [99]

In eddy current NDT, eddy current is induced in the sample though electromagnetic coupling by an AC-driven excitation coil. This circulation of the eddy current induces a subordinate magnetic field which varies in the presence of any defect or corrosion that causes a variation in the magnetic permeability and electrical conductivity or even thickness as depicted in Figure 2.17. This variation in the field is picked up by a coil probe or a magnetic sensor.

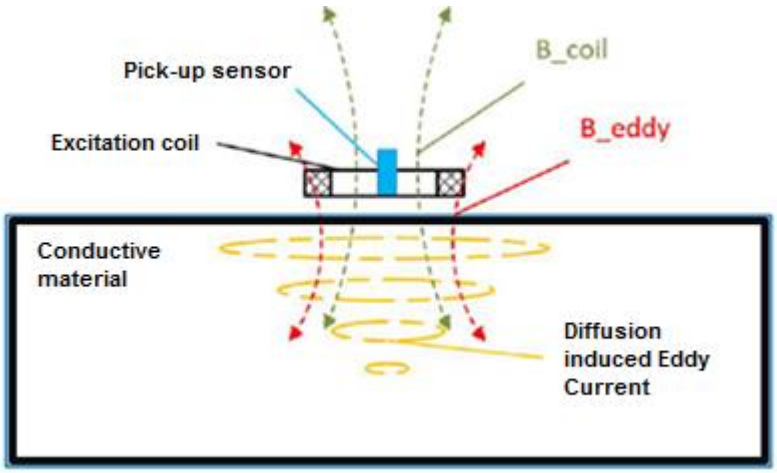

Figure 2.17: Principle of ECT showing the magnetic fields [97]

The penetration and the density of eddy current in the sample is an essential challenge. The depth of penetration is affected by skin effect, which decreases the density exponentially. The depth at which the density is reduced is called the skin depth and is denoted as δ and is defined by:

$$\delta = \sqrt{\frac{2}{\varpi\mu\sigma}} \tag{2.1}$$

where ω is the angular frequency (rad/s), μ is the magnetic permeability (H/m) and σ is the electrical conductivity (S/m). As it can be seen from the equation, that the penetration depth is dependent on the excitation frequency. The higher the frequency, the lower the depth of penetration. One of the advantages of using PEC over traditional ECT is that, conventional ECT is limited to only one frequency component whereas in PEC, a pulse waveform is generated and the frequency component of this pulse waveform can be shown by using Fourier Transform:

$$f(t) = \begin{Bmatrix} A, -\frac{W}{2} \le t \le \frac{W}{2}, \\ 0, |t| \ge \frac{W}{2}, \end{Bmatrix} \tag{2.2}$$

Where A is the pulse amplitude and W is the pulse width.

Even though the excitation of PEC is always obtained by an induction coil, but the sensing device can be categorised in two types; induction coils and magnetic sensors. The output of these two sensors can be shown as:

$$V_{ind\_coil} = -N.A.\frac{dB}{dt} \tag{2.3}$$

$$V_{mag\_sensor} = K.B \tag{2.4}$$

Where N determines the number of coil turns, A is the path area from which magnetic field passes through, B is the magnetic field density and K magnetic sensor coefficient. These two equations generate from the principles of the two types of sensing. This means, the output of the magnetic sensor is proportional to the magnetic flux density on the other hand the output of the induction coil depends on the rate of change of magnetic flux density. This proves that both these types will display similar response characteristics [100].

PEC signals, however, are influenced by numerous elements, including lift-off variation, electrical conductivity, magnetic permeability, inhomogeneity of the material and even thickness variation of the material under inspection, not to forget the noise and the low level signals in other cases. These issues have been continuously addressed over the time through correct signal processing, feature extraction and classification of the modelling. The features that has been used in order to extract the desired information are peak values [101, 102], peak arrival time [103], rising time [104] and zero crossing time [105]. Another most widely used technique was using principal component analysis (PCA) [106-111].

Using FFT, surface and sub-surface defects have been classified in [112, 113]. Also the use of both time and frequency domains have been studied by Ref. [114] in order to detect and characterize cracks under aircraft layered structures. There is also a long list of literatures covering the detection of sub-surface defects of AISI type 316 stainless steels and artificial defects by Tian et al in [105, 106, 115]. Amongst the major issues, many researchers have attempted to solve the problem of lift-off variation or at least reduce them. One of the popular features used to minimise the effect of lift-off is finding the lift-off point of intersection (LOI) which is a point where PEC signal is intersected with lift-off distance variation.

This technique has been adopted well to evaluate the thickness of a material [116] which is basically considered as the corrosion layer and also identify defects location in layered samples [117]. The LOI was also obtained by using derivative of the output signal from a Hall sensor by Tian et al [118]. Experimental measurements of thickness of insulation has also been identified using PEC in [119] along with coating thickness measurement of both magnetic and non-magnetic coatings in [120]. Applus RTD has created PEC system to determine the wall thickness from the ranges of 6 mm to 65 mm and by evaluation the wall thickness, the corrosion under insulation (CUI) can be measured [121]. Another Canadian company called Eddyfi has commercialised their PEC system that is capable of measuring wall thickness of up to 64 mm

and for a non-conductive insulation up to 203 mm [122]. Other research works estimated pipe wall thickness in [123] and [124].

Also, PEC technique is utilized to measure the electrical conductivity of ferromagnetic materials such as carbon steel plates which is inspected by Chen et al [125]. The same work has also proved to show good results for the magnetic permeability measurement. Also, Adewale et al [126] explored the effects of permeability and conductivity on PEC signals and found that conductivity affects the rising edge of the transient response of the pulse whereas permeability affects the steady state region. Apart from these, the inhomogeneity of material has been studied in [127, 128] which affects the defect measurement due to spurious signal responses.

Despite all these, current methods for detecting corrosion over thick insulation (lift-off) without removing, it is still a severe limitation of PEC. Also the inspection area for PEC is very limited as it can only detect any defect under the probe and therefore requires sensing array to be built. Another major drawback is the inability to detect localised corrosion using PEC.

2.3.6.8 Capacitive imaging technique

This NDT technique is also known as electrostatic imaging technique. The general principle of this technique is that, the co-planar capacitive electrode is used to determine any electrical characteristics changes within the sample. The probe that contains two or more electrode will then generate a distribution of the electric field within the sample upon the application of the AC voltage between the positive and the negative electrodes. The resultant electric field pattern will be affected in the presence of any defect. This can be seen in Figure 2.18.

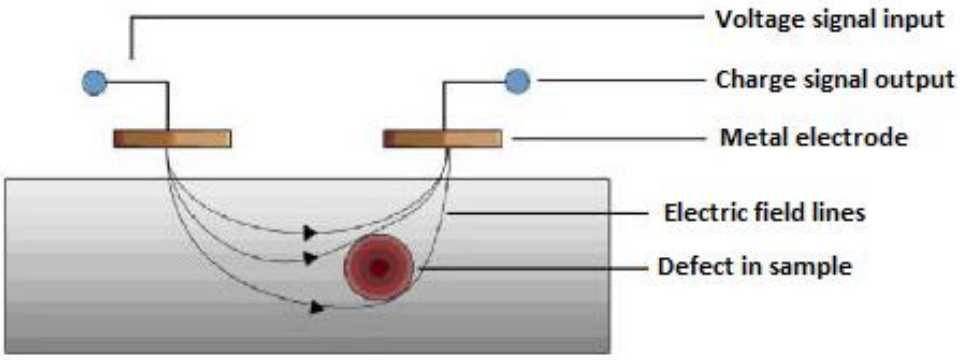

Figure 2.18: Schematic of capacitive imaging technique [129]

Unlike the PEC method, this technique can be used to inspect non-conductive materials such as wood [130], concrete [131] and plastics [132]. Also, since electrodes are used instead of coils, the amount of electric field produced is much higher than the produced magnetic field.

This technique has been applied in order to image surface defects as small as 2 mm in depth by Yin et al in [133]. This sensor has also shown good sensitivity in moisture detection in non-conductive materials [134, 135] and thereby enhancing the scope of detecting water in insulations as a precursor to corrosion development. Though the varying moisture level in the insulation layer may obfuscate the corrosion progression.

2.3.7 Synopsis of NDT&E techniques defect and corrosion detection

The literature review of NDT&E methods for corrosion and other defect detection have been summarised in Table 2.1 below. A comparison of the techniques in terms of its overview along with the pros and cons of the techniques are provided in the table.

Numerous elements that need to be considered before the selection of these NDT techniques can be made. These include accessibility, application scenario, portability of the system, inspection area and its size, types of material under inspection, costs and type of defects to be inspected are amongst the many elements that needs to be considered. Some techniques perform well under certain conditions and are more applicable than the others providing quantitative and qualitative information but maybe only effective for limited materials, while other techniques may just perform abysmally when other factors are taken into consideration. Eventually, the overall target of inspection is to provide an accurate and time efficient technique that can advance the repair/replacement in a cost effective manner.

Table 2.1: Schematic of capacitive imaging technique

NDT&E techniques	*Ultrasonic*	*EMAT*	*ACFM*	*EIS*	*Microwave*	*Radiography*	*ECPT*	*MFL*	*PMFL*	*PEC*	*FSM*	*Capacitive imaging technique*
Advantages	Faster technique; wide area inspection; higher depth of penetration; sensitive to both surface and sub-surface defects	No surface contact required; couplant not required; allows high temperature operations	Uncalibrated defect sizing; less affected by probe lift-off	Higher sensitivity; faster operation; non-visible defects can be detected	Higher resolution; coating properties can be inspected	Better resolution imaging; broad range of materials inspected; inspection film can be recorded	Surface defect detection; higher resolution; wide area inspection	Established method for pipeline inspection; robust measurement of metal loss	Better defect sizing and detection on surface and sub-surface	Higher penetration depth; accuracy in differentiation between surface/subsurface defect; multi-layered defect detection	Continuous corrosion detection	Inspection of non-conductive objects
Disadvantages	Couplant requirement; accessible surface required; difficulty in measuring irregular surfaces	Efficiency of transductio n is poor; lower signal to noise ratio due to backscatteri ng noise	Lower sensitivity to shallow defects; edge effect; geometrical constraints	Costly; complex data analysis for quantification ; prior knowledge of defected area required for localisation	Only surface defect can be detected due to limited penetration depth; complex wave interactions	Radiation safety essential; expensive; access is required for both sides of the material	Expensive technique; complex system requirement ; poor resolution	Axial slot defects are undetectable; surface preparation required; limited penetration depth	Large lift-off limitation	Limited inspection area; lift-off sensitivity; limited in achieving sensitivity in complex geometry; influenced by material	Limited area; costly technique	Immune to interference; change in permittivity due to moisture
Primary defects	Delaminati on; wall loss, SCC	Wall loss, SCC, sub-surface defects, pitting corrosion	Weld inspection underwater	Corrosion under coating; coating properties	Pitting corrosion; General wall loss	General wall thickness; pitting	Fatigue crack, SCC, corrosion	General wall loss; pitting	General wall loss; pitting	Pitting corrosion; sub-surface defects; metal loss	Metal loss; corrosion	Corrosion under coating
Parameters influencing performance	Attenuation coefficient and material properties of the sample under inspection	Material properties; lift-off	Coil geometry; frequency of operation	Coating thickness	Thickness of insulation; material properties	Material properties; radiation scattering	Coating; thickness of material	Sensitivity and calibration of the magnetic sensor	Lift-off; sensitivity of magnetic sensors	Conductivity; permeability; probe geometry; lift-off effect	Delaminati on; sensor geometry	Thickness of coating layer

2.4 Review of passive RFID sensing system

Over the last decades, a swift grown in RFID technology for tracking and identification has been noticed in the industries due to its ability of unique identification (UID). Taking this trend to an advanced level, the processing of the physical behaviour related to the coupling between the reader and the tag, could give even more information about the target without further requirement of any additional electronic devices or sensors [136]. Allowing the ability to sense using RFID technology will provide the system with further information about the state of the real world situations and relate it to the global cyber-physical systems (CPS) and Internet of Things (IoT) [137]. Over the years the research on the exploration of RFID sensors are increasing exponentially. Zhang et al [138] carried out a literature review of the articles related to passive RFID tag antenna based sensors. From the research, it was found that, there were 442 papers on only passive RFID antenna based sensors published till 2015. Also noteworthy to mention that another 70 papers were published by the end of 2016. This research result is shown in Figure 2.19.

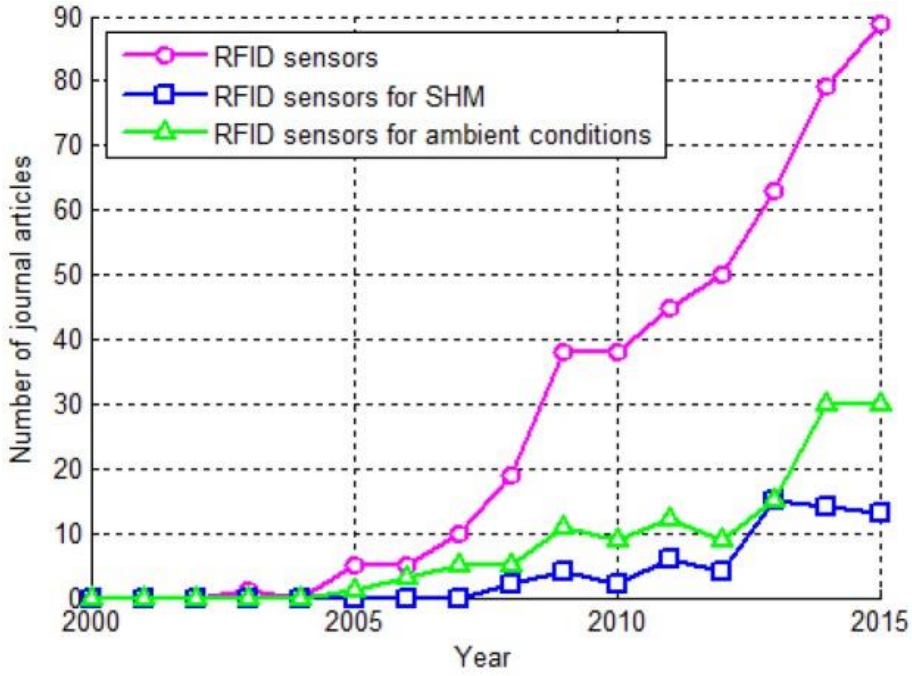

Figure 2.19: Classification of publications made for passive RFID sensors based on years, journals and countries

Passive RFID tags have been used in numerous forms in various applications starting from physical and chemical changes such as strain [139-141], displacement [142, 143], moisture [144-146], gas [147, 148] and temperature [149-152]. They are attractive as a potential system due to their simple configuration, passive (battery free) operation, low cost sensing, UID and flexibility of the tag to be embedded into thick insulation for long term SHM. This section will

give an overview on the use of passive RFID as sensors in SHM and then narrow the scope into the specific case of the usage of passive RFID sensors for corrosion and crack detection will be reviewed in the next section.

Cazeca et al. [142] demonstrated the usage of off-the-shelf RFID tags for making cheap passive wireless displacement sensors. The sensing system was fabricated by dividing the RFID transponder into two components, one being the transponder antenna and the other is the chip-loop. The sensor worked on the principle that the transferred RF energy to the RFID chip is dependent on the distance between the chip-loop and the transponder. Also Paggi et al [143] used a slotted patch as a UHF-RFID sensor for 1D displacement by establishing a mechanic-electromagnetic modulation to determine any changes into the antennas response.

Virtanen et al. [153] presented the use of novel-inkjet printer humidity sensors tag for passive UHF RFID. The humidity was measured based on the permittivity change of the Kapton HN substrate. Any changes in the humidity condition will cause the substance's permittivity to change based on the varying capacitance which will eventually mismatch the impedance of the sensor element and thus changing the tag signal. Later Emran et al. [154] presented clipless RFID tag based sensor for monitoring humidity of the tagged objects. The tag had multiple slots for the data encoding and for sensing the humidity there was an inductive capacitive resonator which would cause a resonant frequency shift due to the presence of humidity.

Occhiuzzi et al. [155] validated the feasibility of RFID sensor tags doped with single wall carbon nanotubes which is sensitive to the presence of ammonia in order to characterise the sensing capability of the RFID tag. The ammonia gas is investigated by analysing the variation of the radiation performances of the RFID antenna in terms of input impedances and the transmission characteristics. One the other hand Potyrailo and Surman [148] implemented the passive HF RFID sensors to demonstrate the multivariate analysis for self-correction of temperature effects in the LCR transducer coated material for gas sensing.

On the other hand, Girbau et al [156] demonstrated the feasibility of using UWB in the RFID based sensing system and used a positive temperature sensor (PTS) to detect the temperature variation from 30°C to 130°C and the reflection coefficient frequency function have been measured. It was found that an increase in the frequency would decrease the temperature sensitivity. Martinez-Martinez et al [157] proposed a novel passive RFID sensor based on planar magnetoinductive-wave delay lines. When the sensor is interrogated in time domain with a pulse, the temperature variation then creates a duplicate of the original pulse modulated in amplitude which depends on the magnitude under sensing. In industry, Intel Researchers have

designed a Wireless Identification and Sensing Platform (WISP) as a passive UHF RFID sensor and implemented as a PCB for better applicable scenarios and worked well over broad temperature range of 70°C [158].

One of the common feature in the aforementioned works is the use of thin films of PCB for RFID tags. Due to environmental changes, there will be changes in the thin film which could be monitored in order to determine various chemical and physical properties of materials or object under test. This is however, a limitation in terms of corrosion or crack detection and SHM because changes in the thin films or the PCB delamination may not be an accurate indication for the changes occurring on material the tag is placed on as corrosion or crack will inflate the material damaging the tag itself. Also another drawback is that these cannot be used for long term monitoring due to the saturation of the films or the unproductive encapsulation.

2.4.1 Passive RFID crack and corrosion sensing

In this part focus is pointed towards the literature on the use of the passive RFID tags for the monitoring of the corrosion and crack. Though the electrical components and the compositions used in engineering are designed very carefully taking into consideration of any kind of fatigue failures, there still exits nearly 50% of the mechanical failures due to the fatigue cracks. The extremity of these cracks depends on the length and the orientation of them. Amongst all, transverse cracks are the common forms of cracks and the even minacious, this is because they reduce the integrity of a structure. Traditional crack sensing systems use wiring for the data collection, the maintenance of these substantial wiring is inconvenient and costly [159]. Patch antennas are often used for crack monitoring. Based on the cavity theory, the underneath area of such antenna are the most sensitive. Also dual-mode [160] and 2D grid [159, 161] are used to detect both the crack length and the orientation. Also a multiplexing antenna sensor was designed to detect different oriented cracks using a multi-patch with spatial division [162]. The backscattered phase of this sensor can function as sensing variable and using the mutual coupling between 2 patch antennas even sub-mm resolution of crack width can be detected [163, 164]. The development of the crack characterization based on the passive sensing are further summarised in the Table 2.2.

Table 2. 2: Crack characterization based on the passive RFID sensing

Measurand	Sensing principle	Feature used	Pros.	Cons.	Ref.
Length and orientation of the crack	Dual resonant patch antenna	Resonant frequency shift	Sub-mm resolution, dynamic ranges	VNA is needed, not suited with Gen2 standards	[160]
Length and orientation of the crack	Spatial division	Power variation	Multi-site crack detection	Specific receiver required	[162]
Fatigue crack	Deformation of patch antenna	Resonant frequency shift	Higher read range of about 2.1m	Size of the antenna is large	[165]
Width of the crack	Mutual coupling using patch antenna	Phase shift	Resolution: sub-mm	Prior knowledge about the crack position is required	[163, 164]
Crack depth	Inductive coupling	Ratio of the voltage change	0.5 mm resolution of depth	VNA required, localisation dependent	[166]

Along with this, the interaction of these materials with corrosive environments and tensile stress such as any kind of directly applied stresses or residual stresses can cause collapse in the form of stress corrosion cracking (SCC) [58]. The damages formed from SCC can be unforeseen and catastrophic as they can be easily hidden under paint coating, later leading to larger failures. Therefore, early detection of these defects are essential to avoid any kind of danger and have enough time for condition based maintenance. Corrosion is a multi-layered structure which has thin oxide layer that brings about variation in the material's conductivity, permittivity and permeability [167]. These changes vary from material to material and the changes can be monitored based on the impedance shift of the tag antenna. The development of the corrosion sensors are summarised in the Table 2.3.

Table 2.3: Corrosion characterization based on the passive RFID sensing

Sensing principle	Feature used	Pros.	Cons.	Ref.
Inductive coupling	Static response	Faster analysis	Limited read range, lift-off dependent	[168]
Inductive coupling	PCA	Lift-off independent	Limited read range up to 2.5 cm, VNA is needed	[169]
Capacitive coupling	PCA	Higher read range of about 1 m	Large antenna size	[170]
Stub resonator	Resonant frequency shift	Chip-less, up to 2 m read range	Not compatible with Gen2 standards and VNA is needed	[171]

Corrosion detection and characterisation under paint and under insulation was demonstrated using the LF RFID coil antenna [168] and also HF RFID [172] by directly monitoring the response of the tag in the time domain. Due to the magnetic coupling, the detection distance is limited. Also feature of static responses used, are lift-off dependent. In order to overcome this challenge, measurement of impedance was carried out using VNA and for feature extraction purposes, PCA has been utilized for lift-off independency [169]. In order to overcome the limited read range challenge, UHF RFID technique have been adopted, where a 3D antenna was designed for the metallic surface that could be read from a range of 1 m [170]. The recent strive to use UHF RFID for defect monitoring can be characterized into two sections: one is the direct changes in the physical parameter of the antenna and the other is the indirect changes of antenna properties. Also inject printing [173] along with embroidery technology [141] have been applied for further cost reduction and enhancing the tag performance in terms of sensing.

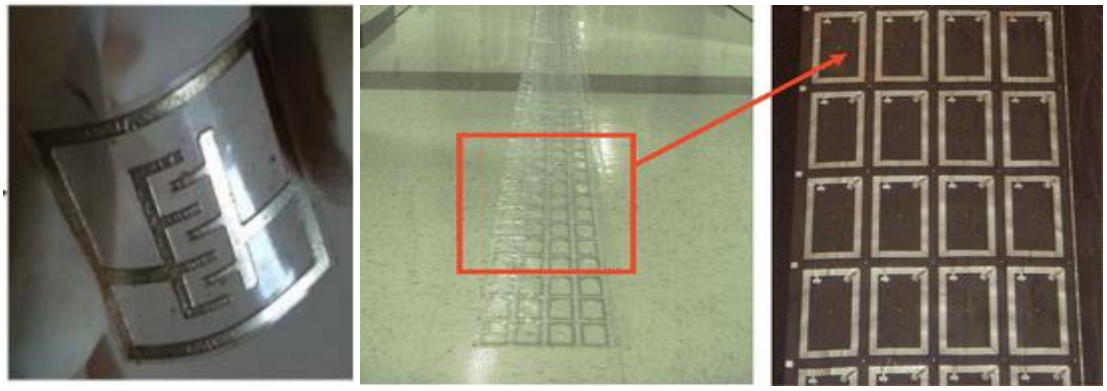

Figure 2.20: Flexible ink-jet printed chip-less RFID sensing platform [169]

Additionally, chip-less antenna have been developed to determine under water corrosion using a stub resonator at 2 m read range but the complexity of the system made it inefficient for practical use as it required VNA and also the system was not compatible with Gen2 standard [171]. Apart from these, Leon-Salas et al [174] have presented smart RFID based corrosion sensor that can be embedded in concrete. The sensor is a custom designed tag inbuilt with a microcontroller and the limitation of the varying reader position is diminished by modulating measured data with carrier signal. Andringa et al [175] on the other hand, presented a RFID based corrosion sensing system for steel reinforced concrete. It simply uses a loop of steel wire connected to the RFID tag. As corrosion begins to develop on the wire, the resistance of the tag increases and therefore there is a shift in the resonance of the tag which is further detected.

A specific limitation of some of the RFID sensors is the use of sacrificial elements. Similar to thin films used, the sacrificial elements may not actually represent the actual corrosion. The optimal impedance matching, lift-off independency and the vast usability in harsh environment of these tags still remain a challenge [176]. Also the compromise between the sensor sensitivity and the communication distance challenges the antenna design as well [177].

2.4.2 Challenge identification and chapter summary

The main challenges posed by cracks and corrosion under insulation are the inaccessibility and detectability of the defects at different lift-off variations caused due to changes in the insulation or the paint coating layer on the material. Additionally, moisture mingling along with variation of temperature within the structure accelerates the development of corrosion. Lift-off variation affects the detection ability of the defect due to reduced sensitivity. In addition to this, challenges associated with the characterisation of defected material requires an understanding of the physical changes in the material. Hidden nature of CUI may often go unnoticed which ultimately leading to catastrophic failures.

A literature survey carried out in this chapter, mentions the most common types of NDT techniques for corrosion and crack detection. However, most of the methods are restricted in terms of online in-situ monitoring of defects due to thick insulation layer or even the accessibility of the sensing systems. Solution to these problems will require using bulky, expensive equipment with much higher power or removal of the insulation layer which will include operation shutdown or using inspection holes to send signals along the structure.

The passive LF RFID sensing system identified in the literature signifies the potential of cost-effective, battery free wireless sensing for long term monitoring. Passive RFID based sensors have been shown to work effectively in various situations. The sensor's battery free nature,

gives them the potential to be embedded in the structures such as under insulation at harsh environmental conditions for long term condition monitoring. Also, majority of the studies have shown to use either thin films or sacrificial elements attached to the tags or even complex designing of the tag antenna based sensors. For long term monitoring, these sensors may not be suitable solutions as the sensing elements of the tag may degrade faster than the structure itself.

To tackle the problems of thick insulation with regards to lift-off variation and for effective blind crack and corrosion characterisation under harsh environmental conditions, the use of passive LF RFID sensing system is proposed in this study. The developed system aims to address the following challenges:

- Miniaturisation of the RFID reader system and the usage of off-the-shelf components, keeping the sensing system cost effective. To further reduce the cost, the tag should be unmodified. The sensing mechanism will be in terms of the interaction between the reader and the tag antenna.
- Lift-off independent defect detection using smart RFID reader with self-sweep frequency ability for long term monitoring of defect under insulation.
- Corrosion progression measurement on mild steel samples correlated with conductivity and permeability changes using transient feature extraction and further enhanced signal sensitivity using ferrite sheet
- Applicability of smart RFID sensing system with sweep frequency ability for defect detection in high temperature conditions and using advanced feature fusion technique to compensate temperature fluctuation. Also further study of ceramic tag to compensate temperature is shown.

In the following chapter, the theoretical background of passive LF RFID is provided along with design and description of the hardware implementation used in this study and explanation of feature extraction is also provided.

Chapter 3. Systematic Approach for the Development of smart RFID sensing system for defect detection

Following on the challenges discovered in chapter 2, this chapter presents the methodology and theoretical background of passive Low Frequency (LF) RFID based sensing, in conjunction with elucidation of the transponder operation as a defect sensing element and it's applicability in high temperature conditions. The research methodology is outlined in the remainder of the chapter.

The theoretical background of the RFID based sensing system is explained in terms of electromagnetic wave interaction and inductive coupling along with physical mechanism. This chapter mainly focuses on the research methodologies. Behaviour of the RFID system near metal along with system setup considerations are discussed in Section 3.1. The geometric consideration topologies are described in Section 3.2. Section 3.3 looks into the RFID reader construction and the transponder selection along with data acquisition designing. Section 3.4 discusses real life scenario for the application and then finally summarise the work.

3.1 Background of passive LF RFID

3.1.1 Theoretical background of passive LF RFID

RFID is considered as one of the most prevalent technologies today. Several basic components used by RFID satisfy the needs of the implementing organization. RFID has now been around for decades and one of the first utilization was during WWII [178]. Since then RFID has been for various applications such as antitheft system, for tracking luggage in the airports, collection of tolls, etc [179]. RFID has also gained attention in industry and research. One of the primary users of RFID technology are the retail industries. Organizations like Wal-Mart, Tesco have adopted RFID in early 2003. This system has replaced some of the traditional systems including Barcode system, Optical Character recognition (OCR), Biometric Procedure and Smart Cards. A comparison of these different ID systems is shown in the Table 3.1.

Mainly an RFID system is composed of two hardware components i.e. the reader and the tag/ transponder. The reader consists of the RF circuitry such as filters and the envelope detectors as per the requirement for the transmission and receiving of the RF energy. The reader is used to both transmit and receive the signal via coil/antenna. The reader's function is to: (1) to energise the tag by transferring enough power to it; (2) via response signal from the tag, receive the data that is stored in the tag's memory; and (3) write data to the tag's memory.

Table 3.1: Comparison of different ID systems [175]

Parameters	Barcode	OCR	Biometric	Smart Card	RFID
Data capacity	1-100 bytes	1-100 bytes		16-64 Kbytes	16-64 Kbytes
Data density	Very Low	Low	High	Higher	Very High
Reading range	0-50cm	<1cm	0-2m	Contact	0-30cm
Speed of reading	Very Low	Very Low	Very Low	Low	Very Fast
Cost of readers	Very Low	Medium	Very High	Low	Medium ~£1-2
Dirt/Damp	Very High	Very High		Possible	No influence
Covering	Completely fail	Completely fail	Possible		Very Low

Also the tags come in passive, active or semi-active forms. Active or semi-active tags require a battery to provide power, making it expensive and larger in size and thereby also limiting the life-time. On the other hand, passive tags obtain power from near field carrier signal produced from the reader via inductive coupling as shown in the Fig. 3.1. As this thesis is concerned with battery free operation, therefore, here onwards only passive RFID will be reviewed.

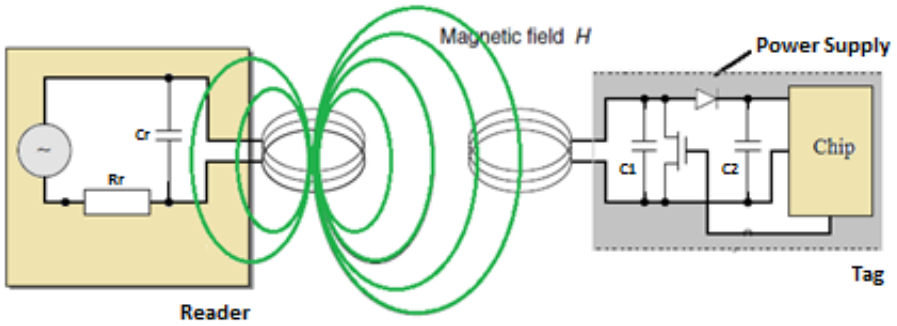

Figure 3.1: Diagram showing inductive coupling between reader and tag coil [180]

Different RFID systems operate at different frequencies which defines various factors such as cost, range and tolerance to different components. The table below shows some of the most common RFID operating frequencies.

Table 3.2: Comparison of different ID systems [172]

Range of frequency	Frequencies	Reading distance	Advantages	Limitations
Low Frequency (LF)	120-140 KHz	10-20 cm	Simple and robust, shapes and sizes available, good penetration, works best around metal and liquid	Limited range, slow data transfer
High Frequency (HF)	13.56 MHz	10-20 cm	Reading range is slightly higher than LF RFID, cheap tags	Performance around metal is poor, through liquid reading is non-viable
Ultra-High Frequency (UHF)	868-928 MHz	3 meters	Good anti-collision, Faster response, longer read range, cheap price, good standards	Vulnerable to interference from liquid and metal
Microwave	2.45 & 5.8 GHz	3 meters	Higher data transfer, Longer transmission range, commonly used in active and semi-active modes	Poor performance around liquid and metal
Ultra-Wide Band (UWB)	3.1-10.6 GHz	10 meters and above	Superior resolution in radar, immune to multipath propagation	Inappropriate for wide area network, UWB devices are all power limited

RFID technology can be divided into two parts in terms of energy and data transmission methods: inductive coupling and electromagnetic wave. For both LF and HF RFID operating below 30MHz, there is generally an inductive coupling between the reader and the tag. The generated magnetic from reader energises the tag via inductive coupling to transmit and receive data from the reader. Due to coupling limitation, the communication range is low.

For UHF RFID which operates at a frequency higher than 30 MHz, the communication via the electromagnetic wave. The principle of far field is via the backscattering phenomena. This

allows much greater communication distance to be obtained in free space. However, due to metal or any conductive object proximity, RFID system operating at UHF region or above suffer serious degradation in performance [181-183]. Though many researches are being carried out for improving the performance of UHF RFID near conductive materials [184, 185], but the performance of HF and LF RFID are more robust [186].

As mentioned in earlier in chapter 2, one of the most important factor in deciding which frequency band is most appropriate for sensing causes is the penetration depth/skin depth as shown in Equation 2.1. Skin depth is known as the depth underneath the conducting surface where the current density falls to about 37%. If this equation is applied to HF, then it can be observed that the skin depth is approximately reduced by a factor of 10. This means, stronger eddy current field will be generated by the surface due to lower skin depths and this will defy the primary field from the reader causing less power to be transmitted to the tag. This will eventually reduce the sensitivity of the tag affecting the quality factor immensely. Taking into consideration of these factors, LF RFID had been chosen to be the most fitting platform to address the challenges mentioned in chapter 2.

3.1.2 Fundamental operational principle of LF RFID

Due to close juxtaposition of the reader and the tag, the electromagnetic field is seen as an alternating magnetic field. This field actuates a voltage on the tag coil. This voltage is then utilized to power up the microchip present within the tag. When enough energy has been obtained by the tag to give power to the chip, it will toggle a load resistance which will cause the binary code in the memory of the chip to turn on and off. This change in resistance will change the voltage of the antenna coil. This will result in amplitude modulation of the coil as shown in Figure 3.2. Though technically the tag does not transmit anything, the function of the passive tag is just to change the load presented to the reader using reflective load modulation.

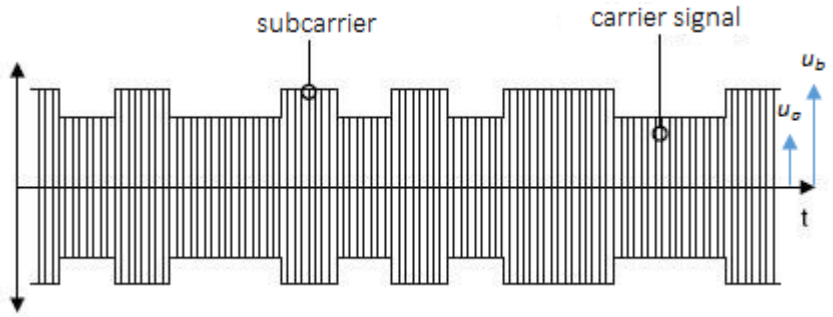

Figure 3.2: Amplitude modulation of RFID

The modulation index of Figure 3.2 can be defined as:

$$m_i = \frac{u_b - u_a}{u_b + u_a} \tag{3.1}$$

Where u_a and u_b are the state of high impedance and the state of low impedance of the FET respectively.

Since this thesis concerns about inductively coupled LF RFID system, it is standing to the reason that the theory of magnetic coupling is essential for explaining the principle. Inductive coupling is based on the common magnetic flux Φ. Magnetic field coupling can be divided in to two types i.e. short-range electromagnetic induction and then mid-range strongly coupled magnetic resonance (SCMR). Faraday's law of induction is applied for the voltage induced in the tag. Faraday's law of induction states any change in the magnetic field will cause a change in the electric field strength which can be given in the simplest form as:

$$u_1 = -N \frac{d\phi(t)}{dt} \tag{3.2}$$

Where u_1 is the induced voltage in the transponder coil and N is the number of windings.

Using the equivalent circuit shown in Figure 3.3 below, the voltage induced across the tag can be determined.

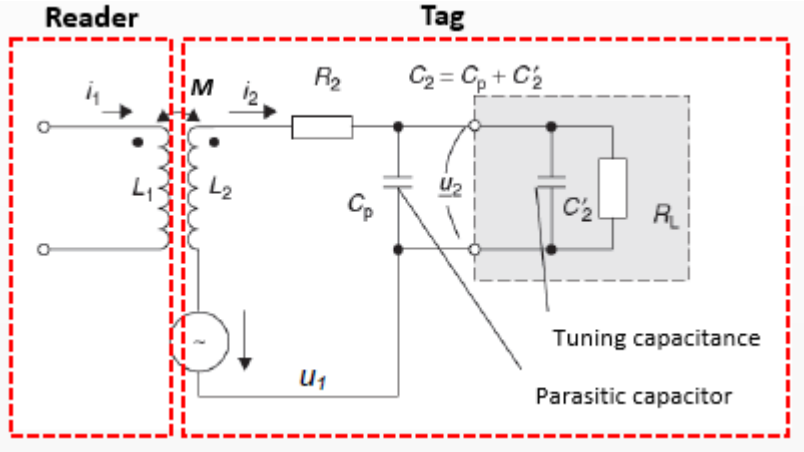

Figure 3.3: Equivalent circuit of RFID reader and transponder coil [187]

A time alternative current i_1 with an inductance L_1 in the reader coil, produces a time alternative magnetic flux $d\Phi(i1)/dt$ due to mutual inductance M. This actuates a voltage in the tag coil which has an inductance L_2 and the induced current is denoted by i_2. A voltage drop across the tags coil resistance R_2 is created due to the current flow. The current produced from the load resistance R_L is calculated using u_1/R_L. The current through L_2 produces additional magnetic flux that resists the magnetic flux of the reader coil $\Phi i\ (i_1)$.

Using a capacitor C_2, the equivalent circuit's efficiency can be greatly improved. This can form a resonant circuit with a resonant frequency corresponding to the carrier frequency. Using the Thomson equation, the resonant frequency can be calculated and shown as:

$$f = \frac{1}{2\pi\sqrt{L_2 C_2}} \tag{3.3}$$

C_2 is the amalgamation of tuning capacitor C'_2 and parasitic capacitance C_p. Thus using the following equation voltage u_2 across R_L can be calculated [9] :

$$u_2 = \frac{\omega k \sqrt{L_1 L_2}\, i_1}{\sqrt{\left(\frac{\omega L_2}{R_L} + \omega R_2 C_2\right)^2 + \left(1 - \omega^2 L_2 C_2 + \frac{R_2}{R_L}\right)^2}} \tag{3.4}$$

3.1.3 RFID based corrosion and crack sensing

For understanding the operation of the RFID system as an eddy current based corrosion sensor, interaction between tag and metallic sample is analysed. There are two significant influences of placing metal near the tag and the reader. First is the distortion of the primary reader near the surface of the metal. According to Maxwell's equations for Gauss's and Faraday's law of induction, only the electric fields and the tangential components are permitted on the surface of an ideal conductor. A metal not being a perfect conductor results in distortion of the magnetic field near the surface. Second effect is the detuning of the tag which is caused by the eddy current field being perpendicular to the metal surface. The eddy current field thus opposes the primary field.

RFID tags that are available commercially, are designed for non-metallic environments. For the applications in NDT&E i.e. characterisation of corrosion on metallic samples, the impedance of the RFID tag needs to be considered. The model for the RFID reader, tag and the metallic sample with corrosion is depicted in Figure 3.4. The resonant circuit is formed by connecting the capacitor across the reader and the tag which results in lower efficiency. The sensitivity, efficiency and the gap between the reader and the tag coil are dependent on the resonant frequency and the operational frequency.

There is a shift in the resonant frequency of the tag coil when it comes in close proximity to the metallic surface [188, 189]. As an alternating current passes through the reader coil, primary magnetic field is generated.

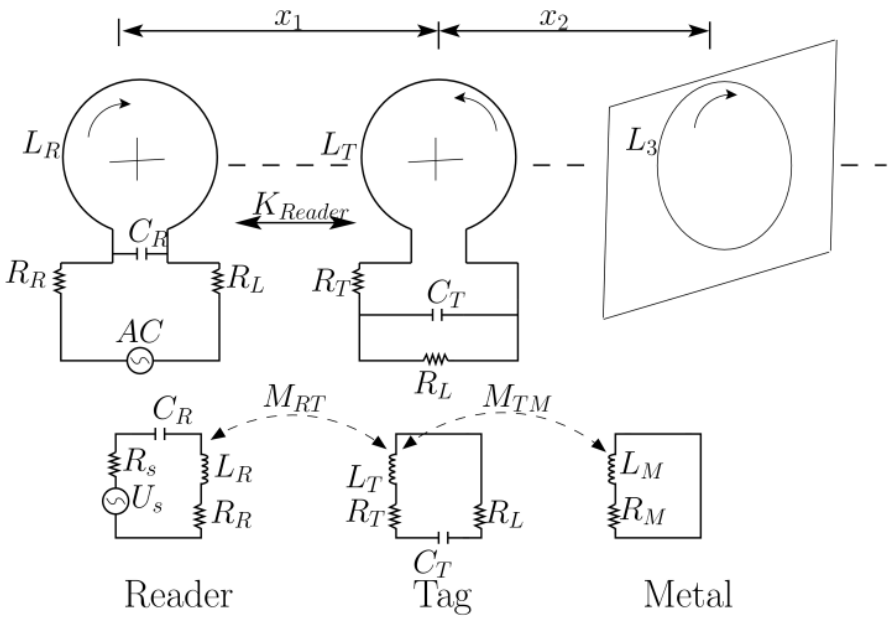

Figure 3.4: Inductive coupling principle between reader, tag and metal

In close proximity to the metal, eddy current is generated on the surface creating a secondary magnetic field opposite to that of the primary magnetic field. Furthermore, with an increase in the corrosion exposure, the thickness of the corrosion layer will also increase. This will cause a variation in the capacitance and the resistance of the RFID tag placed on the corroded sample. Thus causing an impedance mismatch [186] and eventually a change in mutual inductance M_{RT} which is shown as:

$$M_{RT} = \frac{\mu_0 \pi N_1 N_2 \left(r_1 + r_2\right)^2}{2\sqrt{\left(r_1^2 + x_1^2\right)^3}} \tag{3.5}$$

Where:

μ_0 = permeability of free space

$N_1 and\ N_2$= number of turns in the reader and tag coils respectively

r_1 *and* r_2 = radius of the reader and the tag coils respectively

x_1 = distance between the two coils

It can be seen that the reader and tag coils are represented by the inductors L_R and L_T which are coupled with mutual inductance M_{RT} and a coupling coefficient of K_{Reader} which is given by:

$$K_{\mathrm{Re}ader} = \frac{M_{RT}}{\sqrt{L_R.L_T}} \tag{3.6}$$

The quality factor of the system can be determined using the equation:

$$Q = \frac{2\pi f_r L_T}{R_T} \tag{3.7}$$

where, R_T and L_T are the tag coil's resistance and self-inductance; R_M and L_M are the equivalent resistance and self-inductance of the metal shown in Figure 3.4. R_M inversely depends on the eddy current path and conductivity of the metal, L_M depends on the eddy current path and permeability of the metal. Metal near the tag can be modelled as an additional parallel inductance L_M. RFID tags that are present commercially work near the resonant frequency. When the tag comes close to the metallic sample, the eddy current generated on the sample will not only shift the resonant frequency of the tag, but will also reduce the sensitivity of the reader coil.

The expressions provided Cheng [190] and Dodd and Deeds [191] for the change in impedance are modified for the case of planar spiral coil in this section because the transponder that is used in the extraction of crack information is a spiral coil. Firstly, a defect free analytical model is presented which is then modified based on the thin-skin theory of Harfield and Bowler [192] for the change in impedance caused due to transverse crack and applied to the case of planar spiral coil.

In the first case, shown in Figure 3.5, the coil is assumed to be spiral and air-cored with N turns, inner radius a_1, outer radius a_2, thickness Δh, relative permeability μ_r and height of the bottom of the coil windings above the surface of the half-space hl (referred to as the coil "lift-off"). The change in coil impedance ΔZ due to the induction of LF RFID in a defect-free conductor is the difference between the coil impedance measured when the coil is located above a defect-free region of the conductor and the impedance measured when the coil is in isolation and is shown with the following equation [193]:

$$\Delta Z = \frac{i\omega\mu_0\pi N^2}{\left(a_2 - a_1\right)^2}\int_0^\infty \frac{e^{-2\alpha h_1}}{\alpha^4} I^2\left(\alpha a_1, \alpha a_2\right)\frac{\mu_r\alpha - \alpha_1}{\mu_r\alpha + \alpha_1}d\alpha \tag{3.8}$$

where $\alpha_1 = \sqrt{\alpha^2 + 2i/\delta^2}$, δ is the electromagnetic skin depth which is given by δ= $\sqrt{2\rho l(\omega\mu_0\mu_r)}$ and *I* is the radial integral.

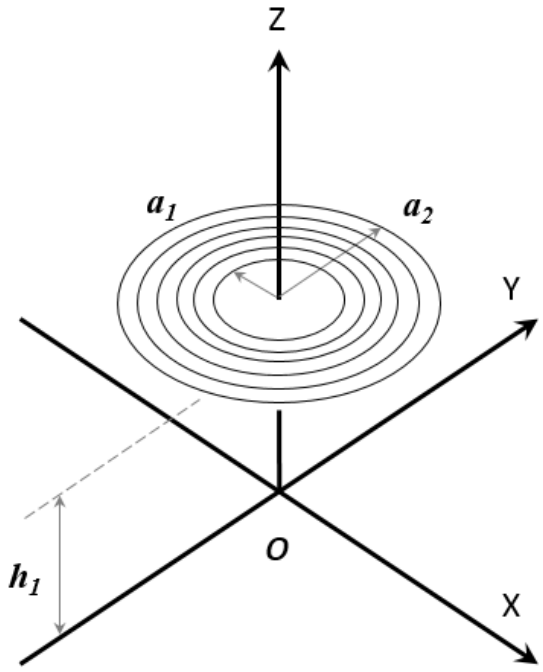

(a)

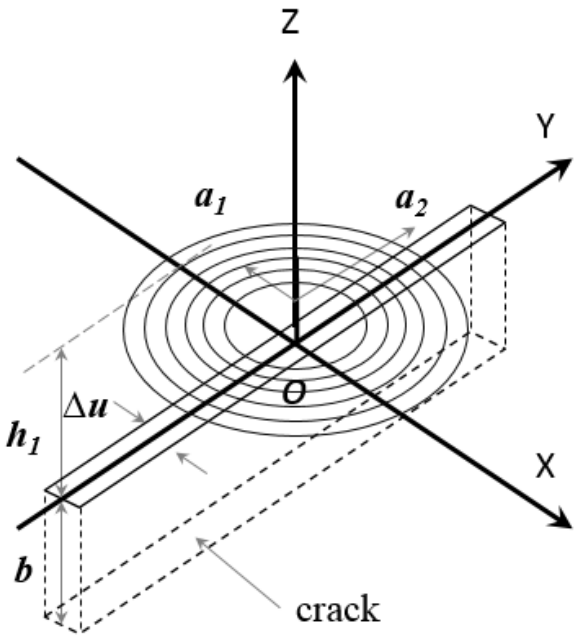

(b)

Figure 3.5: Tag and specimen geometry: (a) spiral coil, (b) spiral coil design over a long crack

Similarly, the change in coil impedance ΔZ due to the induction of LF RFID in a crack area is the difference between the coil impedance measured when the coil is located above a defect-free region of the conductor and the impedance measured when the coil is centred above a crack.

The basic principle of LF RFID system is to discern variation of the tag on the crack with regards to the capacitance, resistance, inductance physical parameters by monitoring resonance frequency, input impedance, or Q-factor [194]. The differentiation method of these parameters can be represented as:

$$\Delta f_s = -\frac{1}{4\pi\left(L_R C_R\right)^{3/2}}\left[C_R,\ L_R,\ 0\right]\times\left[\Delta L_R,\ \Delta C_R,\ \Delta R_R\right]^{\mathrm{T}} \tag{3.9}$$

$$\Delta Q = \left[\frac{1}{2\left(R_s C_s\right)}\sqrt{C_s/L_s},\ -\frac{L_s}{2\left(R_s C_s^2\right)}\sqrt{C_s/L_s},\ -\frac{1}{2R_s^2}\sqrt{C_s/L_s}\right] \times\left[\Delta L_s,\ \Delta C_s,\ \Delta R_s\right]^{\mathrm{T}} \tag{3.10}$$

$$\Delta Z_x = \left[2\pi L_R k^2 Q,\ 2\pi L_R f_s k^2,\ 4\pi L_R f_s k Q\right]\times\left[\Delta f_s,\ \Delta Q,\ \Delta k\right]^{\mathrm{T}} \tag{3.11}$$

Δf_s is the resonant frequency which shwos the point where a variation appears in the frequency response of the impedance. ΔQ is the quality factor which is generally explicated as a sign of the sharpness of the resonance peak. The higher the quality factor of the reader and the transponder coils, the better the efficiency of the wireless power transfer (WPT) [195].

In the following section, the effect of changes in the reader coil position with respect to the tag will be discussed. This is essential because any minor fluctuation occurring between the tag and the reader coil will cause amplitude variation which will give inaccurate results for defect detection.

3.2 Geometric configurations topologies

For the designing of magnetically coupled devices, coil orientation is one of the key parameters. Particularly for RFID, the reader will transmit and receive the maximum power from the tag coil when they are coaxially oriented this is because the measured output signal amplitude is the maximum in this position. There are mainly two misalignments which mainly arise in

practical conditions and these are identified in this section and in order to overcome these misalignments, the designing of the coil rig is illustrated. First misalignment is the lateral misalignment case where the reader and the tag coils are situated in parallel planes. On the other hand, the second misalignment is the angular misalignment where the reader is tilted where the axis of one coil passes through the centre of the other coil. This is depicted in Figure 3.6.

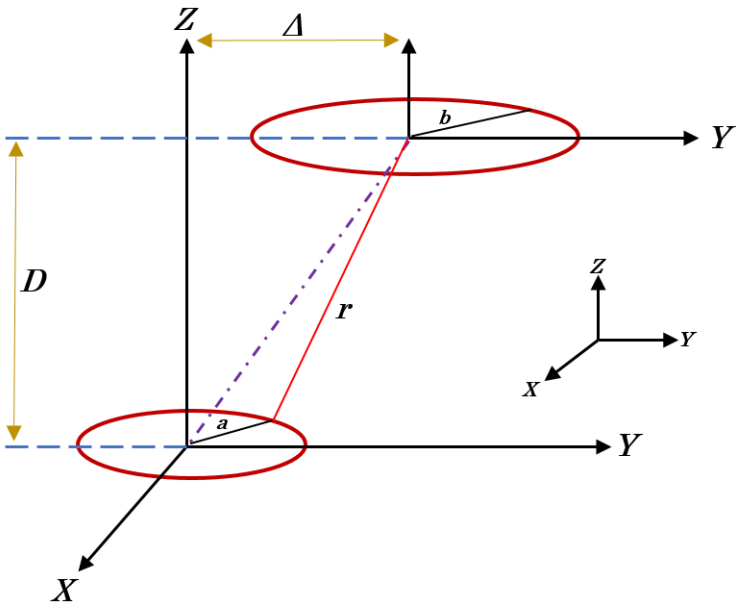

(a)

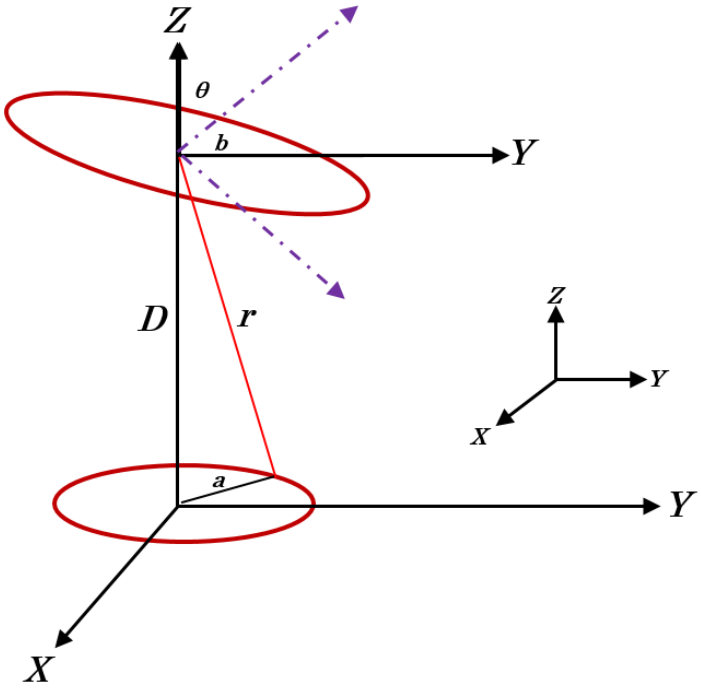

(b)

Figure 3.6: Misalignments (a) Lateral misalignment configuration, (b) Angular misalignment configuration

In the illustration, *D* is the stand-off distance between the tag and the reader coil. Δ is the distance from the centre of the reader and the tag and *a* and *b* are the coil radius. The magnetic field of the reader coil decays rapidly with the distance *r* when the value of *r* is larger than the radius. This is one of the major factors which limits are range in near field inductively coupled RFID. Since, the availability of received power is also determined by the angular misalignment, so the optimum value of the angle is considered to be 90°**.** The positioning is shown in Figure 3.7:

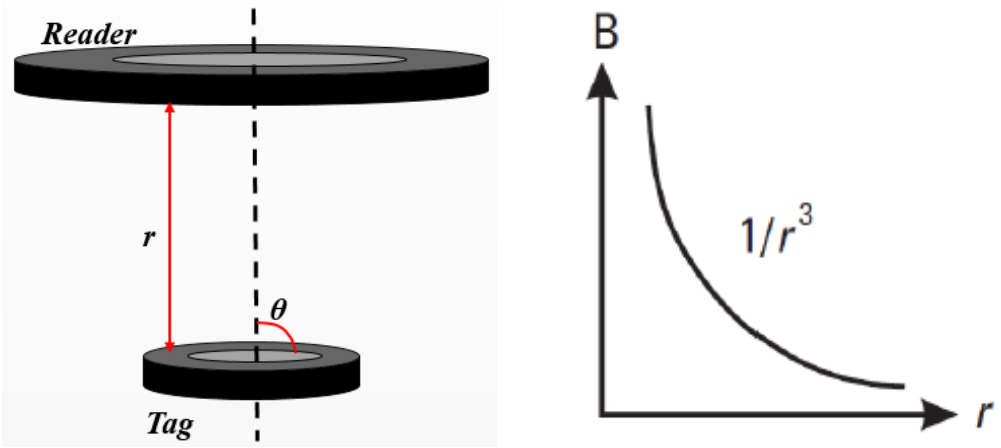

Figure 3.7: Drop in magnetic field generated by the reader coil due to alignment

Any changes between the *r* and the *θ*, can cause serious fluctuation in the power availability to the tag which can lead to becoming an issue for defect detection and monitoring. This is because, any changes in the output signal amplitude from the RFID tag due to the presence of corrosion or crack can be masked by the reader and tag misalignment's output signal amplitude. Therefore, the coaxial orientation, where the magnetic field associated with the reader are perpendicular to the tag coil, resulting in best coupling. The fixed rig designed in SOLIDWORKS has been shown in Figure 3.8 which is used to hold the reader in a fixed position for better robustness improvement of the result.

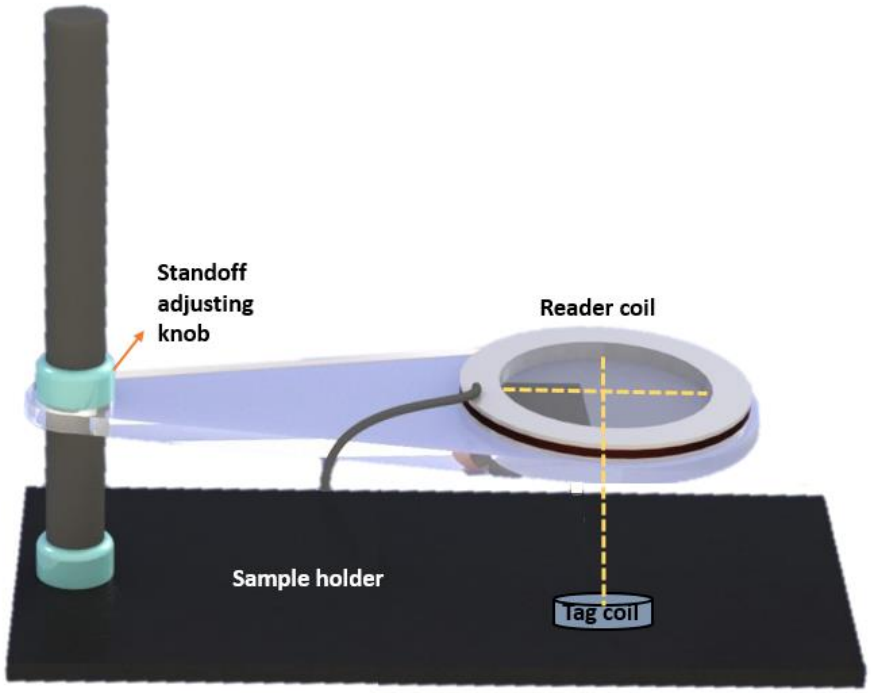

Figure 3.8: LF RFID rig for rigid experimental case

Using the adjustable knob, the lift-off between the tag and the reader coil can be varied. The base is where the samples are placed and the tag is then adjusted accordingly coaxially to the reader.

3.3 RFID System

3.3.1 RFID reader construction

In this research, one of the main focus was given in the reader construction. This is because commercially available LF RFID development kits are not designed to work in metallic environments, therefore the reader unit is custom designed in order to allow easy access to the analogue signal of the tag coil and further intensification is carried out allowing reading of the tag on metal at a larger lift-off distance. The block diagram of the reader unit is provided below in Figure 3.9 following to it is the circuit schematic.

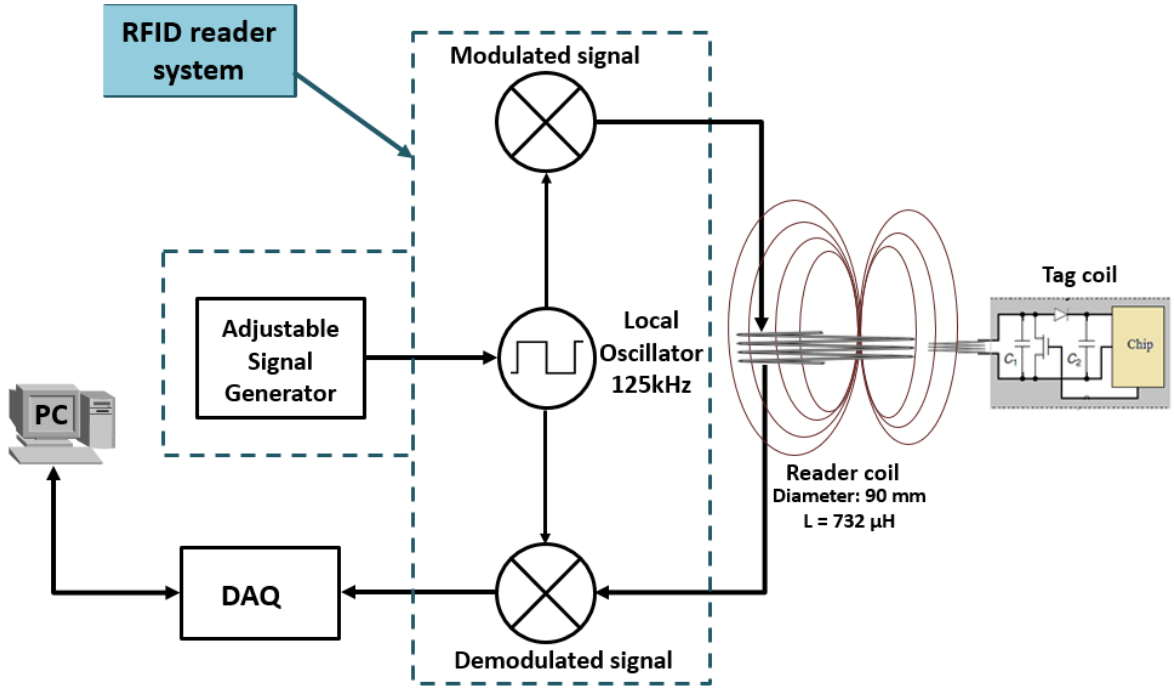

Figure 3.9: Custom RFID reader unit block diagram and the reader properties

The RFID circuitry shown in Figure 3.10 is contains of coil L_1 and C_{res} which are tuned together to resonate at 125 kHz. This resonance is achieved using the Thompson equation shown in (3.3) by adjusting the coil turns. However, in practice it is unlikely to achieve the exact same resonance and hence it is wiser to know the resonance frequency of the circuitry since they are affected by several factors. At the power amplification stage, there are two IRF630 MOSFETS which are driven by 125 kHz square wave at the gate.

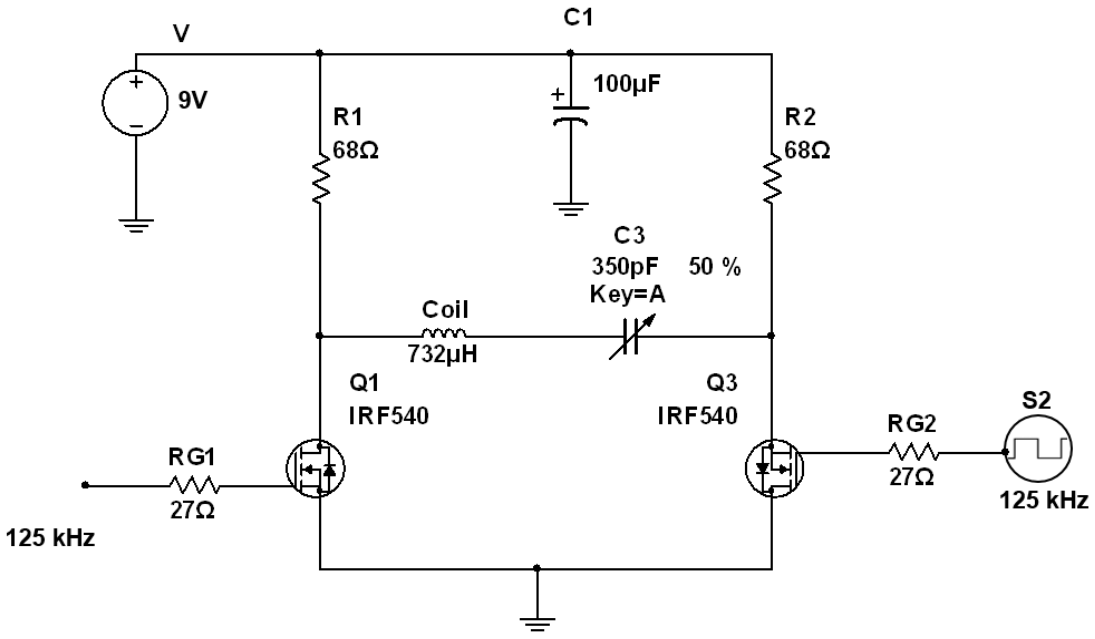

Figure 3.10: Reader amplification circuitry for the RFID system

When one of the MOSFET is turned on, the other is turned off. In this way, the capacitor C_{res} charges and discharges and thereby producing the 125 kHz RF signal. Since the operational frequency is low, there will be a large amount of current drawn at the charging of the capacitor through the coil which is pulled alternatively high by R_1 or R_2 or pulled low by any of the MOSFETS. The capacitor C_1 controls the 9V voltage at a suitable constant value as the instability of the 9V will affect he circuitry. Lower RG_1 and RG_2 (27Ω) are chosen for the faster operation of the transistors at 125 kHz. The 68Ω resistors are a simplification of the bridge circuit which in order to form a full bridge circuit, would be replaced by high side MOSFETs. Ideally all the components require to be of the same value but due to tolerances there will always be a slight difference in them. These are few of the factors affecting the resonant frequency of the circuit.

To carry out the investigation of the RFID sensor for defect monitoring at high temperature conditions, it is essential to know the behaviour of the resonant frequency shift aroused by the changing factors. Therefore, working at only 125 kHz will not be beneficial in this case and hence the sources of the circuitry are connected to the signal generator so that the operational frequency can be changed from the range of 110 kHz to 140 kHz to attain the resonance behaviour based on the material delineation or environmental changes. This is shown in Figure 3.11.

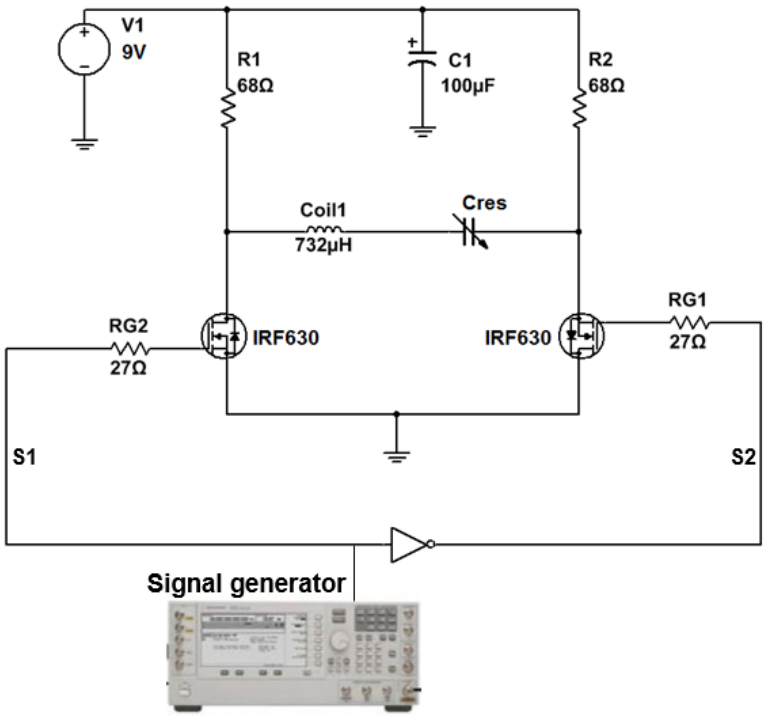

Figure 3.11: Modified reader amplification circuitry for the RFID system for sweep frequency

The frequency response curve for a typical resonant tank circuit is shown in Figure 3.12.

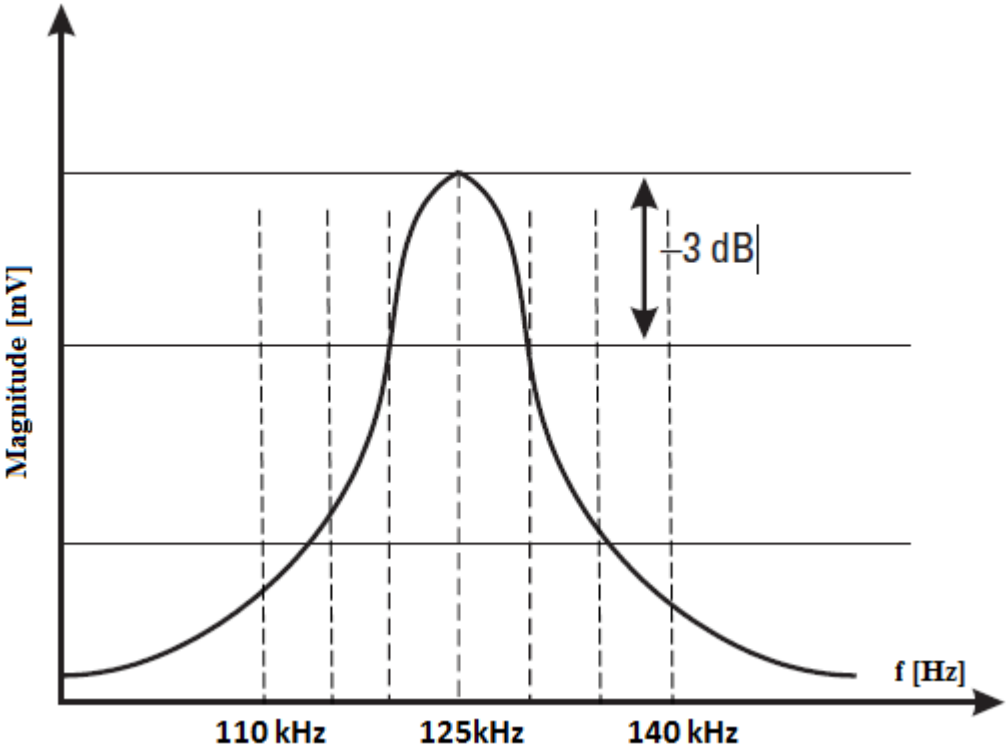

Figure 3.12: Frequency response curve for resonance tank circuit

The design prototype is shown in Figure 3.13. The prototype is made keeping commercial feasibility in mind, hence, the prototype is designed in a box of $15 \times 10 \times 5$ cm in size. This miniaturized design can be well fitted in the industry. The design shows the amplification circuitry in red box, the sweep frequency circuitry in blue and the demodulation circuitry in yellow as per the schematics shown earlier in this chapter.

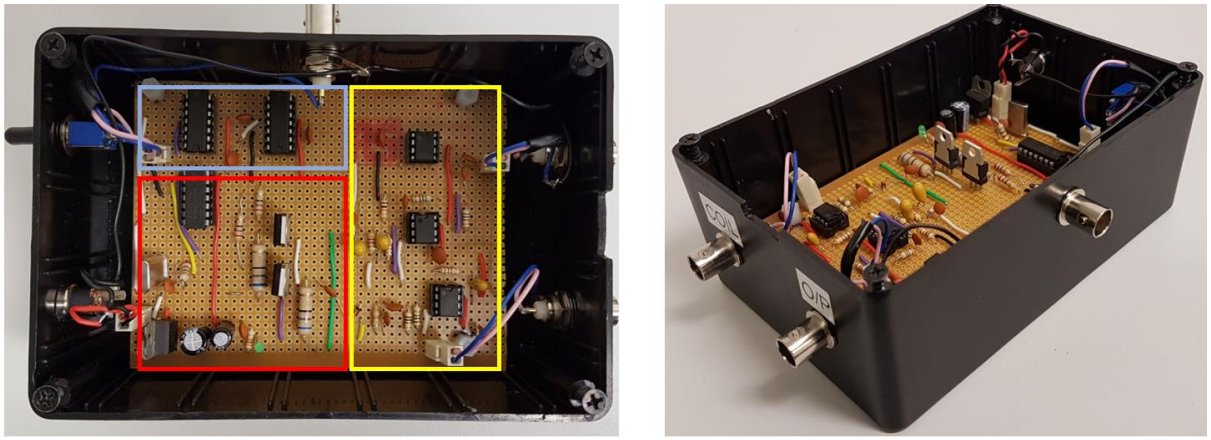

Figure 3.13: Top view of reader unit prototype

3.3.2 RFID transponder selection

For this research commercially available tags which are available for approximately less than pound has been used as sensors. The two types of tags that have been used are the ATA5577

disk tags from Atmel Corporation [196] and HID LF Volcano tags from HID Global [197]. There are numerous types of tags available for LF RFID system and they come in different shapes and sizes [198] depending on the application it will be used for. For the intended application of deploying tags under insulation and for research validity purposes, ATA5577 disk tags and HID Volcano tags have been chosen as the corroded region on the sample are of similar size to these tags.

Figure 3.14: Commercially available off-the-shelf tags used in this study and their dimension

The internal block diagram of the tag is shown in Figure 3.15. The tag coil is attached to the analogue front end which converts ac to dc to power the microchip and all the chip based tags have the same layout. One of the reasons for not using the ATA5577 tag and moving onto HID Volcano tags for temperature based research is because of its encapsulation which is made from the field demonstrated, temperature stable polyphthalamide (PPA). This thermoplastic shell holds its shape despite of high temperature fluctuation, protecting the electronics within for reliable performance.

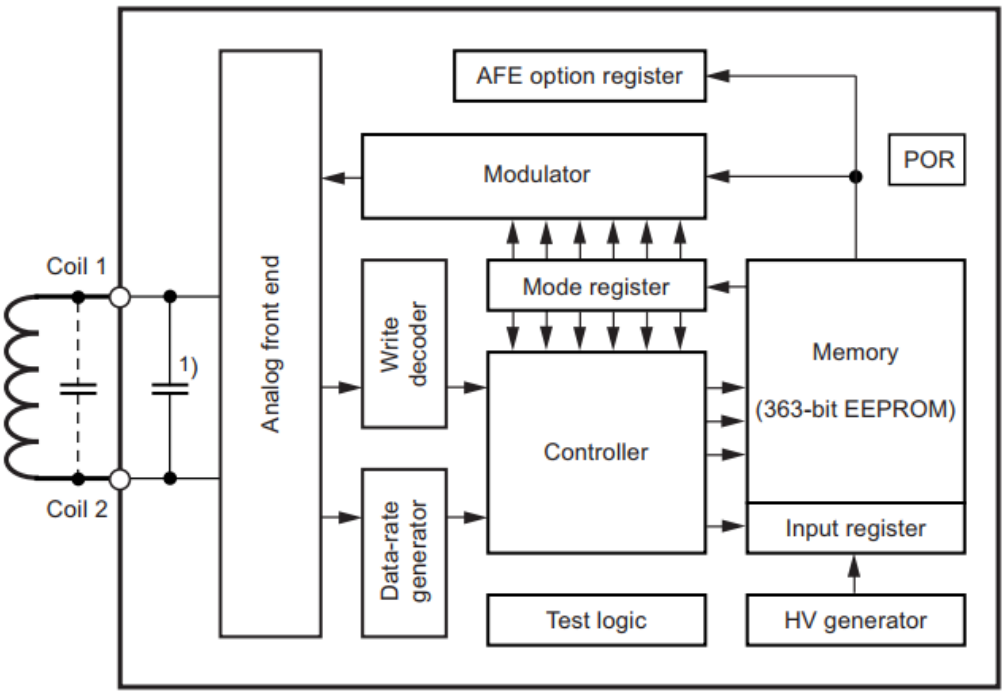

Figure 3.15: Internal functional diagram of ATA5577 tag

3.3.3 RFID transponder modulation code

The modulation code which is stored in the memory of the tag is what gives it its unique ID. Most of the commercial tags including the ones used in this research allow the code to be modified by the user. One of the advantages of modifying the ID to allow us to create our own set of ID for our own benefit of extraction. For example, in this research, the ID used was a uniform stream of 1's by filling the tag's data blocks with 'FFFFFFFF' which makes it easier to process and extract features as it allows to average over number of cycles.

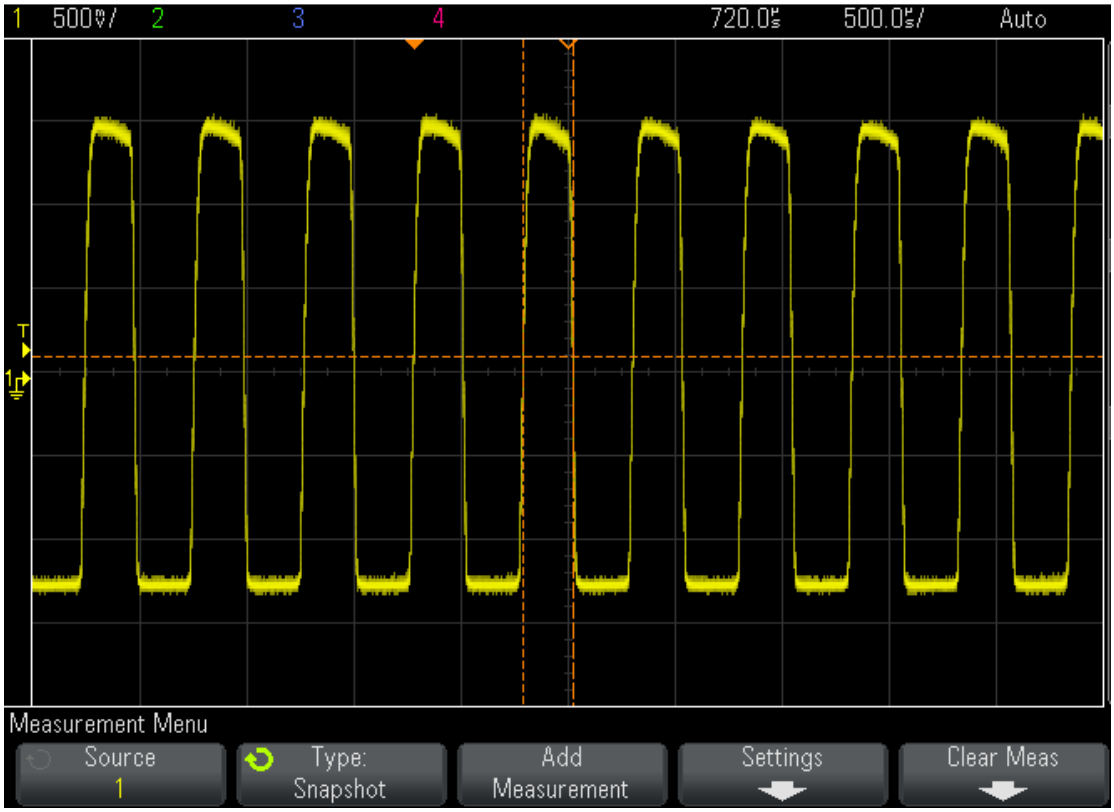

Figure 3.16: Section of the tag's ID from oscilloscope showing the uniform code

The tag have been programmed TS-RW38Plus universal reader and writer module from GiS-Net [199] and are specially used for LF RFID tags. The kit provides PC interface for the easier programming and it also allows the data rate or the tag's frequency to be adjusted. The KIT is shown in Figure 3.17. The tags used in this research contain 7 32bit user rewritable memory blocks.

Figure 3.17: TS-RW38plus RFID reader kit from GiS-Net for programming tags

3.3.4 Data Acquisition

The signal that is taken using the RFID reader coil is passed through the demodulation circuity which is shown in Figure 3.18. This demodulation circuitry removes any unwanted noise from the signal along with the 125 kHz carrier signal. The circuitry involves an envelope detector which is attached to an om-amp buffer. The signal is passed into the op-amp bandpass filter to cut-off the lower and the higher end frequency bands i.e. 160 Hz and 16 kHz. The gain used at this stage is 10. The ending phase of the demodulation circuitry is a non-inverting buffer which is then connected to the data acquisition card. The power supply provided to the circuitry is 9V which is then converted to 5V using voltage regulator in order to avoid any excess amount of voltage which would be detrimental. Also, in order to further minimise noise, the supply of the op-amp is decoupled to the earth.

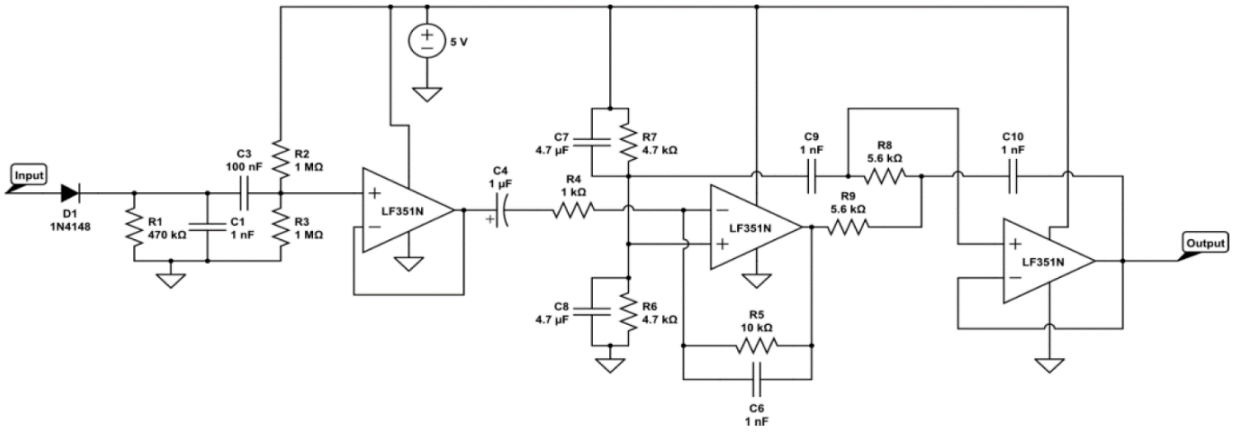

Figure 3.18: Demodulation circuitry of the reader system

The output of the demodulation circuitry is sampled using the 14-bit Adlink 2010 data acquisition card. This card has the capability of obtaining the data at a maximum rate of 2MS/s.

The data acquisition is carried out in the computer using a LabVIEW program which gives the flexibility of setting the sample rate and the number of samples as per the requirement.

3.4 RFID sensing scenario

It is envisaged that the endmost application for the RFID system that is considered and carried out in this thesis will be used for the monitoring of defects i.e. corrosion or crack growth in steel pipelines under thick insulation working at high temperature environments. Tags placed on various positions on an insulated pipeline will be catechized periodically to monitor for crack or corrosion development. Figure 3.19 depicts the general idea of the instalment.

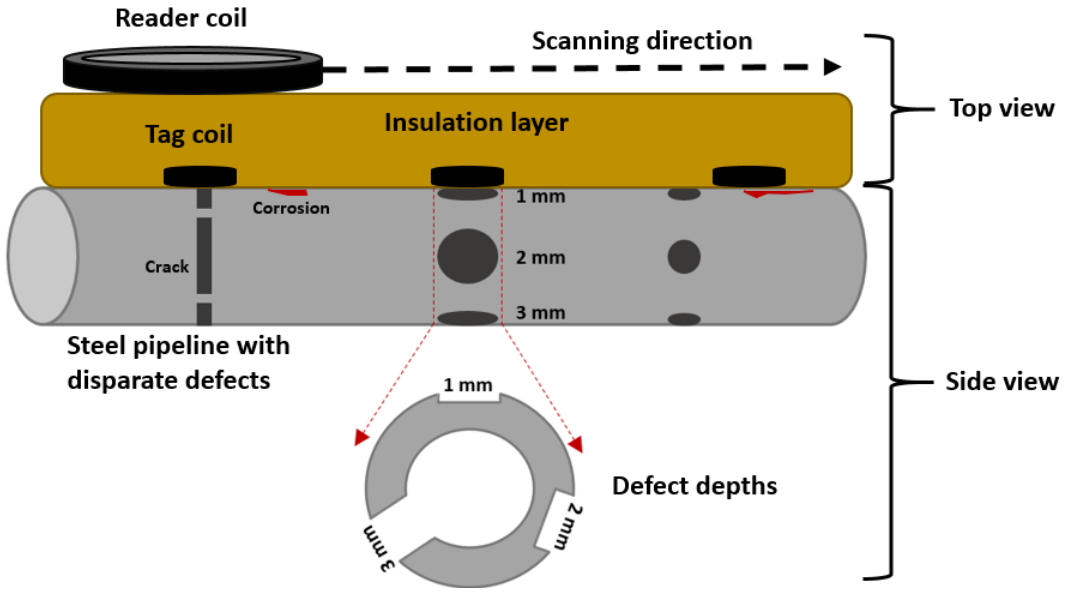

Figure 3.19: Envisioned scenario of RFID tag embedded under insulation for varying lift-off scenario for defect monitoring in steel pipelines at high temperature environments

The passive nature of the RFID transponders allow them to be deployed under insulation for long period of time without having to worry about the replacement of the tags due to battery depletion.

3.5 Research Methodology

3.5.1 Integration of simulation, experimental with the help of signal processing

The research carried out in this thesis involves the experimental investigations of LF RFID sensing system for corrosion and crack monitoring under paint coatings masked by insulation layer. One of the major concerns of practicability of LF RFID sensing system is based on the usage of commercially available tags which are extremely cheap but are not specifically used for sensing metallic defects. Therefore, major attention was given to the development of RFID reader to allow the commercial tags to be read on steel samples at higher standoff distances for

accurate defect monitoring. Signal processing is carried out in order to identify and extract meaningful features out of it.

Along with careful control of certain parameters taken into consideration, such as coil alignment, lift-off variation, the measured features are agreed upon with known qualitative properties of the defected samples to signify the detection capabilities. For practicability of the RFID system in harsh environmental condition, such as high temperatures, the RFID reader has been reconstructed and a self-sweeping-frequency design has been implemented. Multiple parameter estimation such as resonance behaviour of the tag's responses in terms of temperature variation has been explored and demonstrated. All the corrosion sample used in this research have been naturally corroded by the exposure to the atmosphere for different time periods. A summary of these are shown in the subsequent sub-sections and these are detailed in the chapters following. The proposed method flow diagram is shown in Figure 3.20.

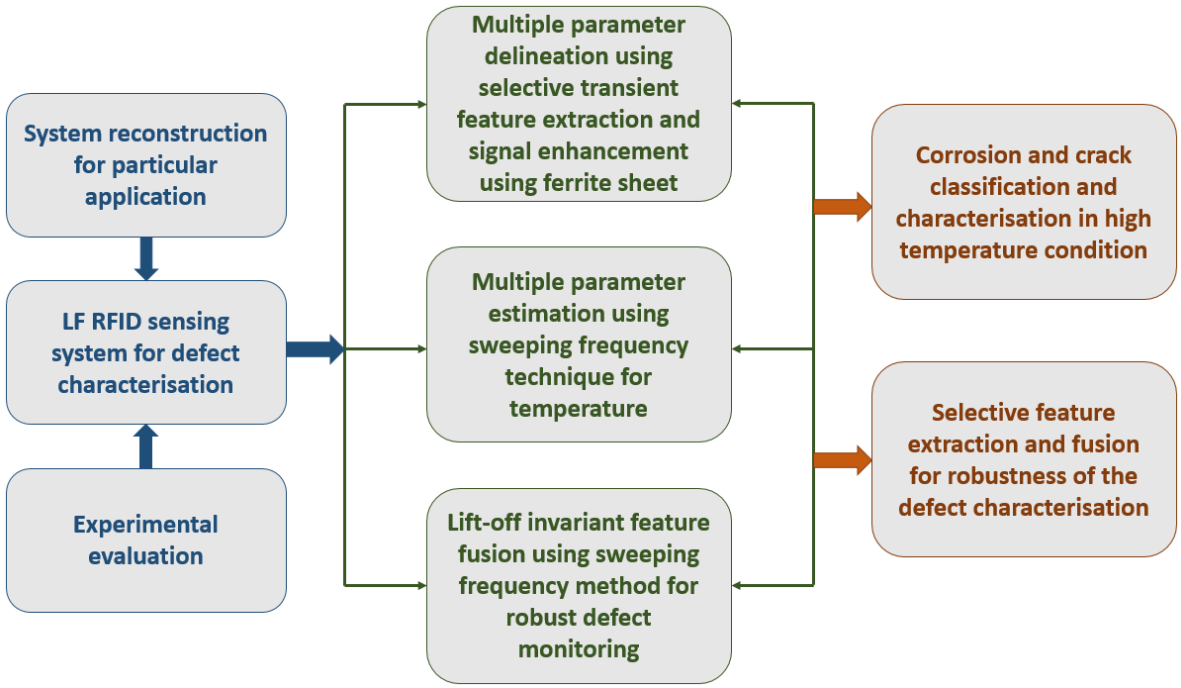

Figure 3.20: Research diagram for RFID sensing system

3.5.1 Study 1: Transient feature based corrosion progression characterisation

A set of paint coated and uncoated steel samples are used which has corrosion patches on them. The samples vary in terms of duration of time they have been exposed to the atmosphere for different level of corrosion to build up. The test is carried out keeping all the parameters unchanged such as reader and tag coil position and environmental conditions in order to obtain a monotonic change with corrosion progression i.e. increasing exposure time. Different features have been extracted and after quantitative analysis best feature has been selected i.e. transient

feature which contains multiple frequency responses of a signal for robust corrosion characterisation. The signal features are correlated with the change in the sample properties.

3.5.2 Study 2: Signal sensitivity and robustness enhancement using ferrite substrate

For enhanced signal sensitivity, FEA analysis has been carried out in COMSOL to demonstrate the capability of ferrite sheet attachment on the RFID tag. Further experimental studies have been carried out on the same set of corrosion progression samples using the best selected feature i.e. transient feature. The variables in this experiment are the presence (or absence) of ferrite sheet attached to the tag for both uncoated and coated samples for corrosion characterisation. The improved performance is demonstrated and tabulated to differentiate with the transient response.

3.5.3 Study 3: Temperature independent disparate crack characterisation using swept frequency and feature fusion

The RFID reader system was reconstructed to apply sweeping frequency capability rather than a fixed operational frequency (125 kHz) in order to understand the multi variate delineation in terms of sample under inspection. The problem of the measured signal dependence on the resonant frequency is tackled in two complementary steps. First, the temperature had been controlled using a hotplate and incremented gradually keeping all the other parameters constant. This allowed to understand the behaviour of the temperature on the RFID tag which has a semiconductor in and as it is known that the resistance of the semiconductor is highly influenced by the change in temperature. Second, the swept frequency study allowed the understanding of resonant frequency shift with regards to crack depth variation along with temperature increments.

Based on the temperature sensitivity of the tag placed on the sample under inspection, best frequency is selected at which the influence of temperature is the lowest. However, for further temperature suppression, new feature have been applied which eliminated any temperature variation and characterises the crack depth progression.

3.5.4 Study 4: Inhomogeneity study using corrosion progression samples and usage of ceramic filled substrate for temperature compensation

This study is an extension to the previous study where instead of crack samples, much more complex multi layered corrosion progression samples are used at different temperature variations. The study is divided into two sections, the first is the inhomogeneity study where

multiple delineation aroused from the sample variation is considered and second study is the effectiveness of ceramic filled substrate attached to the RFID tag for temperature fluctuation.

In realistic environmental conditions, temperature will highly influence corrosion progression thereby giving rise to inhomogeneity. The inhomogeneity will arise from sample variation and also any variation in the distance between the RFID tag and the sample (corrosion thickness) or temperature variation, will change the impedance, inductance and quality factor of the system. The sensing coil will be highly influenced by the conductivity and the permeability changes due to the changes in the sample. These multiple delineation are compensated using feature fusion. Further, the experimental setup is revamped and the robustness of the temperature fluctuation suppression is shown using the ceramic filled substrate.

3.5.5 Study 5: Lift-off invariant feature extraction and fusion for robust crack monitoring on steel pipeline

In this final experimental study, to imitate the real world application and for potential usability, steel pipeline with different sized cracks have been used. Firstly, the common challenge in RFID sensing system i.e. the lift-off variation is suppressed using the normalized feature fusion. This same feature extraction is then applied to the cyclically heated pipe with different cracks and similarly temperature variation is also subdued. Measurements are taken several times for improved accuracy of the results.

3.6 Chapter summary

This chapter looked in to the introduction and the theoretical background of passive LF RFID based corrosion and crack sensing. The reasons for the selection of LF RFID for this particular research is demonstrated in terms of industrial applicability. Geometric configuration topologies and the effect of metal on the commercially available tags are discussed. The reader unit construction and the effective transponder used in this thesis have been thoroughly explained and identified.

The following chapters of the thesis will demonstrate the experimental studies carried out and the effective resolution developed to vanquish the challenges identified. Critical analysis and the discussion of the results are provided.

Chapter 4. Transient Feature Extraction and Selection for Corrosion Characterisation using LF RFID Sensors

In the previous chapter the latent theory behind RFID as a defect monitoring sensor was outlined. This section will look into the experimental studies of the corrosion detection capabilities of RFID system. Firstly, the samples used in this experimental study have been outlined along with the signal processing and feature extraction methods. In order to determine the conductivity and permeability changes, the feature extraction methods and the selection of the features for both the coated and the uncoated samples are discussed further. All the features are extracted, compared and validated. Signal sensitivity enhancement using ferrite sheet are further discussed.

The first study results exhibits the ability of RFID system to not only distinguish between corroded and non-corroded region on steel but four different qualitative surface conditions which are of significant importance to the coating industry. Second study then focused more into the specific samples from the industry which were naturally corroded steel plates. In this investigation, the use of RFID system to differentiate between the corrosion levels which are defined by the different exposure times each samples were placed in the atmosphere, has been demonstrated. Then, several time domain features have been investigated and compared followed by the selection of the transient features which outperformed in comparison to the other features. Lastly, to improve the signal sensitivity in terms of quality factor and robustness, ferrite sheet has been used with the tag and the results are further explained.

4.1 Integration of RFID principle with WPT methods

In SCMR system, the tag and the reader are inductively coupled to the resonator coil resulting in higher Q-factor thus having higher wireless power transfer efficiency. The reader is also inductively coupled with the resonator coil. A resonant frequency is exhibited from the resonator which matches with the reader frequency causing maximum Q-factor. In the same way, another resonant frequency is exhibited from the second resonator coil that coincides with the tag frequency. SCMR requires both the resonators to be resonant at the same frequency in order to achieve WPT efficiently. The resonant frequency f_r can be calculated by:

$$F_r = \frac{1}{2\pi\sqrt{LC}} \tag{4.1}$$

Considering the resonators are identical coils, the efficiency of the SCMR system at its operational frequency can be shown as [200]:

$$\eta(f_r) = \frac{k^2_{(Tx-Rx)}(f_r)Q^2(f_r)}{1+k^2_{(Tx-Rx)}(f_r)Q^2(f_r)} \tag{4.2}$$

where $k_{(Tx\text{-}Rx)}$ is the mutual coupling between the two resonator coils. To obtain greater efficiency of the RFID system, the impedance must be matched for the reader and the tag. In order to realize impedance matching, Fu et al [201] proposed splitting frequency points in the odd or even mode which was only applicable for over coupled areas. Lee et al [202] then proposed an anti-parallel resonant structure that can prevent coupling coefficient. This stabilizes the power transfer despite the change in distance. However this method discards, power transfer characteristics in close range. Chen et al [203] and Duong et al [204] proposed impedance matching method by adjusting the relative distance between adjacent coils. Based on this applied method, this experimental study on impedance matching is carried out by adjusting the distance *x* between the tag and the reader coils to attain proper working range as shown in Figure 4.1. As the distance *x* changes between the reader and the tag, there will be a corresponding change in impedance *Z*, inductance *L* and Q factor by mutual inductance M_{RT} according to:

$$Z,\ L\ or\ Q\ = f(x_1) \tag{4.3}$$

For the scope of the research, theoretical analysis and the experimental validation of the wireless power transfer concept for signal optimisation from tags to reader for different metallic sample inspection is not carried out further rather focus is drawn towards the comparison of transient feature extraction and their sensitivity related to the characterisation of the corrosion from the previous study [168].

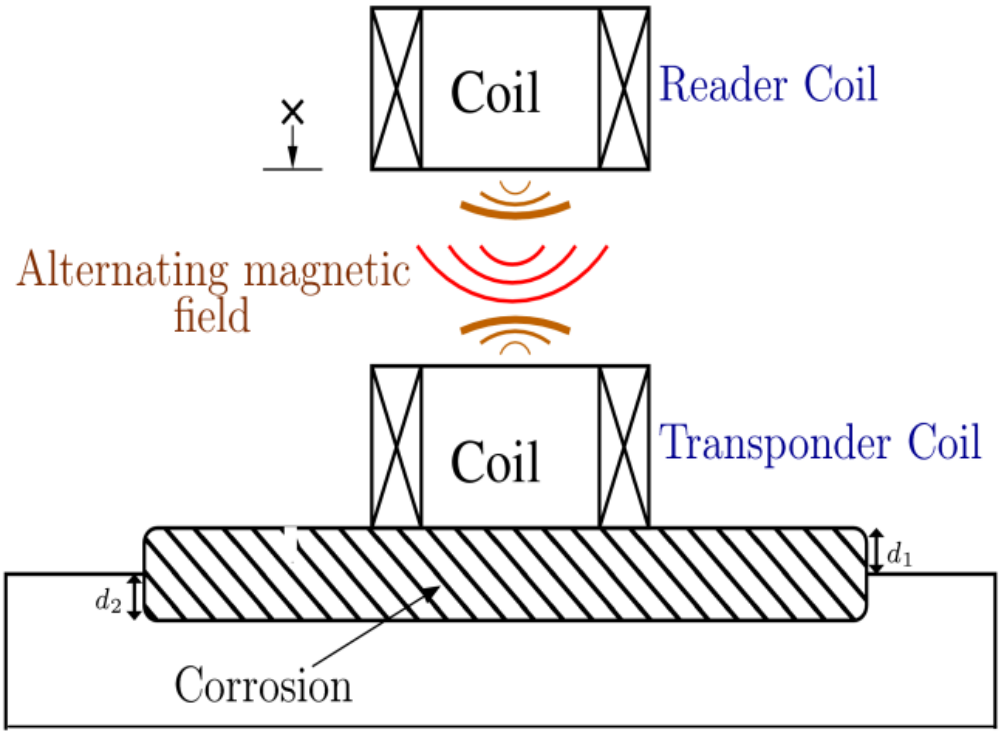

Figure 4.1: Schematic of RFID system on corroded steel

4.2 Samples

In order to investigate the detection capabilities of RFID sensing system, samples prepared by International Paint have been used. These samples show realistic surface conditions and the level of corrosions to determine whether RFID sensors are suitable for detecting and differencing between them. The samples used in this study are low carbon mild steel samples (S275).

There are two sets of samples used. The first set of sample is called the *surface preparation graded* samples, which allows the RFID system to demonstrate its ability to distinguish between four different qualitative surface conditions which are of significant importance to the coating industry. On the other hand, the second set of samples are called the *corrosion progression* samples are specific samples from the industry which were naturally corroded steel plates at different exposure time lengths. These two sets of samples would give more realistic experimental scenario of natural corrosion behaviour.

4.2.1 Surface preparation graded samples

These samples are known as surface preparation samples because it is important to understand the behaviour of different surface grading before anti-corrosive paint is applied into the steel and these samples are also known as UC samples. If the surface preparation is not good, it can

lead to poor adhering of the paint on the steel. There are four UC plates of 300 x100 mm. UC1 plate was blasted using abrasive agent in order to make sure it is free from corrosion. UC2 plate has had been power tooled to obtain the bare metal surface which makes it thinner than the rest. UC3 has had smooth surface corrosion raked away to leave a layer or rust with no notable pitting visible. Finally UC4 has had no corrosion preparation resulting in a very rough surface with a significant level of visible flaking rust. These four plates are shown in the Figure 4.2 and the properties of the samples can be found in Table 4.1.

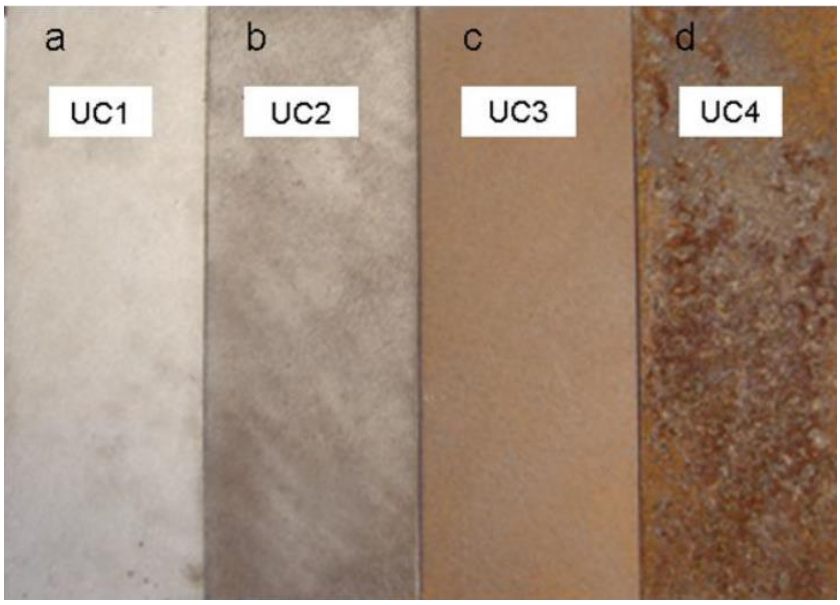

Figure 4.2: Surface prepared grade samples (UC1 – UC4)

Table 4. 1: Samples showing the average thickness measurement and the surface roughness Ra

Specimens	Preparation grade	Average plate thickness (mm)	Average surface roughness Ra (µm)
UC1	A / blasted (Sa2.5)	4.077	18.3
UC2	B / SP11	3.898	16.1
UC3	C / ST2	4.142	29.1
UC4	D / unprepared	4.429	56.7

4.2.2 Corrosion progression samples

Atmospheric corrosion of steel is a general term for an arrangement of iron oxides (hematite Fe_2O_3 and magnetite Fe_3O_4) and hydroxides (ferrous hydroxide Fe (OH) and ferric hydroxide Fe (OH) $_3$). Magnetite mostly in rust is developed in marine climates, which is a ferromagnetic

mineral. Over time, only the proportions of the corrosion constituents have changes with little effect on the composition [17]. This is because density of pure steel is more than that of the iron oxides and hydroxides. During the early stage of the corrosion, the thickness of corrosion will increase but in the long-term corrosion it tends to decrease due to metal loss thereby changing the electrical conductivity and permeability. Additionally, many steel companies apply coating on steel in order to prevent it from rusting; however, over time rust also develops under coating due to blistering or delamination. These have been provided by International Paint with atmospheric corrosion developed in marine atmosphere and the outdoor exposure is shown in Figure 4.3.

Figure 4. 3: Corrosion sample preparation in atmospheric environment

This set of samples consists of coated and uncoated mild steel plates (S275) which have different duration of atmospheric exposure (1, 3, 6, 10 and 12 months) to create different level of corrosion. The plates have dimensions of 300x150x3 mm (length×width×thickness). A 30×30 mm rectangular patch at the centre of each plate was left exposed to allow rust to build up while the remainder of the plate was covered with plastic tape to keep the steel clean and dry. This then formed the uncoated samples. After that, half the plates were spray coated with epoxy phenolic based paint with a typical thickness of 100 microns. The corrosion sample dimension is shown in Figure 4.4 and the images of coated and uncoated rust patches are shown in Figure 4.5.

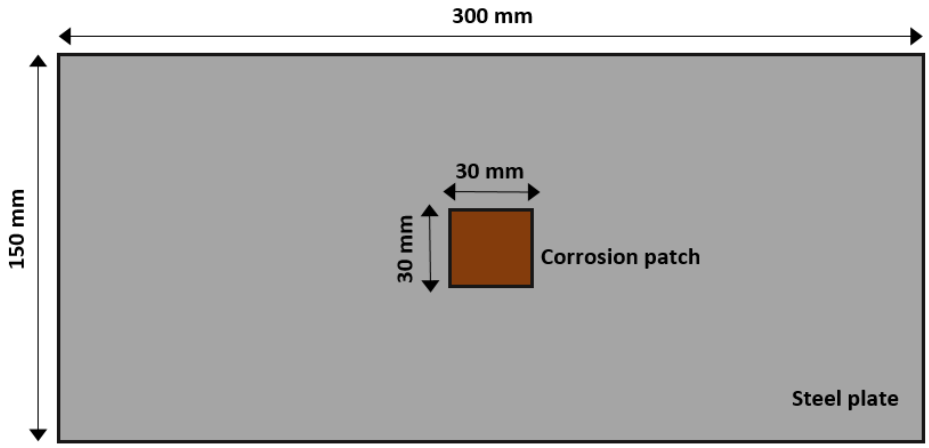

Figure 4.4: Dimension of the corrosion progression sample

Figure 4.5: Images of uncoated corrosion samples (a) 1 month, (b) 3 months, (c) 6 months, (d) 10 months and (e) coated 1 month corrosion sample

As it can be observed from Figure 4.5 above that as the corrosion exposure time increases, the rust begin to spread out while on the other hand in the coated sample, the spreading of the rust is not there. When corrosion expands, it creates a gap between the plastic tape and steel. The oxygen and water can therefore spread to the steel under the tape causing the rust to spread.

4.3 Feature extraction and selection for corrosion characterisation

Many time domain features such as time to peak, amplitude of the peak, rising point and zero crossing, extracted from PEC responses have been used to classify and characterize defects on metallic objects [205], [104] and [206]. In this section, two time domain features have been applied (i. e. transient and static response) from RFID response and analysed and are used to characterize the electrical conductivity and magnetic permeability of the corroded steel sample. Previous related studies on conductivity and permeability changes are shown in Ref. [207], [208] and [206].

Pulse response of RFID is similar to that of PEC, a square wave, which contains rich frequency components. Different frequency components relate to different penetration depth information. The penetration depth in a conductive material is governed by the skin depth δ; this is shown in the equation (4.4)

$$\delta = \frac{1}{\sqrt{f\sigma\pi\mu}} \tag{4.4}$$

where, f is the excitation frequency, σ is the electrical conductivity and μ is the magnetic permeability of the material. It can be seen from the equation that as the frequency increases, the skin depth will decrease.

When testing with ferrous materials, the peak value of the measured magnetic field can vary significantly due to magnetisation effect. The feature characterizing the magnetic permeability variation is the maximum value of pulse *A*, which is the static value of the signal. In this paper, this characteristic is termed as *Max(A)*. The transient response is the rising slope of the pulse which is shown as the first derivative of the signal i.e. $\delta A/\delta t$. Under such convention, a positive pulse of *A* due to the rising edge of excitation current means that the time constant T_c of corroded response decreases faster than that compared to non-corroded response, which corresponds to the decreasing electrical conductivity according to:

$$T_c = L \ / \ R \tag{4.5}$$

where, L is the inductance and R is the resistance of the electrical circuit including the tag circuitry and the test sample. As shown in Figure 4.6, an increase in the positive pulse of *A* in Figure 4.6 (a) will result in the increase of *PVmax(δA/δt)* and decrease of *PVmin(δA/δt)* as shown in Figure 4.6 (b). This is attributed to the fact that as the corrosion progresses, the thickness of corrosion layer will increase [17] which subsequently reduce the electrical conductivity of the material [207, 209, 210]. Therefore, it can be inferred that *PVmax(δA/δt)* reflect the electrical conductivity change of the detected area of the material to be tested. Indication of reduced electrical conductivity caused by the difference of normalised signals from stress measurements in aluminium alloys have already been shown by previous researchers in [207] and [209].

In this section, two time domain features have been selected and are linked to the changes in electrical conductivity and magnetic permeability of the corroded region. In order to evaluate and compare the sensitivity of the features, other features have also been extracted and optimised in order to get a thorough comparison study. Amongst the seven features are, *Max(A)* which represents the maximum value of pulse A, *Adiff* which represents the difference between the maximum and minimum of the pulse and *Aedge* which represent the rising edge of the pulse and is defined by the upper and lower threshold of the rising edge denoted as M_2 and M_1, respectively.

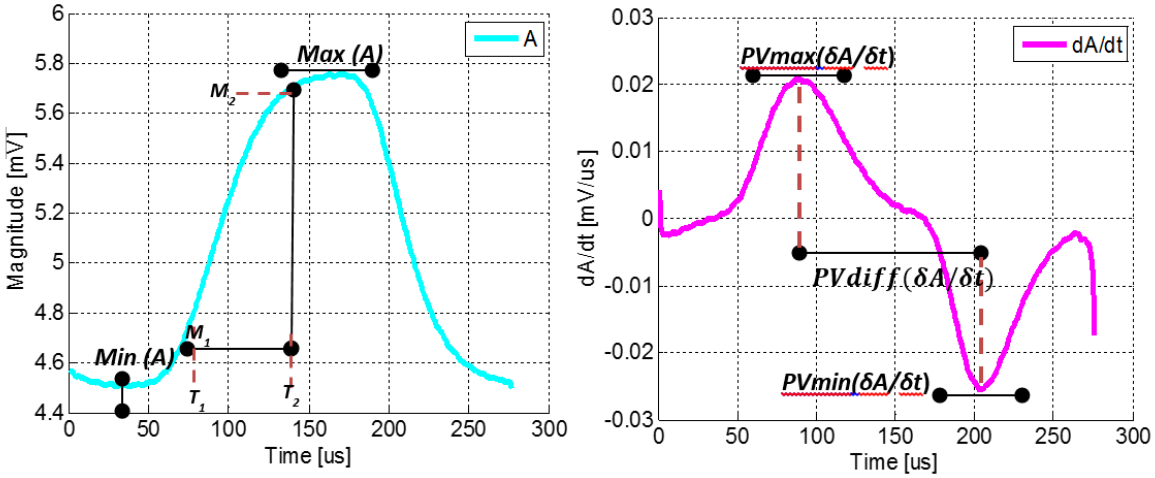

(a) (b)

Figure 4.6: RFID signal (a) RFID response of the proposed system on non-corroded metal, (b) differential response of (a)

As for the differential measurements, the following were extracted, firstly the *PVmax(δA/δt)*, which represents the peak value of the *δA/δt* and then the *PVmin(δA/δt)* which represents the minimum peak of *δA/δt.* Thirdly, the difference between the maximum peak and the minimum peak is found shown as *PVdiff(δA/δt)* and finally the pulse ratio which can be used to determine the quality factor of the signal is denoted as *Pratio(δA/δt)*which is defined as the reciprocal of the duty cycle. All these seven features (three from the pulse response and four from the differential of the pulse signal) are summarised, validated and compared to characterise corrosion (with and without ferrite sheet) in the following section.

4.4 Experimental setup of the RFID system for corrosion characterisation

A LF (125 kHz) RFID reader has been used to perform the experimental work. The tag used is ATA5577 from Atmel Corporation. The tag is programmed with an ID consisting of '1's' at a data bit rate of 125 kHz / 32 = 3.906 kHz with 50% duty cycles. Uniform stream of 1's have been chosen for easier processing as it allows averaging over many cycles. The position of the reader coil and the corrosion patch is maintained at a constant distance and aligned for each measurement while the tag is directly placed in the centre of the corrosion patch.

Experiments were carried out at different stand-off distances and 30mm is found to be the optimum distance for the RFID tag to work best on the metallic samples This is because at a lower stand-off distance, the influence of the reader coil becomes higher than the tag whereas at a higher stand-off distance the tag coil cannot receive enough power from the reader coil thus reducing sensitivity to corrosion. The reader coil used is 90 mm in diameter with parameters of

R = 10.45Ω and L = 732 uH. Both the reader and the tag have resonant frequency of 125 kHz in free space. Due to the metal effect, the resonant frequency of the tag and reader becomes lower. However, the tag is influenced more than the reader since it is in direct contact with the metal surface. The output was sampled at 1 MHz for 0.01 seconds (10,000 data points). Figure 4.7 (a) shows the system setup along with the system diagram in Figure 4.7 (b)

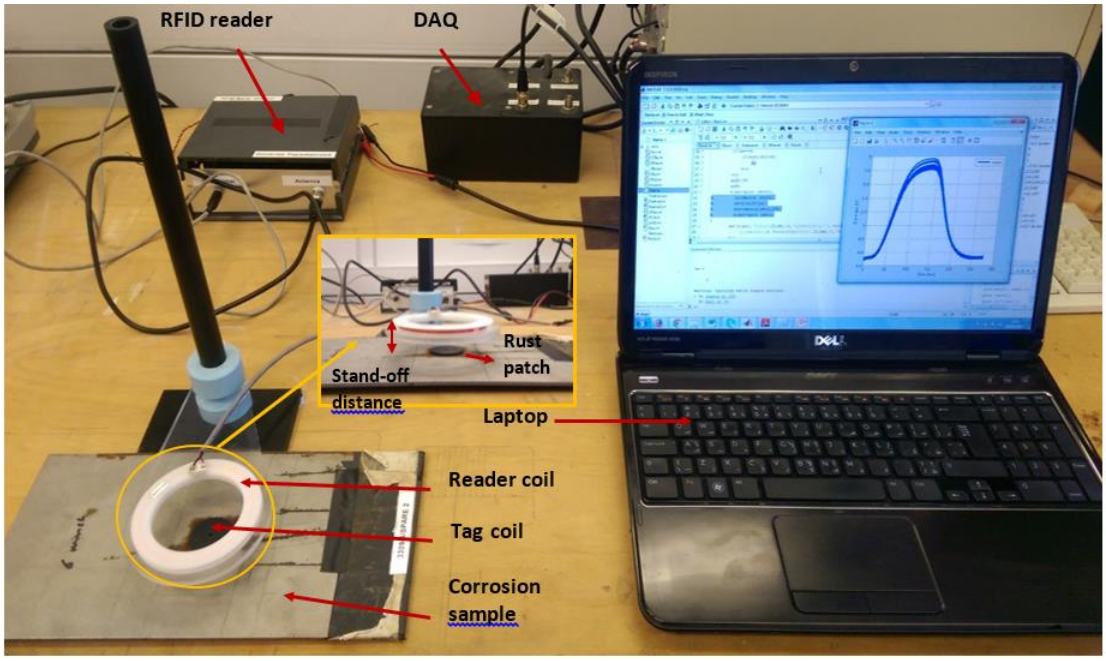

(a)

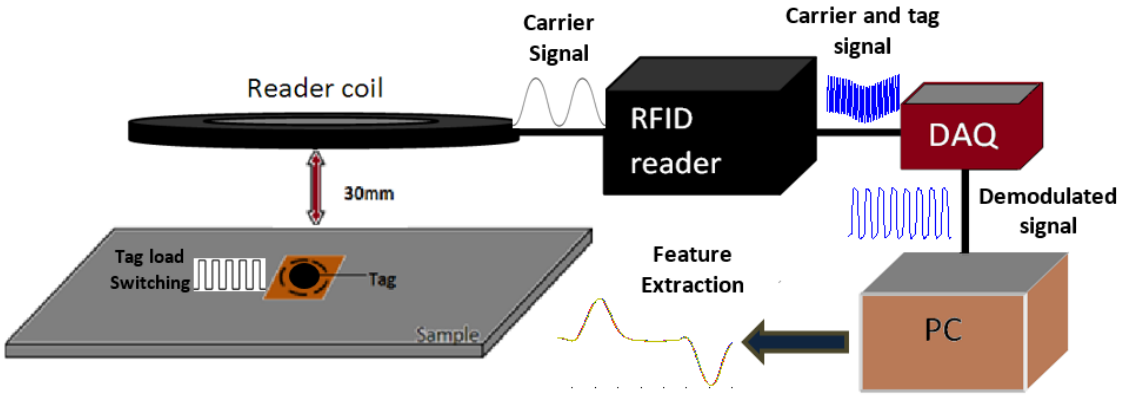

(b)

Figure 4.7: System setup (a) RFID system configuration for corrosion detection, (b) RFID system diagram

4.5 Experimental results and validation

Based on the feature extraction and comparison study mentioned in section 3, it can be inferred that *Max(A)* feature can characterize permeability change and *PVmax(δA/δt)* can characterize conductivity variation and further features prove the robustness of the system and may be useful in future works for other applications. Results for the UC samples are shown in Section 4.5.1. Measurements on uncoated and coated samples taken using the RFID system are shown in Sections 4.5.2 and 4.5.3 respectively. Section 4.5.4 shows the use of ferrite core to enhance sensitivity of the response even further. The measurement was repeated 10 times for each sample and the average from those 10 measurements are then used as the measured value for further extraction.

To ease the feature selection, two equations are introduced and calculated i.e. the absolute variation Δ shown in equation (4.6), and the relative variation ε shown in equation (4.7). In tables, two specific samples i.e. 1 month and 6 months are represented as Sample 1 and Sample 6 respectively. These two samples are chosen for the comparison of absolute and relative variations because of their significant changes in exposure time. The absolute variation Δ between samples 6 and 1 is calculated by:

$$\Delta = max\ value\ of\ sample\ 6 - max\ value\ of\ sample\ 1 \tag{4.6}$$

Relative variation ε is calculated by

$$\varepsilon = (\Delta\ /\ max\ value\ of\ sample) \times 100 \tag{4.7}$$

4.5.1 Surface preparation grade sample

This experimental study is an attempt to provide the proof of concept for the working of the RFID system as corrosion sensors. The experimental setup is same as shown in Figure 4.7. The positioning of the tag-reader coil and the aligning of them has been carefully controlled to prevent having any anomalous signal as discussed in Section 3.2. The average peak voltage for each of the samples is plotted in Figure 4.8 and it first thing can be noticed that all the samples can be differentiated according to their corrosion level.

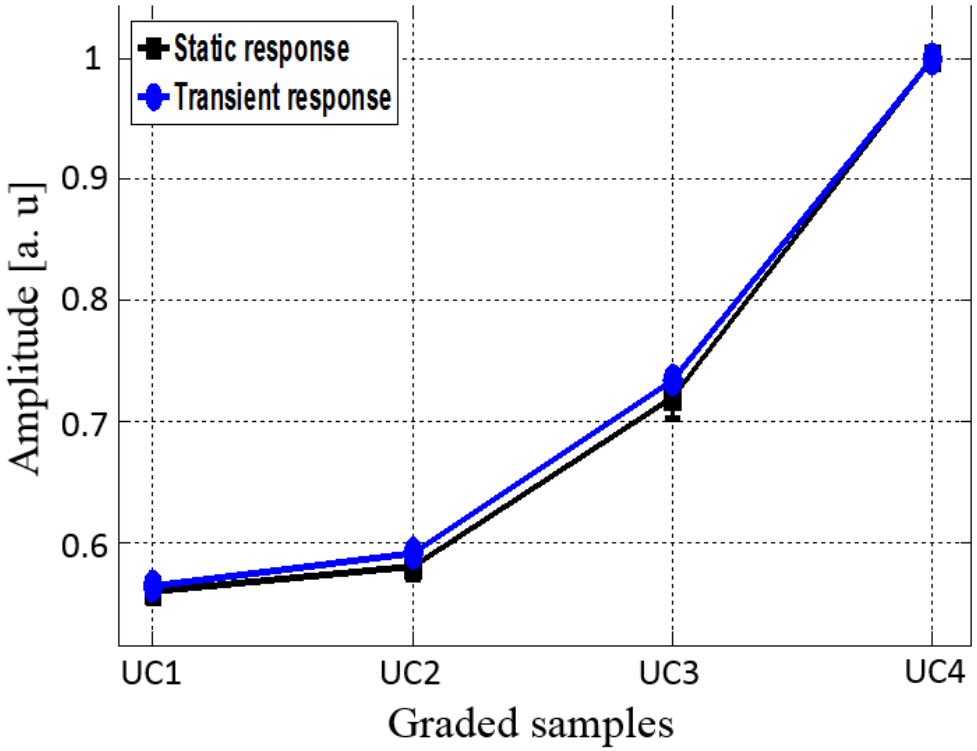

Figure 4.8: The static and transient response for the UC samples

The results for both static and transient responses are shown to be similar with transient response being slightly better. This is because the graded samples are not localised corrosion hence an increase in the overall corrosion of the sample reduces the conductivity σ and overall permeability μ. With this reduction, the resonant frequency of the tag moves towards the free space resonant frequency which results in the tag absorbing larger amount of power from the reader and thereby increasing the amount of peak voltage. Based on the roughness of the UC samples shown in Table 4.1, it can be seen that the results for UC1 and UC2 plates are almost similar and there is very little variation compared to UC3 and UC4 where the roughness increases by a large number.

4.5.2 Corrosion characterisation in uncoated samples

In Table 4.2, all the features have been described and extracted and a comparison between corrosion samples is shown. From the absolute and relative variation of peak values, it is found that transient response has shown 4 times higher sensitivity than that of the static response. The difference between the maximum and minimum values has shown twice as much better sensitivity for the transient response. This shows that transient features have better relative sensitivity than static features. Furthermore, transient features do not depend on the baseline which means that any uncertainty e.g. a change of mutual coupling of the two coils can be minimised increasing the stability when installed permanently for SHM.

Table 4.2: Features for corrosion on uncoated samples for 6 months and 1 month

Features	Descriptions	Sample 6	Sample 1	Δ	ε (%)
Max(A)	Peak value of the pulse response	5.8678	5.8095	0.0583	0.99
Adiff	Difference between the maximum and minimum of the pulse slope	1.3463	1.3117	0.0346	2.57
Aedge	Rising edge of the pulse	0.0176	0.0166	0.0010	5.68
PVmax(δA/δt)	Maximum peak of the differential signal	0.0218	0.0209	0.0009	4.13
PVmin(δA/δt)	Minimum peak of the differential signal	-0.0253	-0.0240	-0.0013	5.14
PVdiff(δA/δt)	Difference between the maximum and minimum peak values of differential signal	0.0470	0.0445	0.0025	5.32
PVratio(δA/δt)	Difference between the maximum and minimum values of the differential signal over time to maximum and minimum values	-4.081e-04	-3.844e-04	-2.37e-05	5.81

The two plots in Figure 4.9 show the changes in peak values (*Max(A)* and *PVmax(δA/δt)*) and the difference between the maximum and minimum (*Adiff* and *PVdiff(δA/δt)*) for both the static and transient responses respectively. The responses have been normalized for better comparison of static and transient features. A monotonic increase with exposure time can be seen from both the plots with very low error bars showing lower uncertainty of the data and an increased accuracy and robustness.

From Figure 4.9 (a) it can be seen that, both the static and the transient responses show a monotonic rise with the corrosion exposure time. Figure 4.9 (b) however shows a slight higher response with the transient response than the static response between 1 and 10 months. From both the figures above it can be noticed that, there is a drop in amplitude at 12 months for static response; whereas the transient response shows an enhanced sensitivity. This is because as the exposure time increases, the corrosion area also increases and when the latter happens, the rust layer loosen up and the flakes fall off as it expands. Thus subsequent corrosion spreads outward rather than increase in thickness.

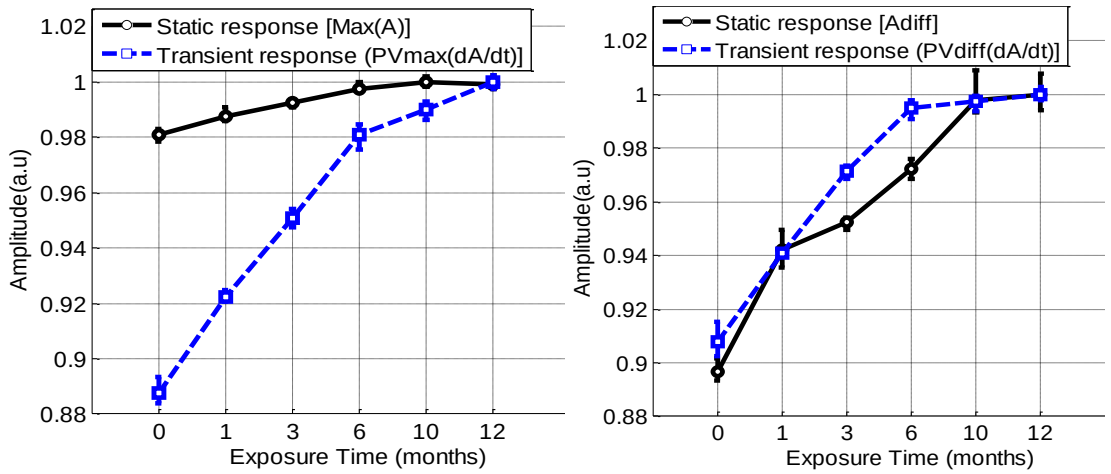

(a) (b)

Figure 4.9: Static and transient responses for uncoated samples showing (a) maximum value of responses (b) difference between the maximum and minimum of the pulse responses

4.5.3 Corrosion characterisation in coated samples

Coating and corrosion layer changes the dielectric properties of the material under test. Corrosion also develops under coating, therefore in this section, coated samples are studied. Coating layer on the samples is approximately about 100 microns thick, hence the effect on RFID characterization is not very significant in comparison with the uncoated samples. This is because RFID system works on low operational frequency hence the dielectric property influence is small. This is also shown in the previous study using PEC carried out by He et al in [210] where it was shown that there is a good agreement in the fitted lines of the measured values drawn between the coated and uncoated samples which are the same samples used in this study.

From Table 4.3, it can be seen that the relative variation between the two samples for the peak value is slightly higher than the uncoated one. This is because the coating layer has prevented any flaking or metal loss and therefore the rust did not spread over the metal causing the thickness of the rust patch to be constant and hence the difference for the peak value between the two samples is higher. Also, the coating layer increases the lift-off between the transponder coil and the sample, thus reducing mutual coupling and therefore the shift in the resonant frequency is smaller.

Table 4.3: Features for corrosion on coated samples for 6 months and 1 month

Features	Sample 6	Sample 1	Δ	ε (%)
Max(A)	5.9426	5.8603	0.0823	1.38
Adiff	1.4536	1.3746	0.0790	5.43
Aedge	0.0185	0.0176	0.0009	4.86
PVmax(δA/δt)	0.0229	0.0219	0.0010	4.37
PVmin(δA/δt)	-0.0270	-0.0253	-0.0017	6.30
PVdiff(δA/δt)	0.0499	0.0471	0.0028	5.61
PVratio(δA/δt)	-4.304e-04	-4.068e-04	-2.36e-05	5.48

Both Figure 4.10 (a) and (b) shows a similar pattern with the static and transient responses over the exposure time. A slight drop in amplitude can be noticed in the 3rd month for both the figures which is thought to be due to the uncertainty of the static response which is however enhanced using the transient response as it shows higher sensitivity. A monotonic trend with exposure time remains. However due to the 10th month's sample deformation as the sample has been receded from its original state, the sensitivity measurement value has dropped slightly for both features.

As illustrated in Figure 4.9, the measured values for uncoated and coated samples are relative. Over time, an increase in the corrosion thickness means an increase in the corrosion contribution to the RFID responses; this lead to a reduction of the electrical conductivity and permeability of the corroded region. In order to enhance the signal sensitivity due to higher magnetic permeability, ferrite substrate is used in the next sub-section and further results are extracted and compared.

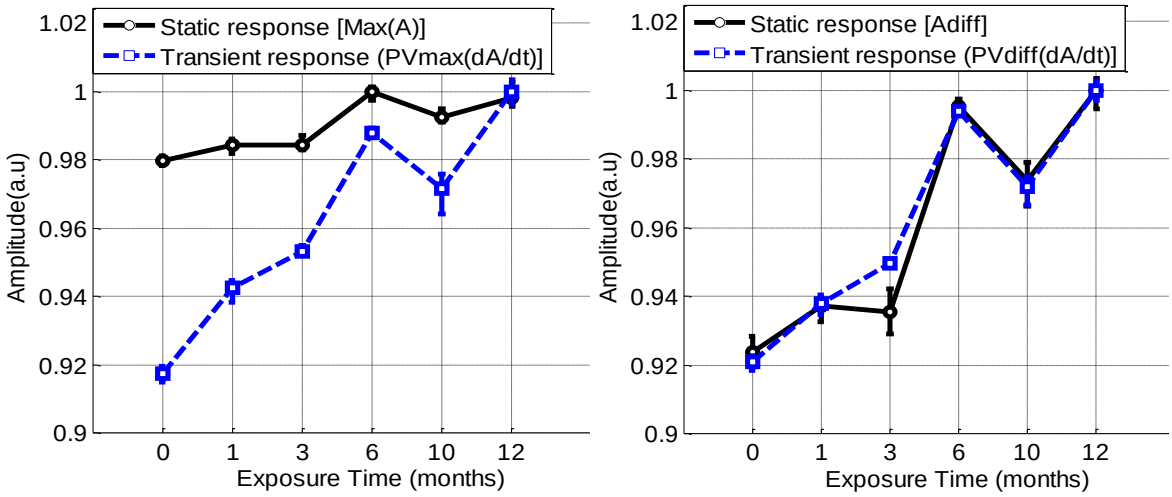

(a) (b)

Figure 4.10: Static and transient responses for coated samples showing (a) maximum value of the responses (b) difference between the maximum and minimum of the pulse responses

4.6 Signal sensitivity improvement using ferrite substrate

As it can be seen in Figure 4.11, that using a ferrite core will shift the tag's resonant frequency $f_{ferrite}$ towards the free space resonance f_0 which is the most sensitive working range. In this section further experimental study is carried out to enhance the performance of the RFID response using a ferrite core for improvement in the signal sensitivity and robustness for corrosion characterisation. From Sections 4.5.2 and 4.5.3, it can be seen that the relative sensitivity is improved by transient feature selection. Using the rising edge of the transient response (*PVmax(δA/δt)*), the sensitivity can be increased by about 3 - 4 times compared to the static response (*Max(A)*) for both coated and uncoated samples respectively. Previous work on both LF and UHF RFID has proved the enhancement of near field coupling using ferrite substrates for RFID applications [211, 212].

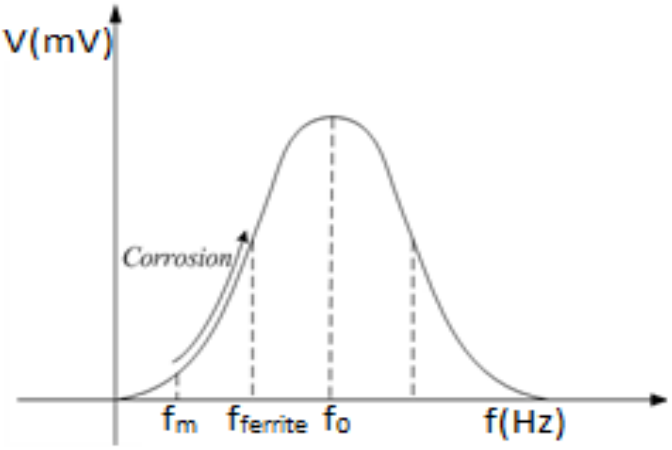

(a)

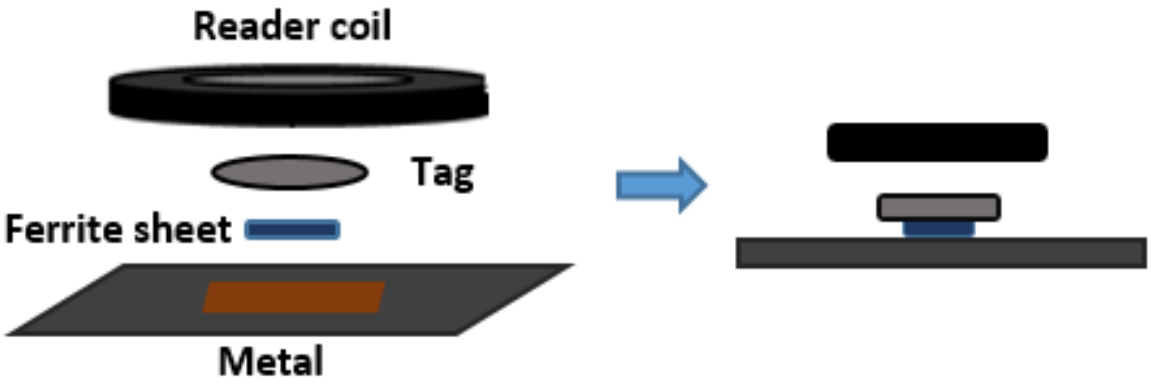

(b)

Figure 4. 11: Setup design with ferrite sheet (a) Operational frequency response curve and resonance frequency (b) setup using ferrite sheet

In order to understand the areas of dominance of the influence of ferrite sheet on RFID signal, a simulation model is exploited. This is the forward process which is then followed by the inverse process in the next step where it is verrified by experimental results.

This modelling is carried out using RFID module of Comsol Multiphysics 4.3 [213]. 3D time-domain simulation for the sensing system with ferrite sheet attached to the tag have been modelled. Figure 4.12 shows the magnetic flux density of both for both with and without ferrite core designs. It can be seen from the model that the magnetic induction is very low on the model without ferrite shown in Figure 4.12 (a) whereas for Figure 4.12 (b) where the ferrite sheet have been used under tag shows the eddy currents are concentrated in the corrosion region of the steel sample below the sensor. The results are further verfied by experimental studies and the results are shown in Figure 4.13.

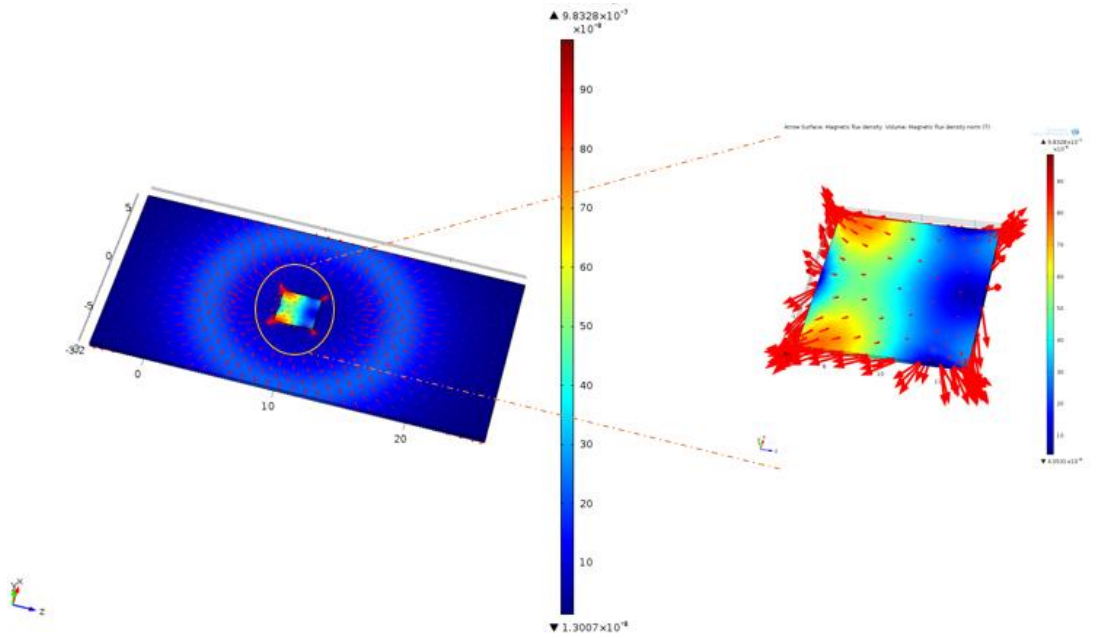

(a)

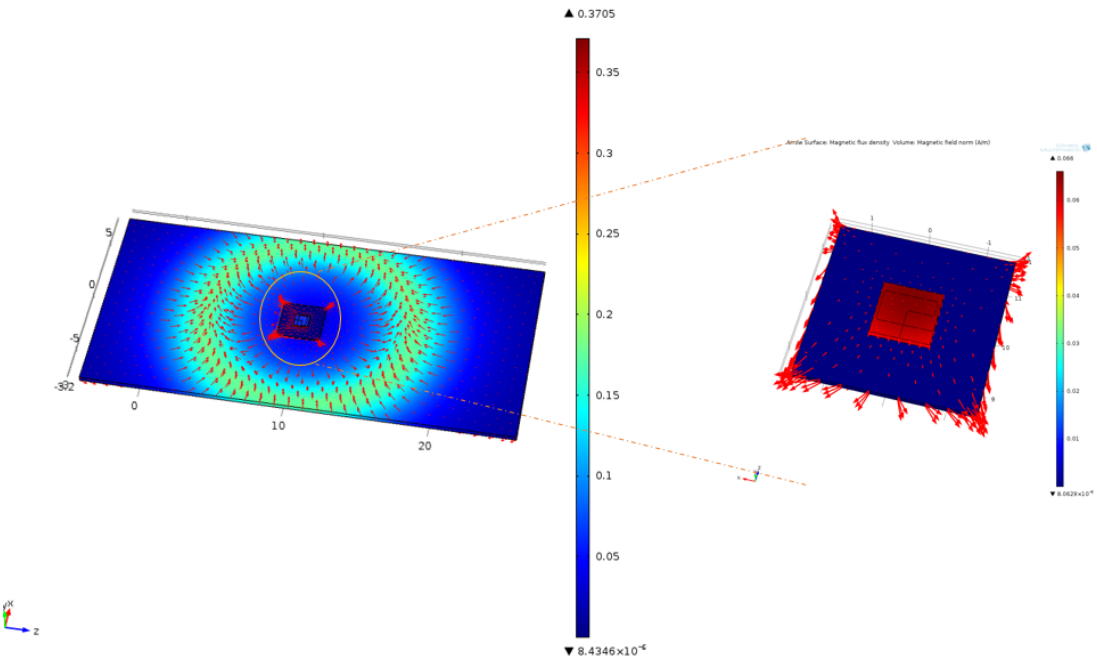

(b)

Figure 4.12: COMSOL simulation (a) Model without ferrite sheet showing a magnetic flux density of 9.833x10-7 T (b) Model with ferrite sheet showing a magnetic flux density of 0.371 T

Table 4.4: Comparison of uncoated and coated samples with and without ferrite core

	Sample type	Features	Sample 6	Sample 1	Δ	ε (%)
No ferrite core	Uncoated	*Max(A)*	5.8678	5.8095	0.0583	0.99
		PVmax(δA/δt)	0.0218	0.0209	0.0009	4.13
	Coated	*Max(A)*	5.9426	5.8603	0.0823	1.38
		PVmax(δA/δt)	0.0229	0.0219	0.0010	4.37
With ferrite core	Uncoated	*Max(A)*	5.9916	5.9124	0.0792	1.32
		PVmax(δA/δt)	0.0242	0.0231	0.0011	4.55
	Coated	*Max(A)*	5.9866	5.8770	0.1096	1.83
		PVmax(δA/δt)	0.0256	0.0240	0.0016	6.25

Measurements in Table 4.4 show that using ferrite cores, sensitivity is further improved even when compared to transient responses. However it needs to be kept in mind that the changes in absolute variation are small since the tag is commercial therefore the amplitude variation between samples are also small.

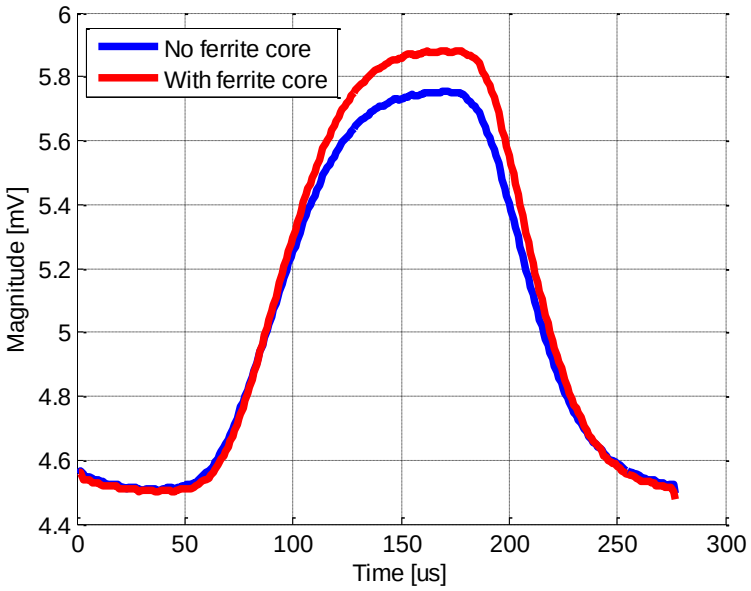

(a)

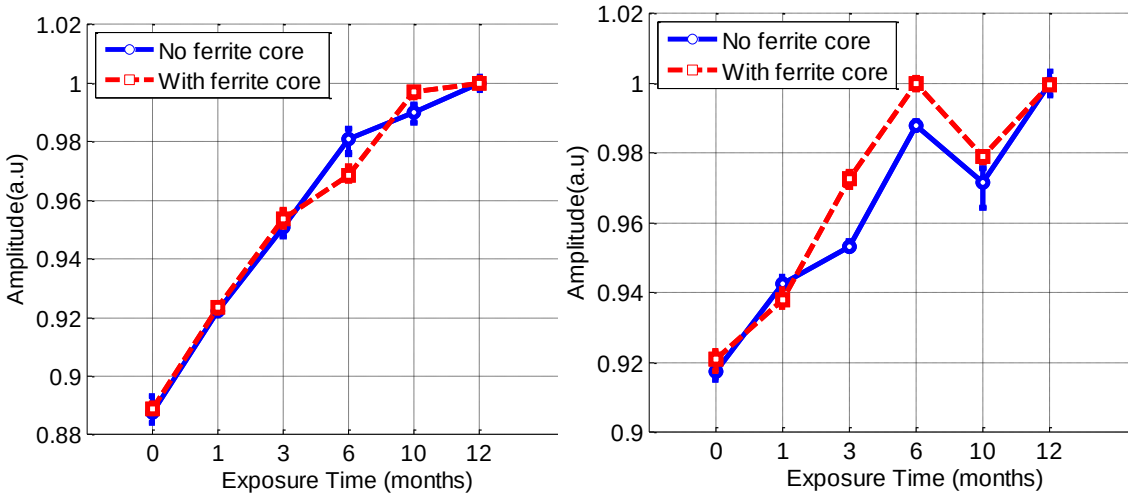

(b)

(c)

Figure 4.13: Results after using ferrite sheet (a) Pulse response on non-corroded metal (b) transient response for both with and without ferrite core on uncoated sample (c) transient response for both with and without ferrite core on coated sample

Even with commercial tags, an increase of ~10 - 45% for both uncoated and coated specific samples respectively have been achieved. Further work will be carried out on tag fabrication for LF RFID with ferrite core or rod. It is expected that sensitivity and detection distance can be further improved by taking into consideration of the shift in resonant frequencies caused by metallic samples, lift-off distances and coupling factors of tag and readers.

4.7 Chapter summary

In this chapter, both coated and uncoated mild steel samples with corrosion exposure between 1 to 12 months have been measured using proposed LF RFID system. The concept of WPT is applied in order to attain the working range for RFID sensing system. Also the distance between the reader and the tag is adjusted to match the impedance variation of commercial RFID tag on metallic sample. The corrosion layer based on the different conductivity and permeability changes has been identified for different stages ($t < 1$ year).

Several features are extracted and compared. Two features have been selected, namely static (*Max (A))* and transient (*PVmax(δA/δt))* response to determine permeability and conductivity changes respectively with corrosion exposure. From selected features, transient responses have proven to be significantly more sensitive and robust with corrosion progression compared to conventional static features.

Further prediction in terms of increasing sensitivity of the tag has been shown using ferrite cores with an enhanced pulse response from which more useful features related to corrosion characterisation can be extracted. An additional about 10 - 45% increase in sensitivity has been estimated using ferrite core without changing the distance between the RFID reader and the tag. Further sensitivity enhancement can be expected using WPT concept by optimally adjusting the distance between the reader and the tag.

These findings are valuable for understanding the behaviour of the resonant frequency further with regards to environmental changes such as high temperature and this is be discussed in Chapter 5.

Chapter 5. Temperature Independent Defect Monitoring using RFID Sensing System

Previous chapter discussed the detection capability of the RFID system and the enhanced sensing capability was experimentally proved. Corrosion is only one of the parameters that affects the resonance of the RFID system. All the other parameters such as effect of resonance on different defect orientation or depth or any other environmental factors such as temperature variation, have been considered to be fixed which may not always be practical. This will limit the usability and applicability of RFID as a defect monitoring sensor. It is therefore essential to study each of these parameters for the wider acceptance of RFID as a defect monitoring sensing system for harsh environmental conditions. In practical situation, the temperature variation will be unknown in a priori and hence will give rise to uncertainty and unreliability in the defect detection as any variation in temperature will also vary the resonance which will be confused with defects.

Therefore, this study, demonstrates the potential use of low frequency (LF) RFID tag antenna based wireless sensors to characterise corrosion and crack progression in high-temperature conditions for potential structural monitoring. Consideration of the parasitic parameters which depend on the temperature variation is presented. The key factors that influences the sensing accuracy with regards to different materials due to inhomogeneity are presented. A cost-effective self-compensation method is proposed by means of a self-swept frequency measurement through selection and fusion of temperature dependent feature near the tag's resonance region. The experimental work validates the effectiveness of the method and some initial results demonstrate the efficiency of the technique to overcome the inhomogeneity caused by different materials and defects.

5.1 Methods and Measurement Principles

The possible interferences of using RFID sensing system can be roughly categorized into three types: *system configurations* such as the communication distance and the circuit bandwidth, *sample interferences* such as roughness, geometry, thickness, permittivity and permeability and *operating conditions* such as temperature. In practical situations, the unknown temperature variation and defect will be mixed. This section presents the temperature modelling, test instrumentation, and feature extraction of LF RFID sensing system.

5.1.1 RFID sensing principle for crack monitoring with varying temperature

For NDT&E applications in high temperature environments e.g. crack depth detection on metallic samples, the detuning of RFID tag's impedance at presence of nearby conductor needs be considered. The Bolch-Grüneisen formula mathematically represents the relationship between temperature and resistivity for metal [214].

$$\rho(T) = \rho(0) + A(\frac{T}{\theta_R})^n \tag{5.1}$$

Where, *ρ(0)* is the residual resistivity due to defect scattering. θ_R is the Debye temperature and *A* is constant. At high temperatures, the metal resistivity increases with an increase in temperature whereas in case of semi-conductors, the fractional change in resistivity is negative which means that the resistivity of semi-conductor decreases exponentially with an increase in temperature [215]. The coil is assumed to be planar spiral and air-cored with *N* turns, inner radius x_1, outer radius x_2, μ_0 is the permeability of free space. Therefore, the inductance of the spiral coil can be written in the form [193]:

$$L_0 = \frac{\mu_0 \pi N^2}{(x_2 - x_1)^2} \int_0^\infty \frac{1}{\alpha^4} I^2(\alpha x_1, \alpha x_2) d\alpha \,, \tag{5.2}$$

where I is the radial integral. The integral in Eq. (5.2) can be expressed in terms generalized functions. The crack is assumed to have constant depth *b* and width Δu . The results derived by Harfield and Bowler [192, 216, 217] can be used to derive the results for the tag's impedance. Semiconductor components of an RFID tag, such as tag IC, also have a temperature dependence given by the Steinhart-Hart equation. The resistivity of semiconductor decreases with an increase in temperature and thus reducing the magnitude of the tag's response [214].

$$\frac{1}{T} = A + B\ln(\rho) + C(\ln(\rho))^3 \tag{5.3}$$

Where, *T* is the temperature in degrees Kelvin and A, B, C are the coefficient constants that determines the expected resistance variation along with the temperature change. The electrical capacitance present in the RFID tag is a dielectric constant function of tag substrate. When the tag is exposed to change in temperature, there is a variation in the dielectric constant. This capacitance change in response to the temperature is expressed as:

$$C_T(T) = \frac{\varepsilon_0 \varepsilon_r(T) A}{t} \tag{5.4}$$

Where, ε_0 is the permittivity of free space and ε_r is the dielectric constant of the material which changes with temperature variation. A shows the area of the electrode plate and *t* is the thickness of the dielectric material.

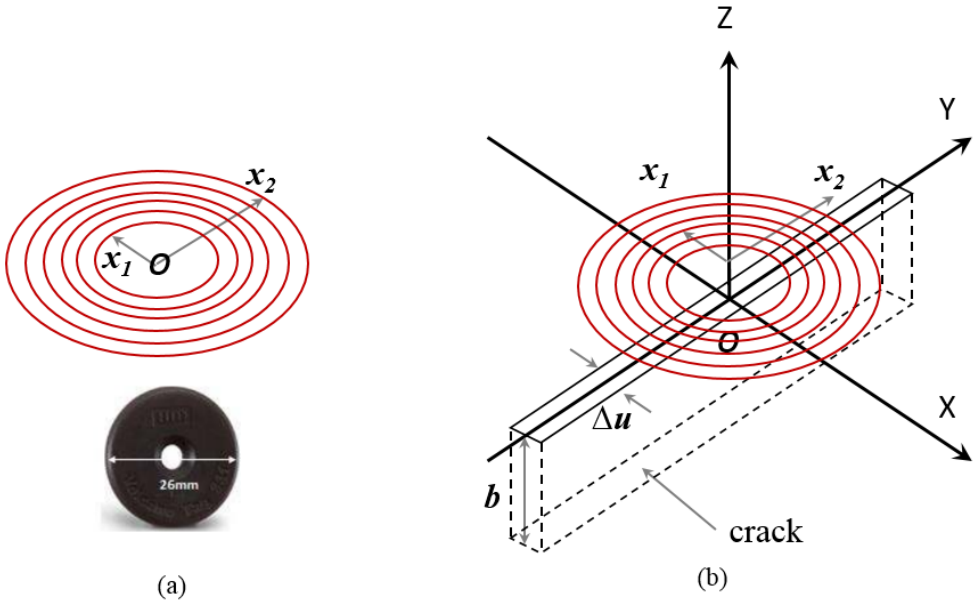

Figure 5.1: Tag and specimen geometry. (a) LF RFID tag and spiral coil and (b) spiral coil with infinitely long crack in a conducting magnetic half-space

5.1.2 RFID readout instrumentation with swept frequency measurements

Due to the tag's resonance oscillation the input impedance of the reader coil changes [218]. In order to measure the resonance frequency range, a readout circuit generates a swept-frequency signal in a specific frequency range is depicted in Figure 5.2. The changes in the physical parameters such as the resonance frequency, input impedance, or Q-factor are already derived and shown in section 3 equations (3.9) to (3.11). Any changes in the temperature causes a change in the permittivity ε_r of the sample following a change in the capacitance. This results in the shift of resonant frequency of the sensor. Any shift in the resonant frequency can be detected by the reader coil which is also magnetically coupled with the transponder coil. A swept frequency response is obtained in order to cover the resonant frequency shift caused by the tag. Resonance oscillation followed by change in the input impedance of the reader coil occurs when the transmitted frequency equals the tag's resonant frequency [218]. Detailed circuitry of the RFID system is described in section 3 Figure 3.10.

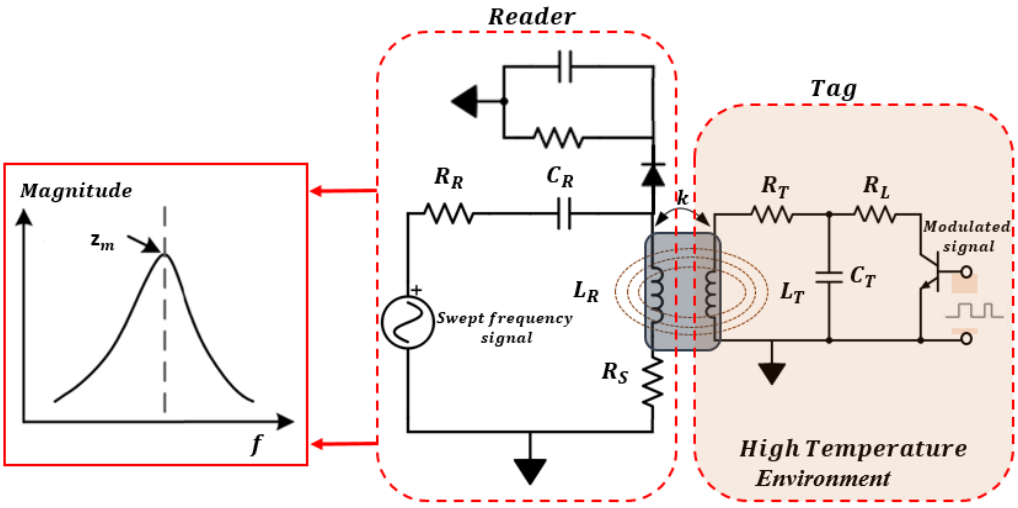

Figure 5.2: Schematic of RFID sensing system

5.1.3 Feature extraction and selection

The tag's resonance response can be obtained by changing the AC source frequency. From this, the impedance can be measured using *peak-to-peak* response. The *peak-to-peak* response is shown in Figure 4.6 (a) in Section 4. Then, the temperature coefficient across the swept frequency is compared, where the summation from both sides of the resonant frequency point i.e. the lower frequency points and the higher frequency points is taken in order to enhance the robustness of the RFID sensing system. The sweep frequency technique gives the advantage of selecting various frequency ranges to extract information, the detailed behaviour is going to be analysed in the following section. The processing technique is shown in Figure 5.3.

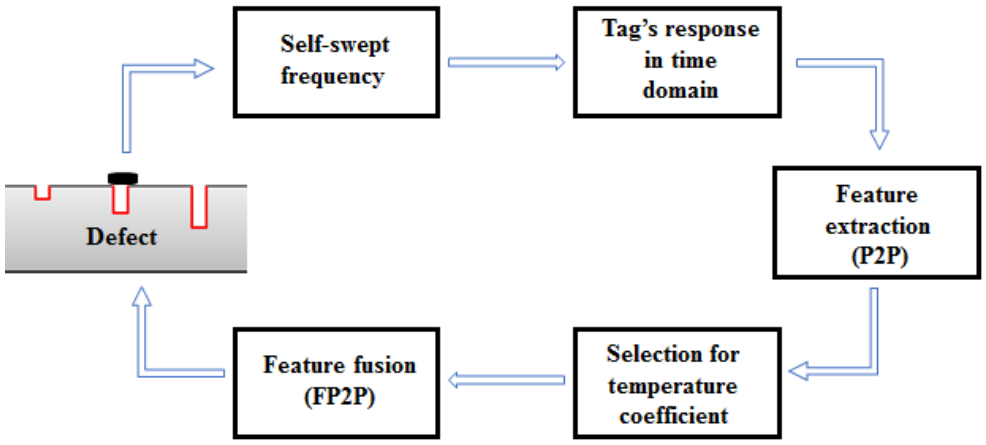

Figure 5.3: Feature extraction processing diagram with a fusion based on combination of positive and negative temperature coefficients

5.2 Experimental validation for RFID data

5.2.1 RFID system

The experimental study carried out in this section consists of the modified circuitry as shown in chapter 3. In this section, the sources of the circuitry are connected to the signal generator using NOT gate so that the operational frequency can be changed from the range of 110 kHz to 140 kHz to attain the resonance behaviour based on the material delineation or environmental changes.

5.2.2 Samples

The samples used for this section of the study are the initially described corrosion progression set of samples in Section 4 in Figure 4.5 and a new crack sample. The crack sample is an aluminium sample with electrical conductivity of 25.8 MS/m and a geometrical dimension of 210 mm × 50 mm × 12 mm. This sample has machined slit defects of constant width of 3 mm. with crack depths of 3 mm, 5 mm, 7 mm and 9 mm. This sample is shown in Figure 5.4. Along with this, the corrosion samples are used for the study of inhomogeneity based on the material difference as the corrosions samples are steel samples which has a much higher electrical conductivity in comparison to aluminium. Also the multi-layered corrosion on the sample will be different to that of the crack depths, producing varying resonance shift. The cracks in this section are denoted as C0 for crack 0, C1 for Crack 1 and so on.

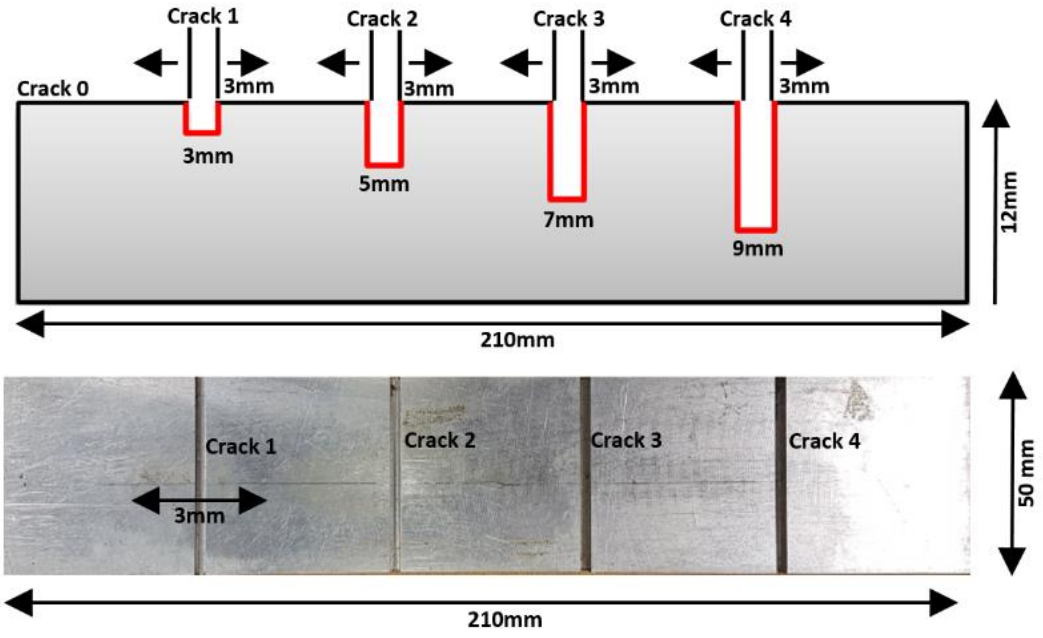

Figure 5.4: Aluminium sample with different crack depths

5.2.3 RFID experimental system setup

A similar system setup as Figure 4.7 in Section 4 is considered for this experiment. One of the changes in this system is the usage of tag. The tag that is used is the HID LF Volcano tags from HID Global. These tags are used for temperature based applications because of its encapsulation which composed of field demonstrated, temperature stable polyphthalamide (PPA). This thermoplastic shell stays rigid even though there are temperature fluctuations, protecting the electronics within for reliable performance. The experiment was carried out at five different temperatures which are 25°C, 60°C, 95°C, 130°C and 160°C. The varying 25°C is being considered the room temperature, therefore, remainder of the variations were carried out using a hot plate (VWR VHP-C7). These temperature increments were monitored using an electric thermometer. The system setup followed by the system diagram is shown in Figure 5.5.

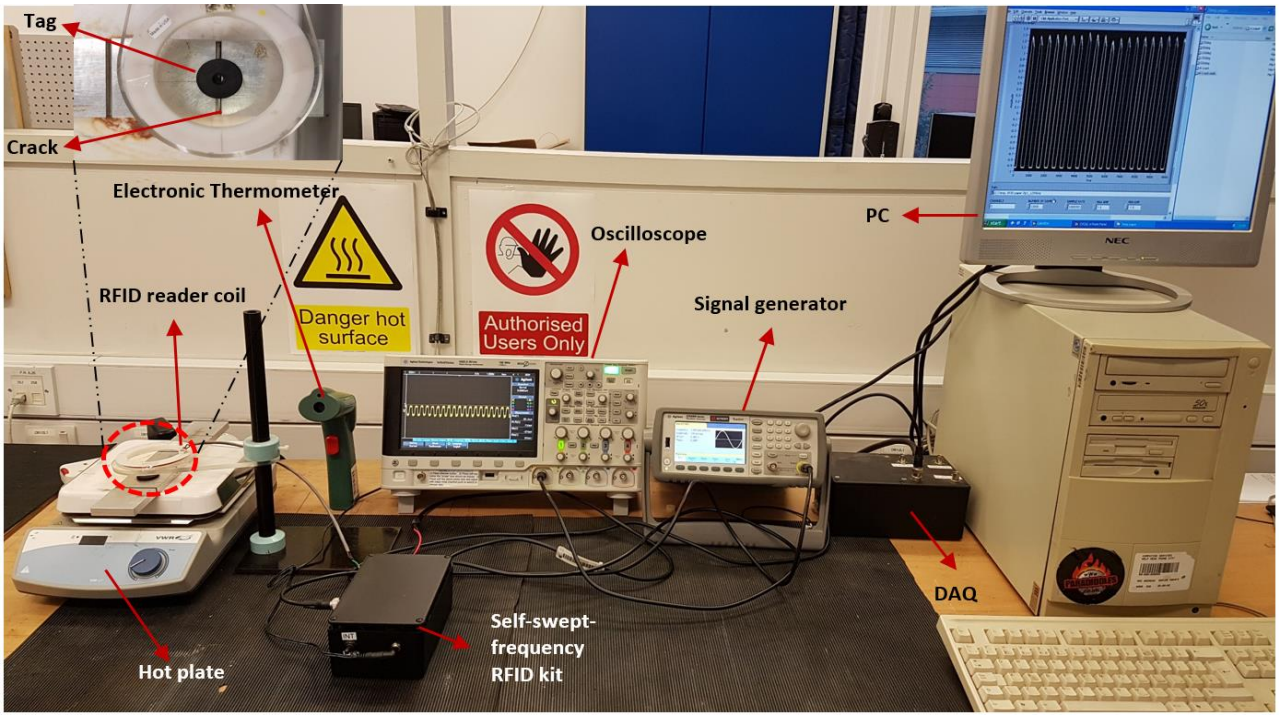

(a)

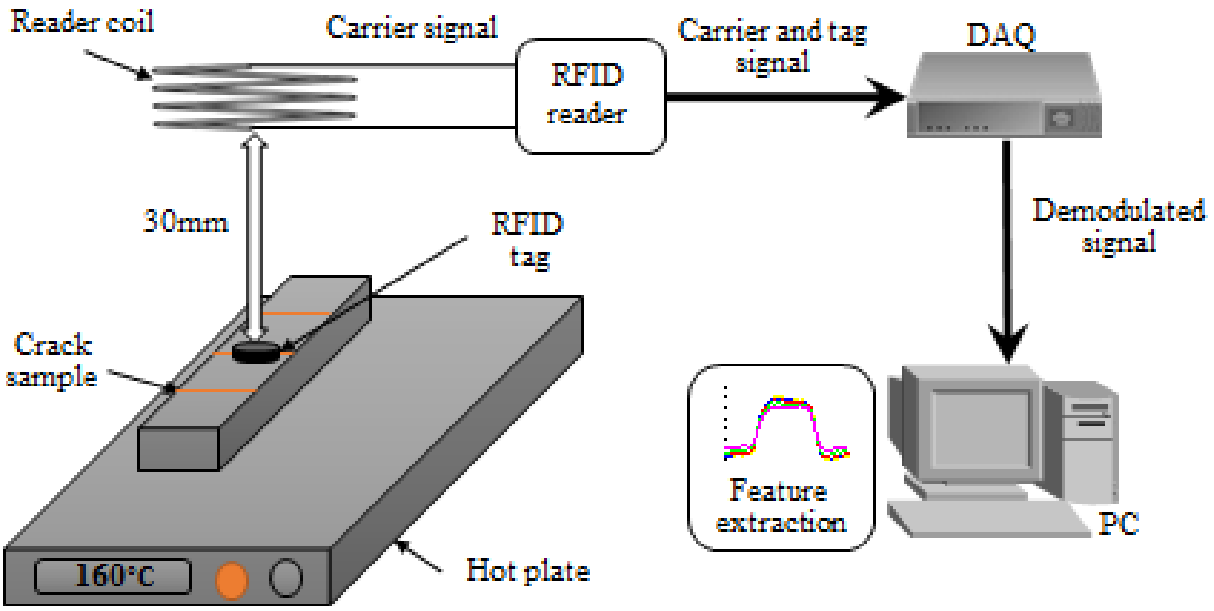

(b)

Figure 5.5: Fabrication of RFID sensing system, (a) RFID system configuration and (b) system diagram with well-established reader and tag configuration

5.2.4 Results and discussion

The envelope of the RFID signal is captured with temperature increment from 25°C to 160°C. Due to the quality factor of the reader coil being lower, the overshoot in the step response casued by limit bandwidth is not apparent. As the carrier frequency is swept, the excitation frequency will match the resonant frequency from the tag causing an increase in the tag's impedance. The sweep frequency technique gives the advantage of selecting various frequency ranges to extract robust information from it. In this case, two frequency points have been have been selected to show positive and negative temperature coefficient and these are 130 kHz (lower frequency region with positive temperature coefficient) and 144 kHz (higher frequency region with negative temperature coefficient) and this is depicted in Figure 5.6 (a) and (b) respectively which shows that temperature variation have significant influence on the tag's response that has been captured by the reader. The variation of the signals can be seen to be complete opposite in these two figures.

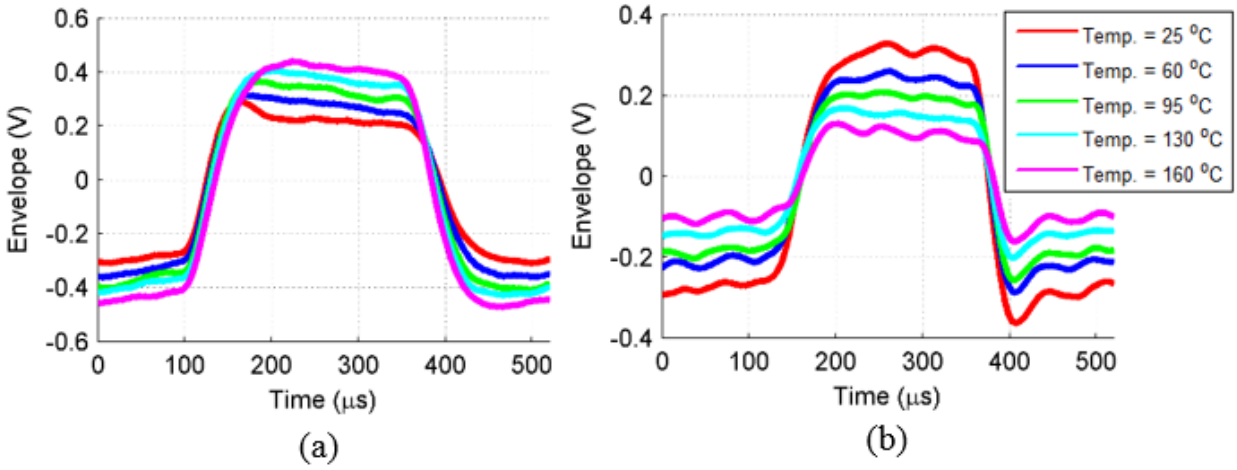

Figure 5.6: Influence of temperature variation on the RFID signal (a) 130 kHz and (b) 144 kHz response

As explained in Section 4 Figure 4.6, the similar time domain feature have been used to do further feature extraction for finding the peak to peak response. The results of feature extraction of the time domain in the swept frequency range are shown in Figure 5.8. The metal effect can be described as the shift in the resonant frequencies of both the reader and the tag towards the higher frequency region compared to the air, showing strong agreement with the sensing principle in Section 5.1.2. There is also changes in the resonance caused due to temperature variation along with the penetration depth variation of the cracks. In Figure 5.8 (a) at 25°C the resonant frequency shift towards the lower frequency region can be obtained with an increase in crack depth. From (b-e), the temperature is incremented at 35°C reaching 60°C, 95°C, 130°C and finally to 160°C respectively.

The figures show the shift in resonant frequency towards the lower frequency region with an increase in both temperature and crack depths but both the crack and the temperature are invariant in the higher frequency region. From Figure 5.7 (a) it can be seen that the maximum resonance of C4 is at 136 kHz whereas in (e) at 160°C the resonance have been shifted at lower than 132 kHz. This is showing the effect of temperature on the resonance frequency. Similarly, at a fixed temperature for example, in Figure 5.8 (b) at 60°C, there is also a decrease in the resonance frequency for all the cracks i.e. as the depth of the crack increases from C0 to C4, the resonant frequency also shifts from approximately 138 kHz to approximately 134 kHz.

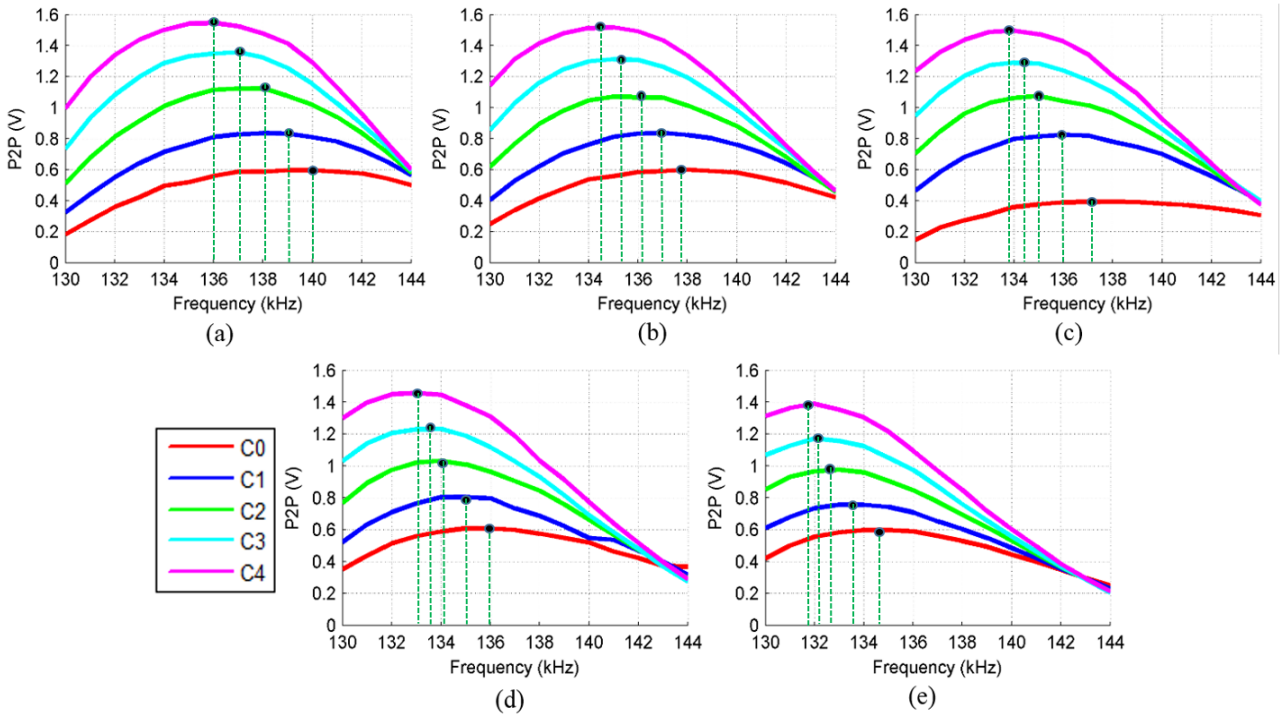

Figure 5.7: Influence of temperature variation on P2P response of the RFID signal. (a) At 25°C, (b) 60°C, (c) 95°C, (d) 130°C and (e) 160°C

At 144 kHz, due to negative temperature coefficient, the P2P decreases with an increase in temperature and so does the magnitude of the crack depth decreases as well. Due to the resonance, we can see that P2P in the frequency region lower than the resonant point has a positive temperature coefficient with crack growth while the frequency higher than the resonant point has a negative temperature coefficient with the crack growth. This is more clearly understood in the following Figure 5.8 where the temperature sensitivity have been calculated using:

$$Temperature\ sensitivity = [P2P(160°C) - P2P(25°C)] \Big/ 135°C \tag{5.5}$$

From the result shown in Figure 5.9 (a) it is evident that the temperature influence is maximum at 139 kHz which is the resonant frequency. Figure 5.9 (a) presents the RFID response for the temperature sensitivity along the crack depth at varying frequencies respectively. At 133 kHz, a near zero temperature coefficient is obtained. At 139 kHz, because it is at resonant frequency, so with an increase in temperature the resistivity of semiconductor decreases and thus reducing the magnitude of the tag's response as described in Eq. (5.3). However, the, magnitude of the tag's response increases with an increase in crack depth due to higher coupling coefficient and an increased quality factor of the tag's coil.

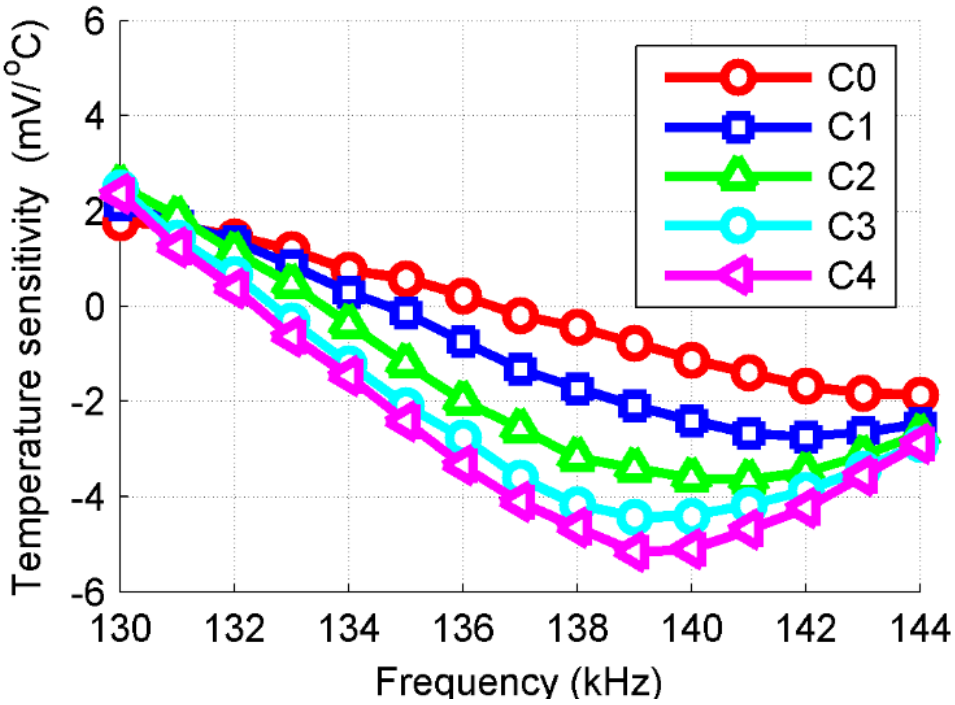

Figure 5.8: Temperature sensitivity under variation of frequencies for crack sample

Figure 5.9 depicts the resonant frequency response for both the crack progression and temperature increment and it can be observed for both the increments, the sensitivity decreases. As it can be seen that these variations are undesirable in NDT&E and SHM as they may be misinterpreted. Any changes in the environmental condition which is temperature in this case, may be misread as defect which may ultimately lead to shutdown of industry for unscheduled time as it is an important economic consideration, and therefore, a monitoring method with temperature compensation ability is highly desirable. In order to suppress the temperature influence on the system a feature fusion have been proposed in this section. It was observed that using this fusion of feature best mean have been obtained with lowest error.

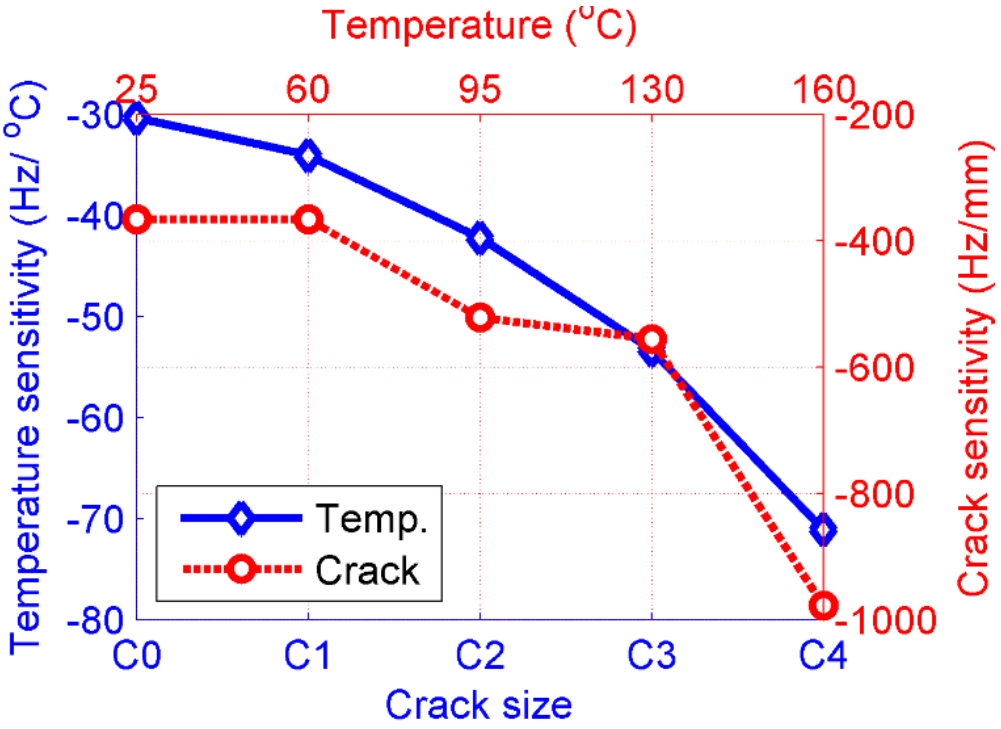

Figure 5.9: Shows the respective temperature and crack sensitivities

The temperature uncertainty for different frequency response and the fusion is shown in Table 5.1.

Table 5.1: Temperature induced uncertainty at different frequency points

Crack (mean ± error)	**SP2P at 130 kHz (V)**	**SP2P at 133 kHz (V)**	**SP2P at 133 kHz (V)**	**SP2P at 144 kHz (V)**	**FP2P (V)**
C0	0.293 ± 0.145	0.458 ± 0.126	0.536 ± 0.103	0.345 ± 0.141	0.638 ± 0.119
C1	0.496 ± 0.168	0.701 ± 0.046	0.731 ± 0.130	0.367 ± 0.190	0.863 ± 0.022
C2	0.743 ± 0.206	0.951 ± 0.034	0.884 ± 0.215	0.337 ± 0.205	1.079 ± 0.013
C3	0.998 ± 0.197	1.176 ± 0.060	1.00 ± 0.274	0.312 ± 0.210	1.311 ± 0.023
C4	1.273 ± 0.196	1.400 ± 0.082	1.06 ± 0.310	0.303 ± 0.218	1.577 ± 0.022

From the table, it is evident that the mean response and the error is the maximum at 139 kHz which is the resonant frequency showing the maximum influence with the temperature variation. Whereas, near zero response shows the lowest variation at 133 kHz. Therefore, this frequency can be selected in order to compensate temperature. The result of this frequency selected compensation is depicted in Figure 5.10 where zero temperature coefficient was obtained and this is named as SP2P since this is the 'Selection of Peak-to-Peak' feature.

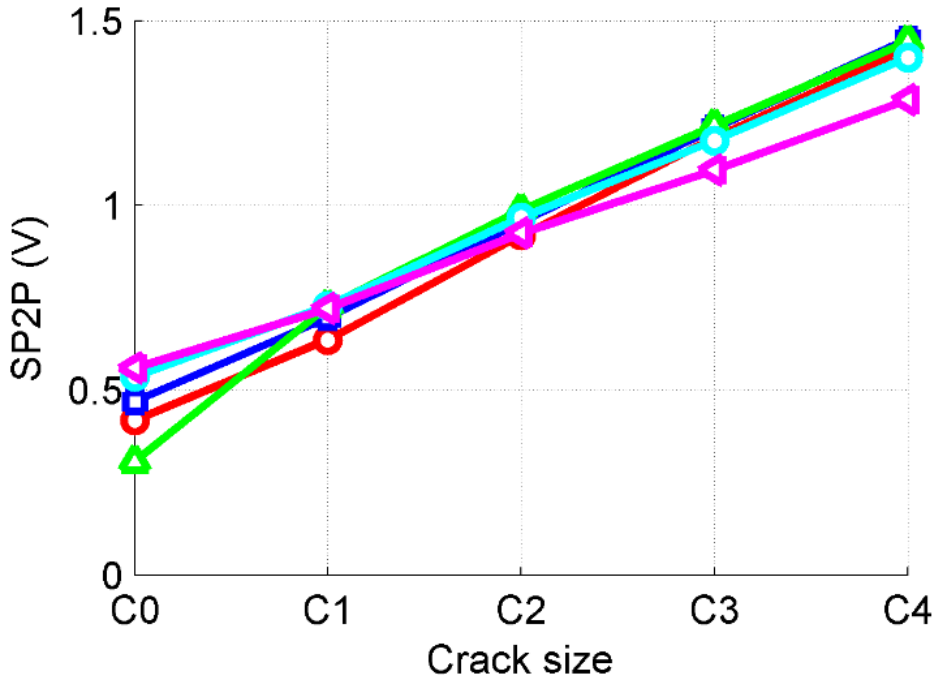

Figure 5.10: Response showing for four different temperatures using selected frequency (133 kHz) at zero temperature coefficient

Furthermore, by the summation of the positive temperature coefficient at 130 kHz and negative temperature coefficient at 144 kHz, we can obtain the lowest error in comparison to the rest of the frequency responses and this is known as the fusion of feature which enhances the robustness even in comparison to 133 kHz by approximately 3 times. This is further depicted in the Figure 5.11.

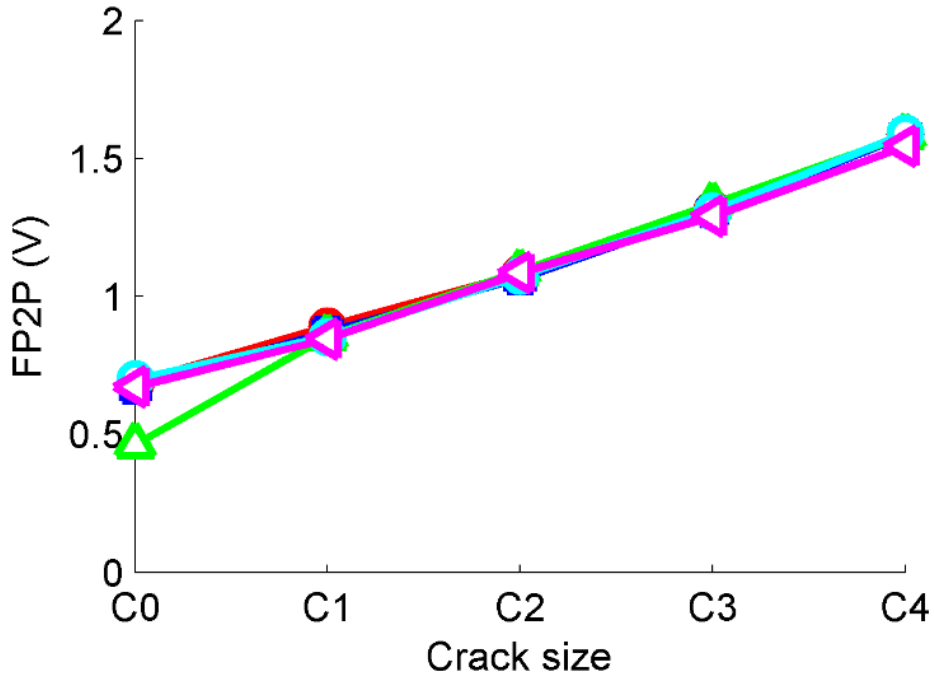

Figure 5.11: Feature fusion for further temperature suppression

Figure 5.10 shows the response at 133 kHz and it can be observed that the crack progression can be easily characterized from the figure but however, there is still a variation in the temperature and for this reason, feature fusion is carried out. Figure 5.11 shows robust temperature independent feature based on a combination of negative and positive temperature coefficients near the resonance region. This is obtained by the summation of both the signals i.e. SP2P at 130 kHz and SP2P at 144 kHz which means by the addition of both the positive and negative coefficients, the temperature influence can be suppressed. However, if only the single frequency is used for the feature extraction, the crack can somehow be detected but the effect of temperature and its influence will still persist. This may result in ineffective crack detection and characterization. The feature is named as FP2P since this is the 'Fusion of Peak-to-Peak' feature, by which the temperature influence is removed while enhancing the sensitivity of LF RFID sensing system for robust NDT monitoring and robust crack progression monitoring by at least approximately 3 times.

5.3 Inhomogeneity study using steel corrosion progression samples

Any variation in the distance between the RFID tag and the sample or any temperature variation, will change the impedance *Z*, inductance *L* and quality factor *Q* with coupling coefficient *k*. The parameters *Z*, *L* and *Q* can be shown as [219]:

$$Z, L \text{ or } Q = f(x, \rho, \mu) \tag{5.6}$$

Where x is the distance between the RFID tag and the sample, ρ is the sample's resistivity and μ is the sample's permeability. Mainly ρ and μ of the measured sample which highly influences the sensing coil. This influence shows the quantification errors which is known as inhomogeneity (electrical run out). Inhomogeneity will muddle the spreading of the eddy currents and generate an effect on the reader output such as noise and thereby demean the resolution. The ρ and μ in steel corrosion samples are different to that of the ρ and μ in the aluminium crack samples. As mentioned in Section 4, proposed transient method has been used to characterize the magnetic permeability variation which is caused by variation in corrosion level. However, in this case study, the peak amplitude with resonant frequency shift for steel corrosion sample is considered and then the proposed feature fusion technique is implemented to reduce the effect of inhomogeneity which would further prove the robustness of this technique for all kinds of ferrous and non-ferrous materials having complex defects.

An increase in the excitation/oscillating frequency can reduce the influence of the resistivity of the sample. The effect of inhomogeneity is monitored at different oscillating frequency for the corrosion progression samples. The measurement is taken from 117 kHz to 127 kHz with increments of 1 kHz. From Figure 5.12, it is evident that the inhomogeneity in ferrous materials (steel) is higher than that of the non-ferrous materials (aluminium) as shown in Figure 5.7. One of the main influences is due to the higher resistivity ρ and permeability μ in steel corrosion samples compared to aluminium sample. For proving the concept and the feasibleness of the fusion technique, only four temperature variation have been considered in this case.

The resonance frequency of the RFID tag can be seen to be shifted by about 10 kHz from aluminium to steel sample. It is clear that the conductivity influence is higher than that of the amplitude change, therefore, in order to reduce uncertainty in the measurements of the RFID that is caused by the inhomogeneity, electrical conductivity must be reduced. However, using the proposed fusion technique where the positive and the negative temperature coefficients are added together, these influences can be vanquished. Figure 5.13 shows the temperature sensitivity over the range of frequencies for all the corrosion samples. The temperature sensitivity is obtained using the same Eq. shown in (5.6). It can be observed that even though the variation in corrosion levels cannot be differentiated at any given frequency, but using the fusion feature technique, the corrosion progression level can still be identified. Each of the month's corrosion progression is denoted as Mn where n is the number of months for the progression.

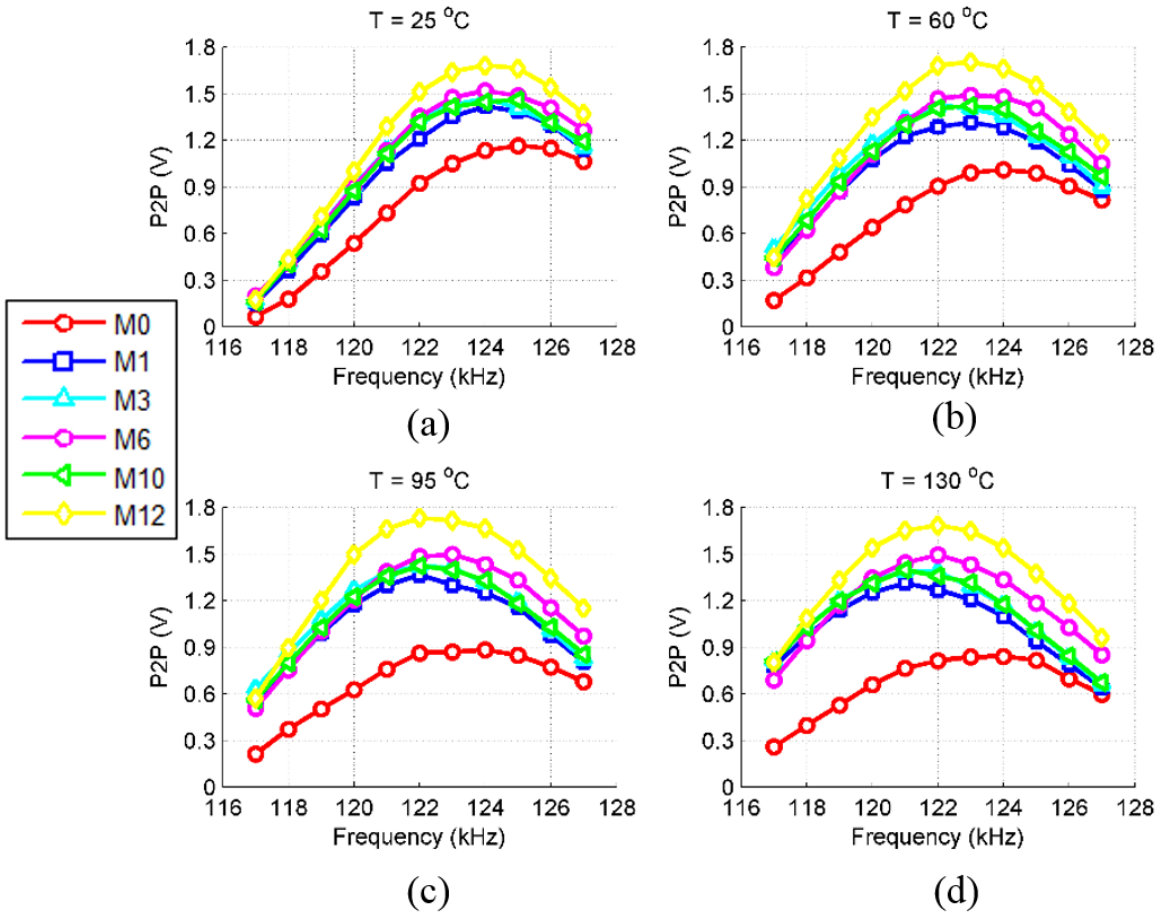

Figure 5.12: Influence of temperature variation on P2P resonant frequency response for corrosion progression samples at (a) 25°C, (b) 60°C, (c) 95°C, (d) 130°C

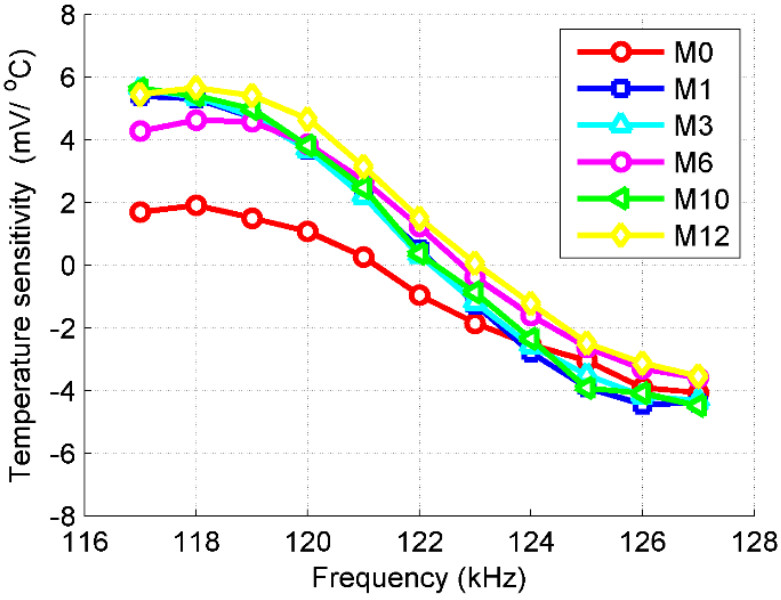

Figure 5.13: Temperature sensitivity under variation of frequencies for corrosion sample

From the response it can be seen there is a sharp drop in the thermal sensitivity with the increase in the frequency because with the increase in temperature the resistivity of semiconductor decreases and thus reducing the magnitude of the tag's response. The sensitivity is reduced from nearly 6 mV/°C to -4 mV/°C which is approximately about 10 mV/°C. Further resonant response with the four varying temperature is shown in Figure 5.14.

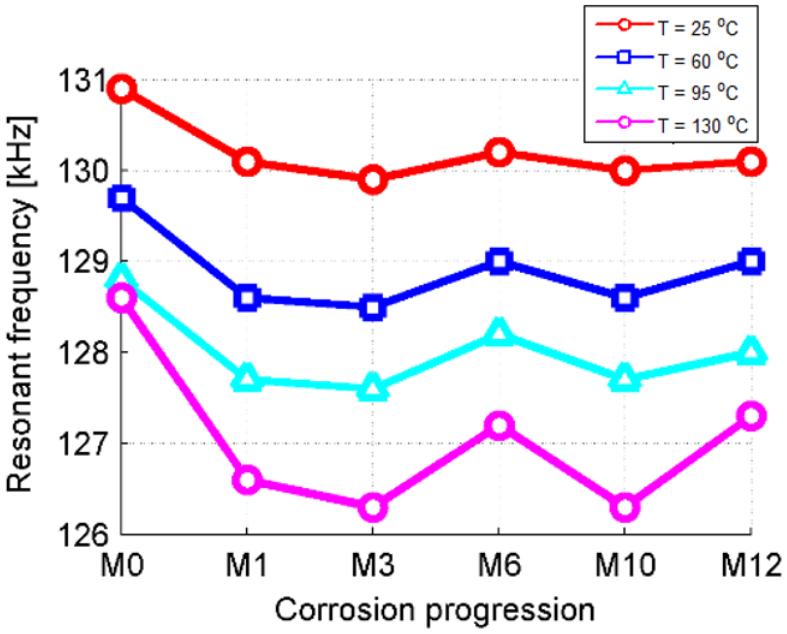

Figure 5.14: Resonant frequency response for varying temperature

In comparison to the crack samples resonant response shown in Figure 5.10, the changes in resonant frequency behaviour with respect to varying temperature is slightly different. In this case, the variation of resonant frequency with an increase in temperature still reduces. However, the corrosion progression behaviour with resonant frequency is not monotonic and this is because the variation in thickness due to metal loss as per the corrosion samples are very negligible which makes it even harder to characterize them. Using the feature fusion technique, this would be characterized and is shown in Figure 5.15.

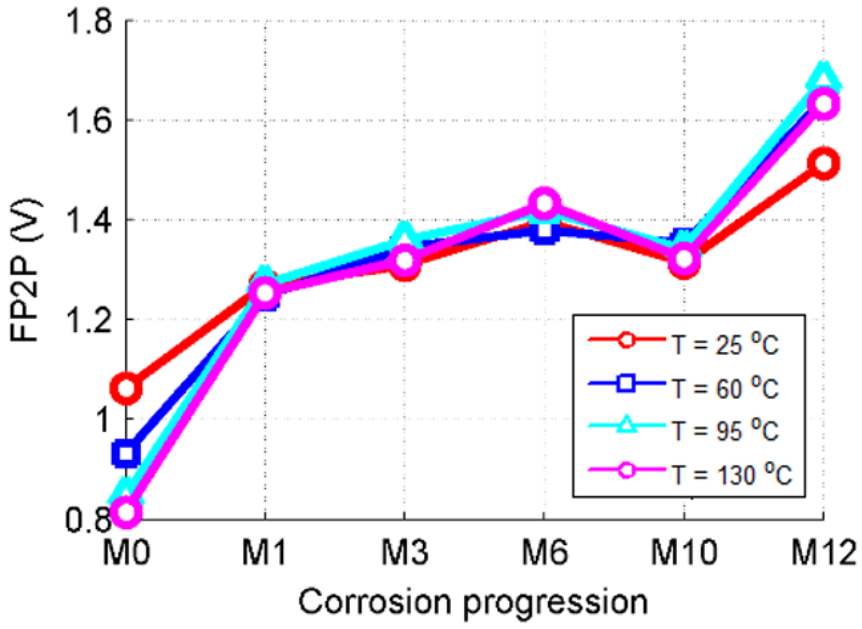

Figure 5.15: Temperature independent corrosion progression characterization using feature fusion

From the trend shown in Figure 5.15 as compared to Figure 4.9, the robustness of the technique can be confirmed. An increase in the thickness of the corrosion means, a depletion in the electrical conductivity and permeability of the corroded region. Though this is the signal processing method that can be implemented for practical use but industry seeks more feasible method for reducing temperature fluctuation in terms of RF techniques. Therefore the following section will focus on improving the RFID sensing performance using a new ceramic filled substrate.

5.4 Thermal reduction and system robustness improvement using ceramic substrate

For field application, sensing stability against environmental temperature change is crucial. Based on the findings in Section 5.3, it can be inferred that RFID sensing system using swept frequency and feature fusion is an effective method to minimize the temperature fluctuation and can be used for SHM. However, in SHM system, there are also other types of sensors used side by side with RFID system which are usually deployed for long-term monitoring. Therefore, an advanced solution is essential from the sensing side itself where the sensing data can be directly extracted from the deployed sensors without further complex feature extraction. Hence, in this section, thermal effects on the RFID sensor performance are explored using ceramic filled poly-tetra-fluoro-ethyulene (PTFE) substrate.

For the proof of concept, both with and without ceramic filled PTFE substrate have been used on RFID tags to understand the behaviour of temperature fluctuation and corrosion

characterisation. To ameliorate the sensing performance under varying temperature conditions, the ceramic filled PTFE substrate material Rogers RT/duroid 6202 [220] is attached to the RFID tag as shown in Figure 5.16.

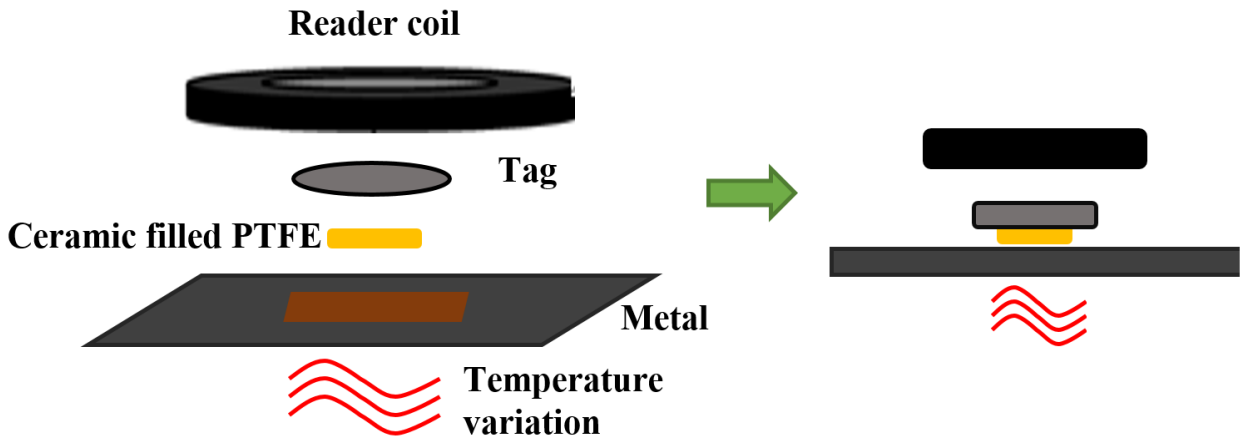

Figure 5.16: RFID system setup using ceramic filled PTFE

The tag, ceramic substrate and the steel corrosion sample are modelled in COMSOL to show if the ceramic blocks the detection capability of corrosion or not. This simulation result is compared to the results obtained in Figure 4.11 (a) in Section 4 which is modelled without any substrate. The model without any substrate showed a magnetic flux density of 9.833×10^{-7} T as can be seen in Figure 4.11 (a). Keeping all the parameters same, only the ceramic substrate of 15mm of diameter is attached to the tag (26mm). The substrate diameter is kept short and centred so that more magnetic field can be drawn and focused on the area underneath the tag. The simulation results is shown in Figure 5.17. It can be seen that with the addition of the ceramic substrate, the change in magnetic flux density is only about 1.6% increase i.e. 9.992×10^{-7} T. This result confirms that further experimental data based on the ceramic filled substrate would not block the corrosion sensitivity but rather minimize temperature influence as the substrate has a thermal conductivity of 0.68 W/m/K and a dielectric constant ε_r of 2.9.

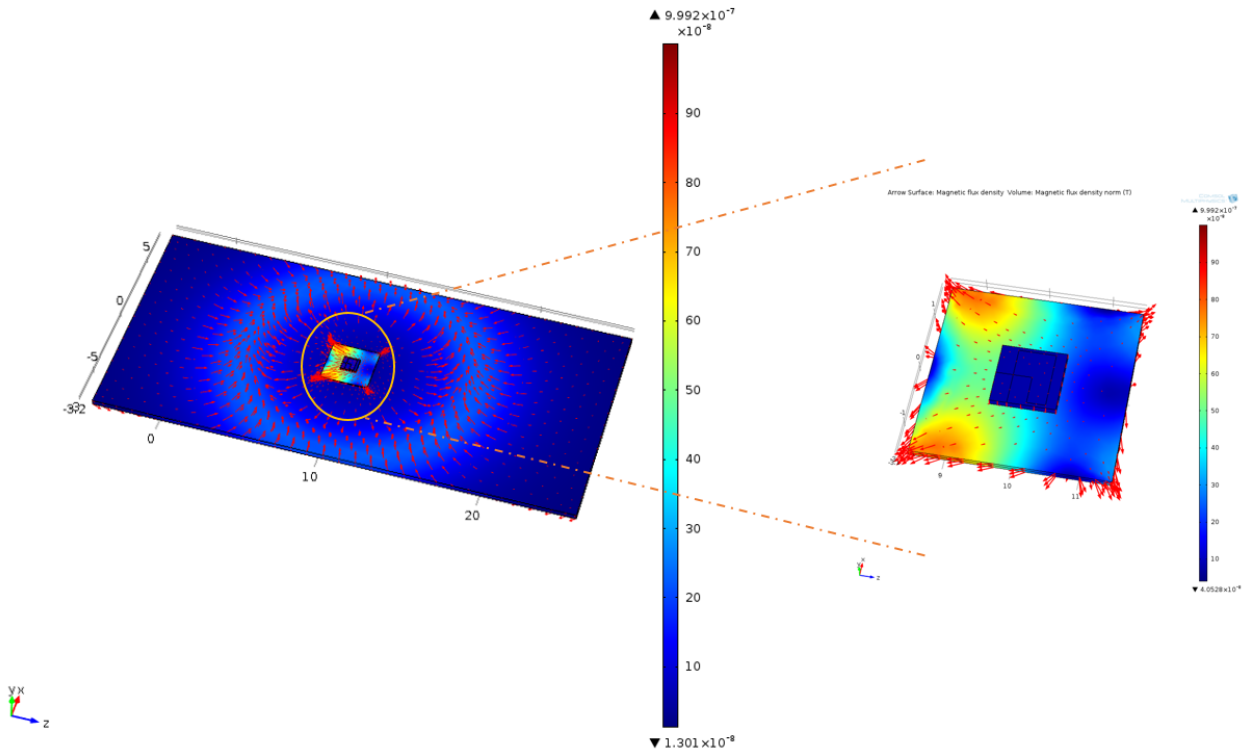

Figure 5.17: Model without ferrite sheet showing a magnetic flux density of 9.992x10-7 T

From the results shown in Figure 5.18, first noticeable thing is the huge shift in the resonant frequency. In Figure 5.13 for without any substrate the peak resonance was mainly obtained near about 122 kHz to 125 kHz, however, for Figure 5.19 it can be seen that the peak resonance is mainly near about 127 kHz to 130 kHz. But one of the major benefit is that the resonance frequency shift due to temperature fluctuation is much lower. The temperature sensitivity is obtained using the Eq. (5.6). The temperature sensitivity for ceramic substrate is shown in Figure 5.19.

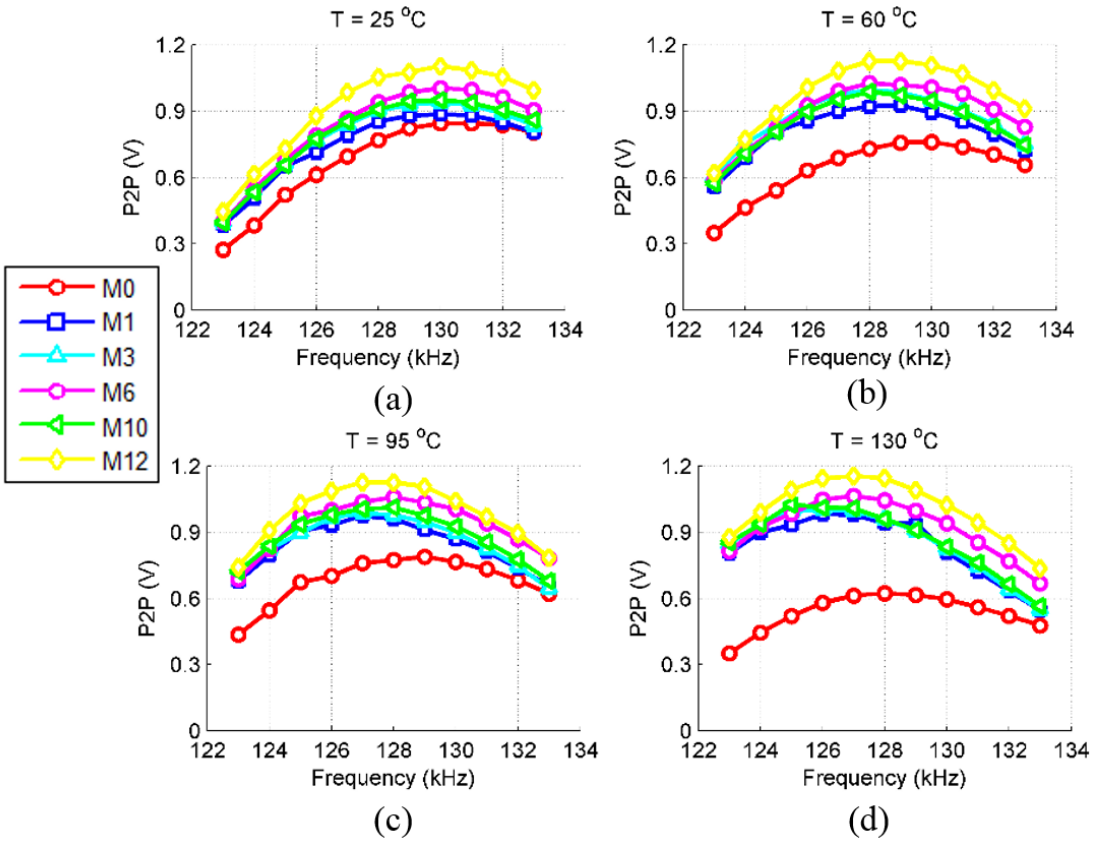

Figure 5.18: Influence of temperature variation on P2P resonant frequency response for corrosion progression samples with ceramic filled substrate on RFID tag at (a) 25°C, (b) 60°C, (c) 95°C, (d) 130°C

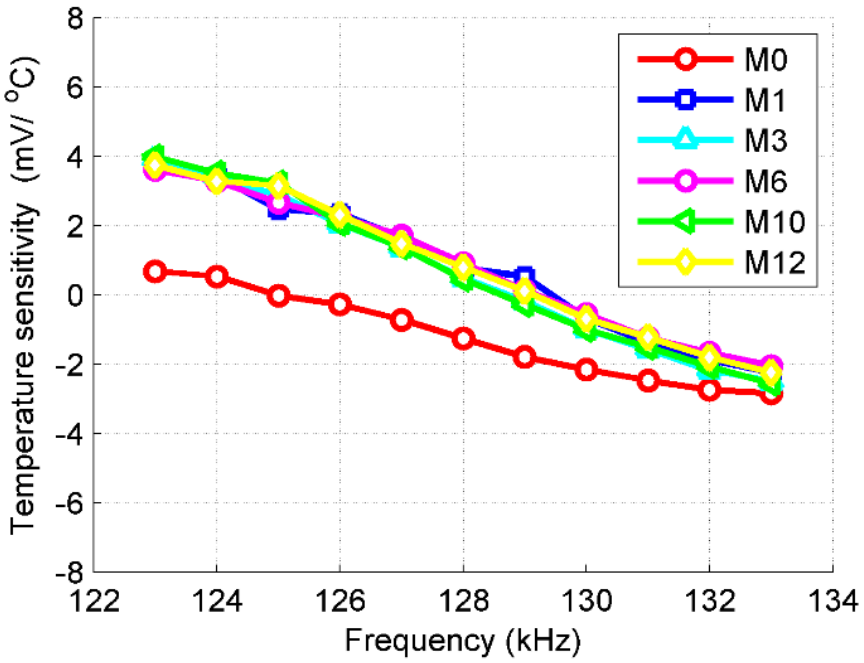

Figure 5.19: Temperature sensitivity under variation of frequencies for corrosion sample with ceramic substrate

From the response it can be seen there is a sharp drop in the thermal sensitivity with the increase in the frequency but in comparison to Figure 5.13, where the sensitivity drop was approximately 10 mV/°C drop, here after the usage of ceramic filled substrate the temperature sensitivity is improved from nearly 4 mV/°C to -2 mV/°C which is approximately about 6 mV/°C, so the improvement is about 40% after using the ceramic substrate. Further resonant response with the four varying temperature is shown in Figure 5.18. Since the temperature influence is already reduced, therefore, only frequency selection feature at the zero temperature coefficient provides good enough result to suppress the temperature fluctuation and characterize corrosion. This is shown in Figure. 20 where SP2P is the 'Selection of Peak-to-Peak' feature which is this case is 129 kHz as it can be seen from the Figure 5.19, that at 129 kHz is the near zero temperature coefficient.

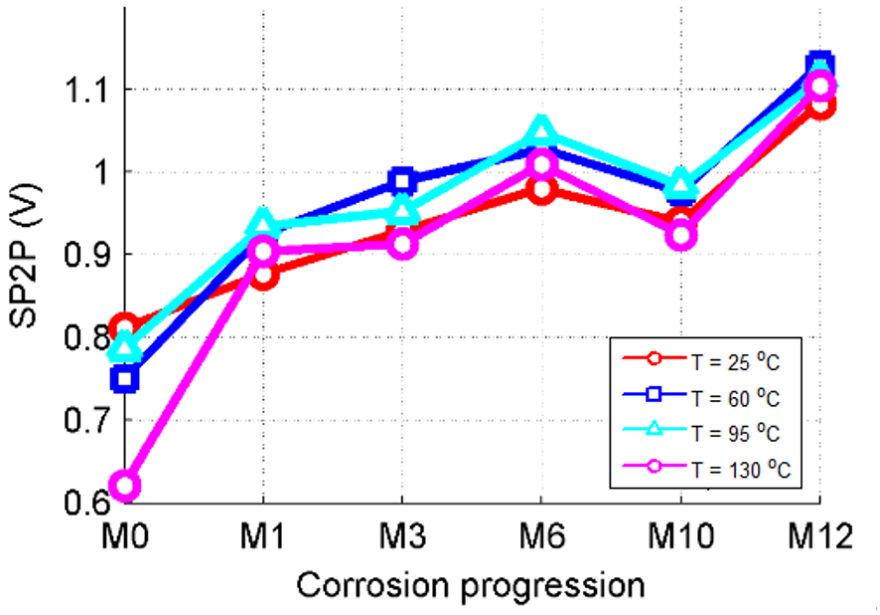

Figure 5.20: Temperature independent corrosion progression characterization using ceramic filled PTFE substrate

5.5 Chapter summary

In practical situation, the unknown temperature variation will give rise to uncertainty and unreliability, affecting the robustness in defect detection and characterization using LF RFID sensing system. Therefore, this chapter addressed the use of a new feature technique known as feature fusion method to solve this problem. Through a sweep frequency measurement, negative and positive temperature coefficients in the left and right side of tag's resonant frequency are reported in this paper. Fusion method involves the summation of both the negative and the positive temperature coefficients to extract the defect information. This phenomena is used to

compensate the uncertainty caused by the temperature variation in both crack and corrosion characterization.

Next, due to the effect of inhomogeneity and the complex multi-layered structure of the corrosion samples, further quantification of magnetic permeability and electrical conductivity required addressing. Therefore it was worth considering and exploring the RFID measurements in order that multiple parameter estimation can be achieved (corrosion progression and crack depth) with an extension to permeability and conductivity estimation as well and hence feature fusion have been used to suppress the temperature influence and effectively characterize corrosion progression.

Also, for practical usability and further sensing deployment for long term monitoring, Rogers 6202 ceramic filled PTFE was proposed on which the future RFID antenna could be fabricated in order to minimize the influence of temperature. As a proof of concept, the last case study carried out in Section 5.4, showed the potential of ceramic substrate attached to LF RFID sensor to further improve the temperature sensitivity and reduce the fluctuation by about 40%. These potential uses of passive LF RFID sensing system demonstrates the prospect of connecting the gap between the NDT&E and SHM.

Chapter 6. Lift-off mitigation and defect detection on steel pipeline under insulation

In the previous sections, the samples were pre-prepared with a certain surface corrosion level that was already known and also the lift-off between the tag and the reader was adjusted beforehand in order to match the impedance. In this chapter, a more realistic experimental study has been conducted. In this section, a steel pipe have been subjected to various defect depths for testing. To improve the robustness of the low-cost LF passive wireless RFID sensing system, feature fusion and extraction have been presented that can automatically mitigate the influence of lift-off variation between the tag and the reader. Finally based on the proposed lift-off mitigation method, defect detection have been carried out on the steel pipeline at varying temperature. The factors that made the study more realistic are the high temperatures experienced by the tags and the surface curvature of the pipe which restricts the types of tags that can be attached.

6.1 Effect of lift-off variation

The influence of the lift-off distance and other interferences such as the environmental conditions, surface roughness of the samples and the response from the circuit are all mixed up in the time domain which requires separation. In the PEC technique, the lift-off influence have been removed partly through the normalization method of the transient responses [221]. In LF RFID, sensing and communication are a contradiction where both of these work in the near field region. Sensing is based on the MRC while the communication is based on the magnetic inductive coupling. From the communication range point of view, higher quality factor leads to narrow bandwidth which limits the data rate whereas from the sensing point of view, higher quality factor means improved effectiveness of the wireless power transfer between the reader and the tag. Therefore, this chapter will look into improving the robustness of the system using the feature extraction without affecting the sensitivity.

6.1.1 Sensing principle

The theory behind using a coil to detect defect can be equivalent to the complex method used in reference [222]. The magnetic field produced by the sensor generates eddy currents in the targeted sample which in turn generates a secondary magnetic field that opposes the initial one which results in a magnetic coupling appearing between the sensor and the target. As the targets position is moved, the parasitic series resistance of the sensor moderately decays. This can be

described using the Lenz's law where moving the target means a little secondary magnetic field is produced and therefore small amount of eddy current or lesser dissipated energy [223]. This reduction in mutual inductance means an increase in the wire's inductance. The sensing principle can be described in Figure 6.1.

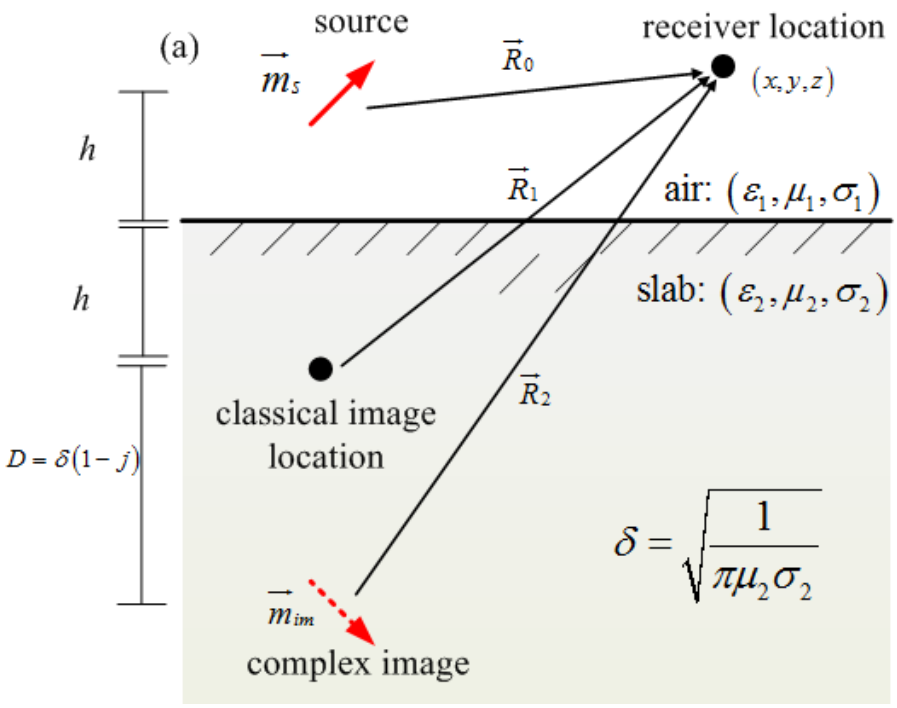

Figure 6.1: Sensing principle of RFID over a conductive slab

Considering the wire length l, height h above a perfectly conducting screen, the mutual inductance can be shown as [224]:

$$M_{p12}^{wire/screen} \approx \frac{\mu_0}{2\pi} l\left(\ln\left[\frac{l}{h}\right]-1\right) \tag{6.1}$$

where the approximation is good for $l >> h$. Through complex image method for a conductive slab, h can be replaced by $h + D$, where D is determined by the penetration depth (shown in Figure 6.1). The impedance of the wire can also be represented as the following:

$$Z_p^{wire/slab} = R_1 + j\omega\left(L_{p11}^{wire} - M_{p12}^{wire/slab}\right) \tag{6.2}$$

The sensing information is contained in the mutual inductance of $M_{p12}^{wire/slab}$. Through an integral over the whole length of the wire, its input impedance can be obtained as $Z_p^{wire/slab}$. In parallel connection between the capacitor and the resistor, the inductor can form an RLC resonance circuitry. The equivalent circuit here is similar to the one used in Figure 5.2. In simulation

shown in Figure 6.2 is implemented by the change of the resistive load of R_{LX} . Any presence of defect such as either corrosion or crack on the target surface will cause a change in the impedance. The basic principle of the RFID sensing system is already discussed in Chapter 3 as it relies on the detection of the changes in the capacitance, resistance or inductance of the tag in response to the parameter of interest such as corrosion or crack. This is done by observing the resonant frequency, input impedance or the Q-factor of the system through the tag response in the reader system. This theory is thoroughly explained earlier followed by equations in section 3.1 equations (3.9-3.11).

It is already known, that, in general RFID sensing system can only get single frequency information using the reader which is fixed to a frequency. These types of RFID sensing is suitable for in-situ monitoring. This section also uses the sweep frequency reader that has been developed and used in Section 5. The sweep frequency will provide the system resonance behaviour for robustness enhancement. The system resonance behaviour is observed in Figure 6.2 which shows that the resonance frequency is independent of the mutual coupling (or communication distance) between the tag and the reader. In this simulation, it is assumed that there is negligence coupling between the reader and the metal surface.

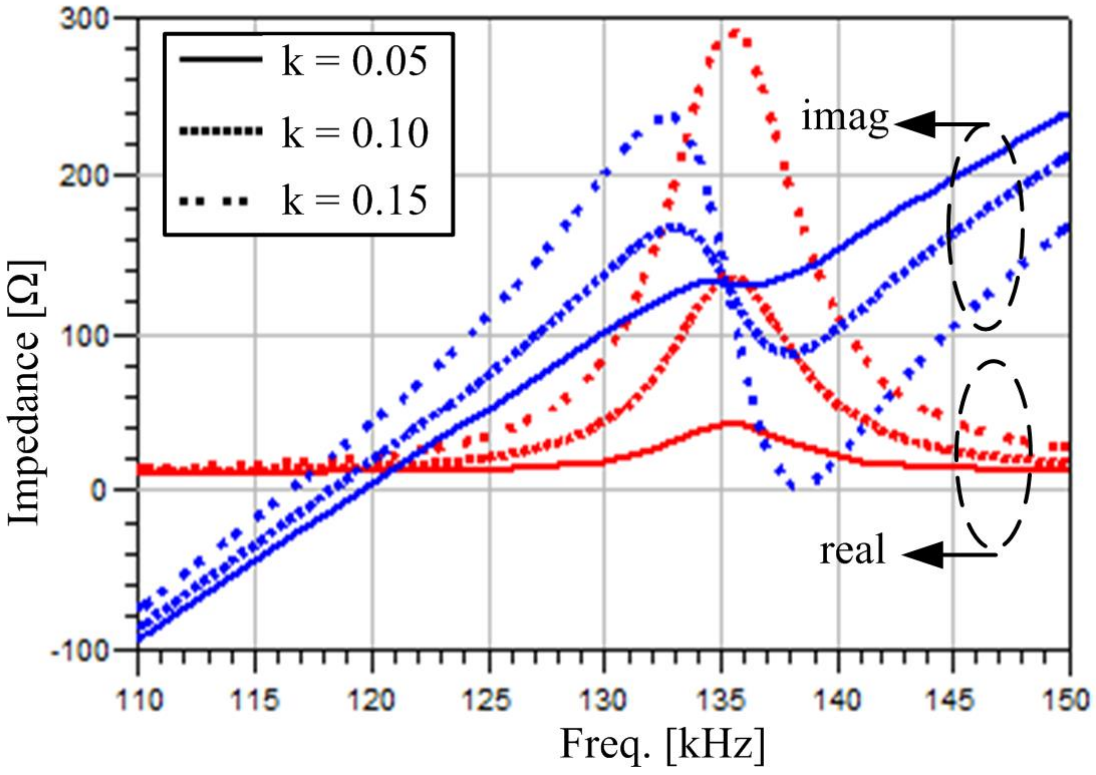

Figure 6.2: System behaviour for interrogation of LF RFID system

6.1.2 Feature extraction and selection of feature fusion

The data processing technique that is used in this section is shown in Figure 6.3. In general, the features of ΔZ_{mx}, ΔQ, Δf_s in (5.9 - 5.11) can be extracted from tag's response in the reader to characterize the physical parameter of interest. The first feature, ΔZ_{mx}, is dependent on Δk, which means that in the signal acquisition, the communication distance may influence the sensitivity. This can be mitigated using either ΔQ or Δf_s, which is relying on the perturbation of the flaw on the inductance, capacitance, or resistance of the coil.

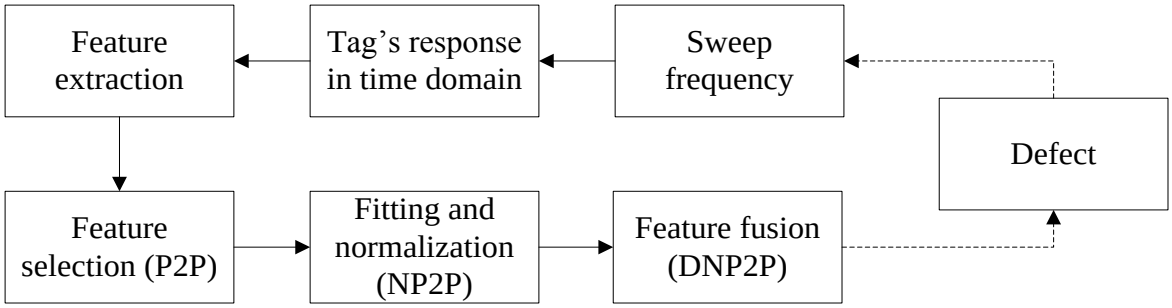

Figure 6.3: Time-frequency feature extraction and fusion technique

By sweeping the source frequency of the reader, the impedance variation can be indirectly measured through P2P feature when the amplitude of the source is constant. To minimise the influence of the mutual coupling (k) along with the noise, the P2P feature is first fitted using the polynomial curve fitting technique and then normalized to its maxima (i.e. the resonant frequency point) over the swept frequency range. This normalization is followed by the fusion procedure where the differential is taken from both sides of the resonant point i.e. the lower frequency ranges and the higher frequency ranges. This will further improve the robustness of the proposed fusion technique.

6.1.3 Sample and Experimental setup

The experimental setup used in this section is similar to the one in Section 4.4 along with the description. The tag that is used is the same as the tag shown in Figure 5.1 i.e. Volcano 231 LF RFID tag that resonates at 135 kHz. The ID which is programmed in the tag are all '1's' at a data bit rate of 32nd of source frequency.

The material of the defect sample is aluminium which has a conductivity 25.8 MS/m and a geometrical dimension of 210 mm × 50 mm × 12 mm. The detailed explanation and the depiction of the sample can be found in Figure 5.5 in Section 5.2.2. The experiment was carried out at 3 different communication distances: L1 = 20 mm, L2 = 30 mm, and L3 = 40 mm. The

selection of communication range is also a trade-off between communication and sensing. The block diagram is shown in Figure 6.4.

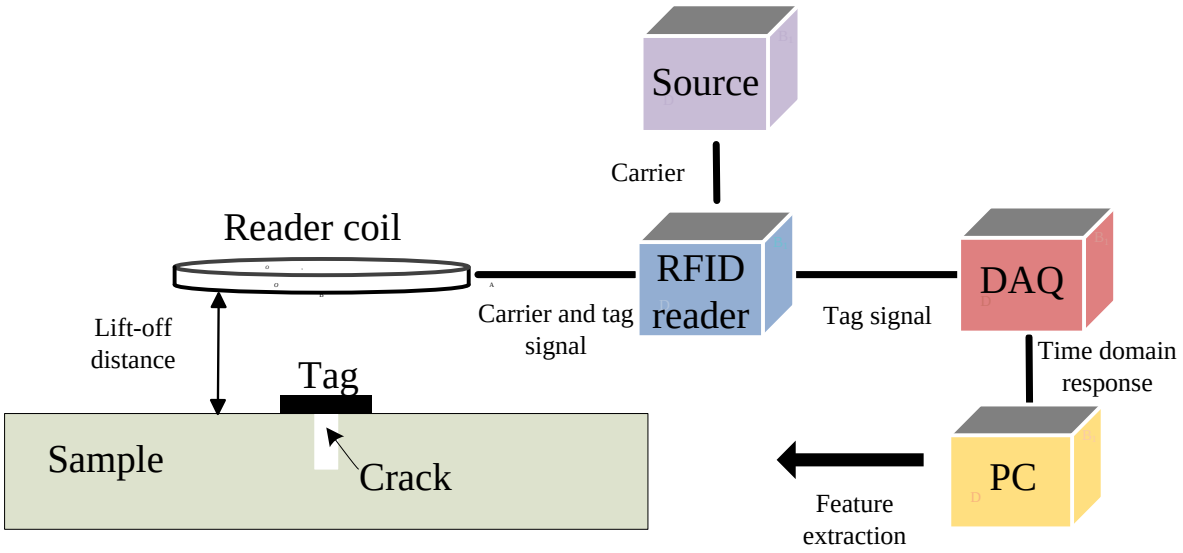

Figure 6.4: Block diagram for the RFID sensing system for crack detection

This selection of the communication range is considered to be a compromise between the sensing and the communication. This is because, at a larger communication distance, not enough power can be received by the tag from the reader to activate the IC within it which will ultimately limit the sweeping frequency. On the other hand, at a shorter communication range, the resonant shift of the reader coil due to proximity of metal cannot be neglected. Therefore an optimal range is acquired to study the behaviour system.

6.1.4 Results and Discussions

Firstly, the response of the tag is acquired at different crack depths on the aluminium sample and these responses are depicted in Figure 6.5.

From the responses, it can be easily observed that cracks have a significant influence on the tag's performance which is then wirelessly captured using the reader before any further processing can take place. The responses were taken at L2 distance for depiction of the signal purposes. Due to the reduction in the Q-factor of the reader coil, the overshoot due to the limit bandwidth of the reader is not apparent. The influence is suppressed using normalization and this is shown in Figure 6.6.

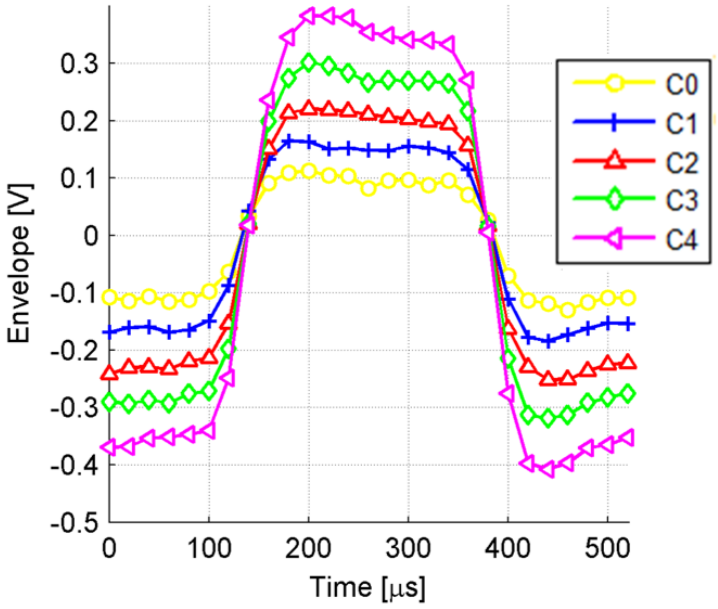

Figure 6.5: Tag's response at 135 kHz on different crack depths

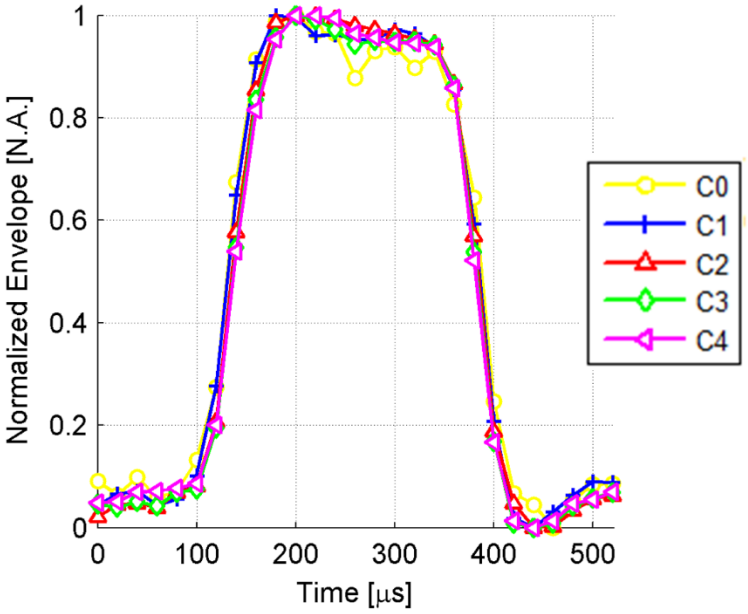

Figure 6.6: Tag's response at 135 kHz on different crack depths after normalisation

From the normalized signal shown in Figure 6.6, the P2P feature is selected which is used to extract and characterise the crack information. The results for feature extraction of the time domain in the swept frequency range are depicted in Figure 6.7. It can observed from the figure that the influence of the crack to the P2P feature is more than that of the communication distance in this particular case. As agreed on the sensing principle mentioned in the earlier sections, both the resonant frequency of the reader and the tag shifts towards the higher frequency region compared to the situation in the air. These resonance shifts are due to the different crack depths and the varying communication distance. From Figure 6.7 (a-c), shift in the resonant frequency

can be seen to the lower frequency region when the crack depth increases thus increasing the P2P. Since the tag is placed on the target, so the shift in the tags response is expected to be more than that of the reader. It can be said that the growth of the crack will continuously improve the coupling coefficient between the reader and the tag. This means that the magnetic flux penetrating into the tag coil will be increased. Through normalization to the maxima in the time frequency feature extraction results, we can get the results of NP2P in the swept frequency range, which is presented in Figure 6.7 (d-f).

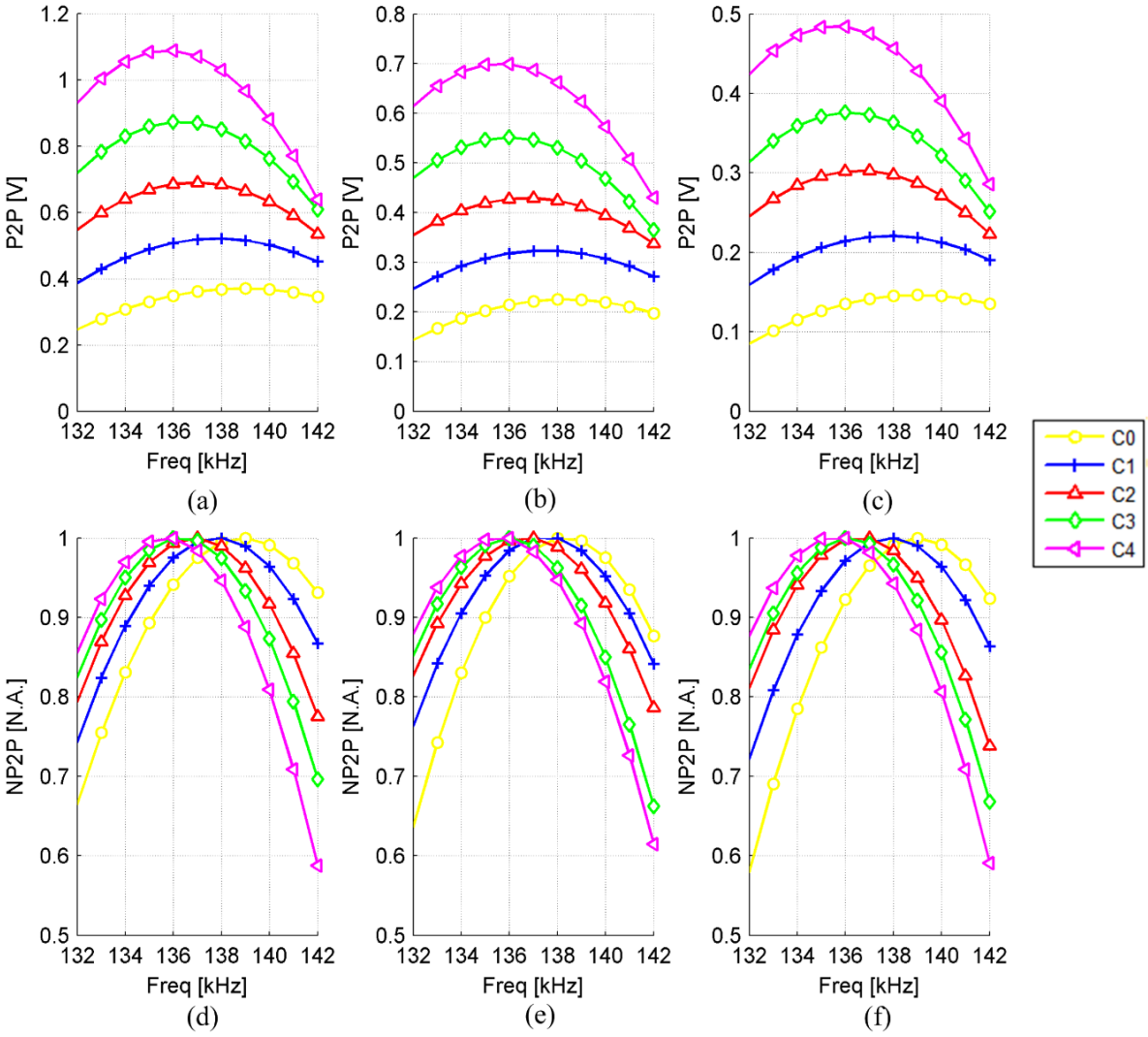

Figure 6.7: Extracted features (a-c) before normalization when the communication distances are L1, L2, and L3 respectively, (d-f) after normalization when the communication distances are L1, L2, and L3, respectively

From the results it can be observed that the communication influence is essentially reduced through normalization. By comparing the C0 in L3 and L1 at the frequency of 132 kHz, we can find the variation of P2P is from 0.08 to 0.25 V (3.1 times) before normalization. After normalization, the variation, however, is from 0.58 to 0.66 (1.1 times). It can also be observed

that NP2P in the frequency lower than the resonant point has a positive coefficient with the crack growth while on the other hand frequency higher than the resonant points has a negative coefficient. These two coefficient responses can be observed in Figure 6.8. Looking at the figure it can be observed that for the Figure 6.8 (a) where the maximum amplitude is showing the highest crack depth C4, on Figure 6.8 (b) the similar magnitude is shown for the lowest crack depth C1. This vagueness near the transition point of the negative and the positive coefficient due to the resonance of the tag makes it difficult for the crack to be differentiated. A single frequency response here would not be able to discriminate between the C1 and C4 from the responses. And ultimately resulting in poor resolution in crack characterization.

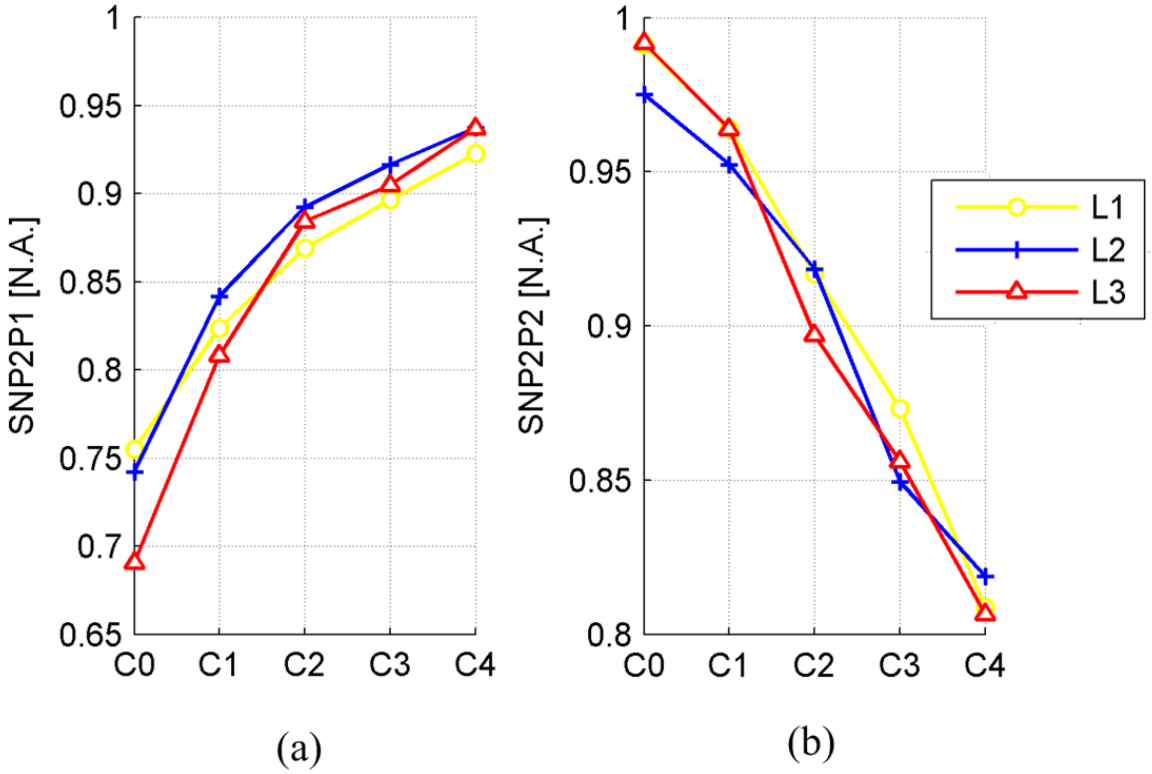

Figure 6.8: Crack characterization at three communication distances: L1 = 20 mm, L2 = 30 mm, and L3 = 40 mm at (a) SNP2P1 = NP2P @ 133 kHz, (b) SNP2P2 = NP2P @ 139 kHz

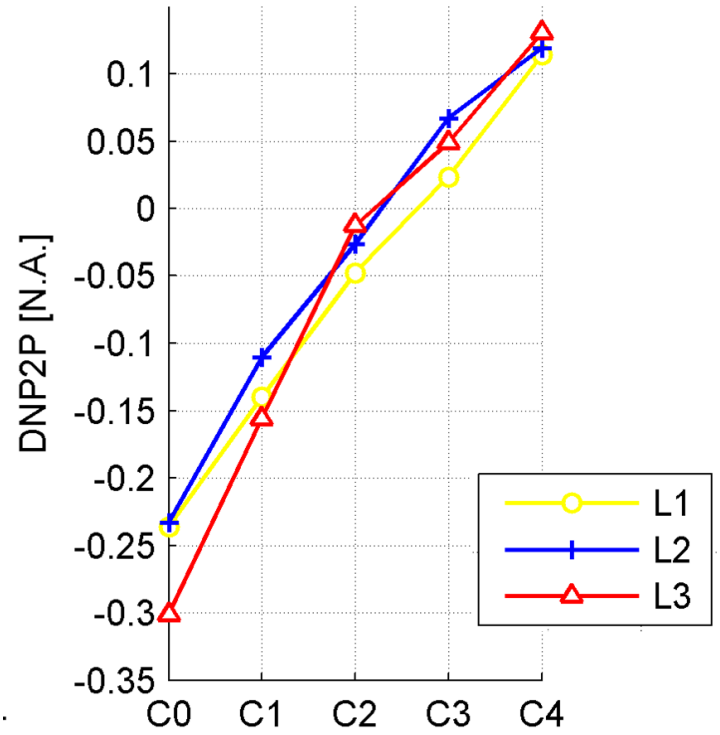

Figure 6.9: Feature fusion technique showing DNP2P = NP2P @ 133 kHz − NP2P @ 139 kHz

To make the crack characterisation more robust, feature fusion technique have been applied in this section. The technique subtracts the responses from the signal at 133 kHz from 139 kHz. By doing this, the influences of the communication distance is further reduced while both the sensitivity and the resolution of the LF RFID sensing system are highly improved. This is further verified in Figure 6.9. From the response it is evident that the subtraction of both the positive and negative coefficients will result in correct characterisation of crack depth detection at variant lift-off distances. This feature is completely invariant to any such lift-off changes making it more applicable for industrial use. It is also worthy of mentioning that the change of communication/lift-off distance is mathematically equivalent to the change of orientation angle of the reader coil, this means, any angular variation can also be suppressed using this feature fusion technique.

6.2 Temperature independent crack monitoring in steel pipeline

The purpose of this section is to replicate an actual field test scenario by testing the steel pipeline sample with several defect types and depths in it. This is to create and experiment which simulates some of the conditions found in actual operation such as curvature structure, under insulation pipelines working at high temperature conditions.

Typical defects on a pipeline are geometrical anomalies, metal loss and crack-like defects. The tests involved a coated 60 cm long sections of steel pipe with 6 cm diameter and 3 mm thickness. The defects on this sample were prepared based on the BSI standards publication [59]. The section is focussing on the depth of the long crack, however, for further characterisation, three different defects were made on the sample and they are long crack of 30 mm length, pit cracks of 10 mm diameter and 5 mm diameter. Crack depths are 1mm, 2mm and 3mm (through hole). This is shown in Figure 6.10.

Three different types of cracks are named as follows: long transverse crack (lc), large pit hole crack (lhc), small pit hole crack (shc) and no crack for reference (ref). The pipe had tags placed at each of these positions and the results were obtained at varying depths and temperatures using swept frequency. The tags were attached on the coated steel pipe surface using high temperature resistant silicone based adhesive. The pipe was covered using calcium silicate insulation.

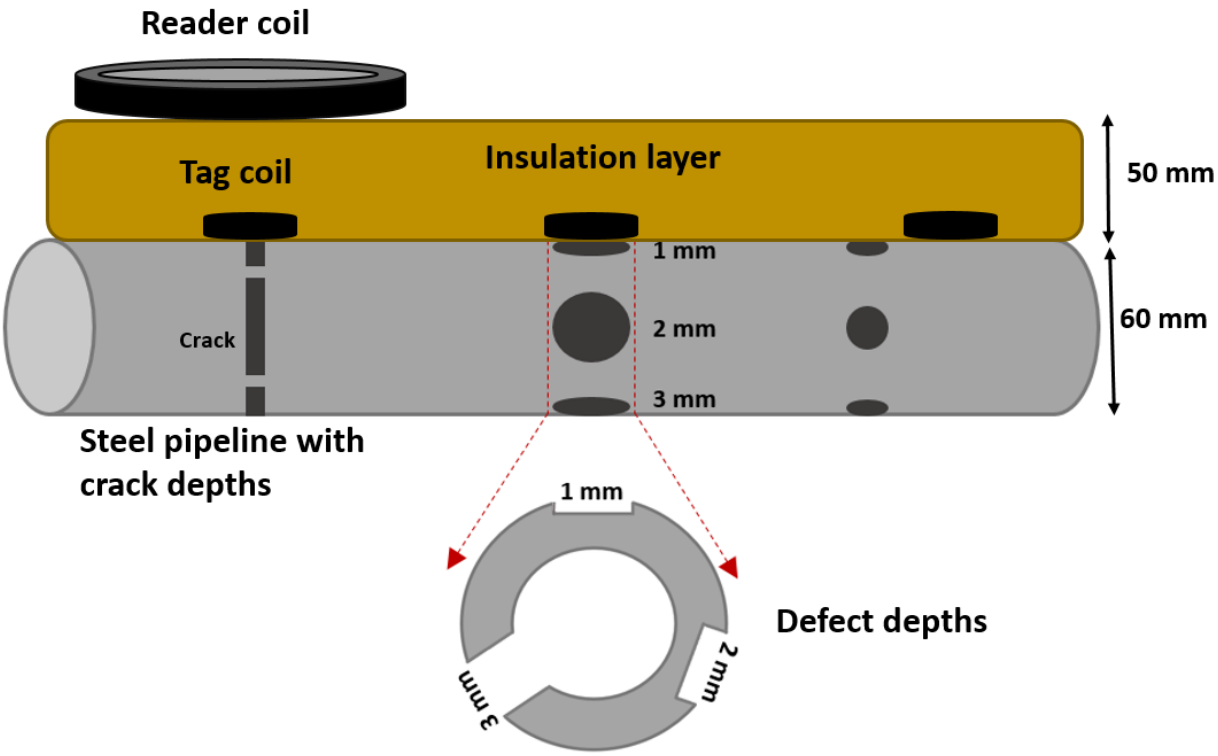

Figure 6.10: Steel pipeline sample with different defects

The experiment was carried out at five different temperatures as earlier which are 25°C, 60°C, 95°C, 130°C and 160°C. These temperature increments were measured using an electric thermometer. The system setup is shown in the Figure 6.11.

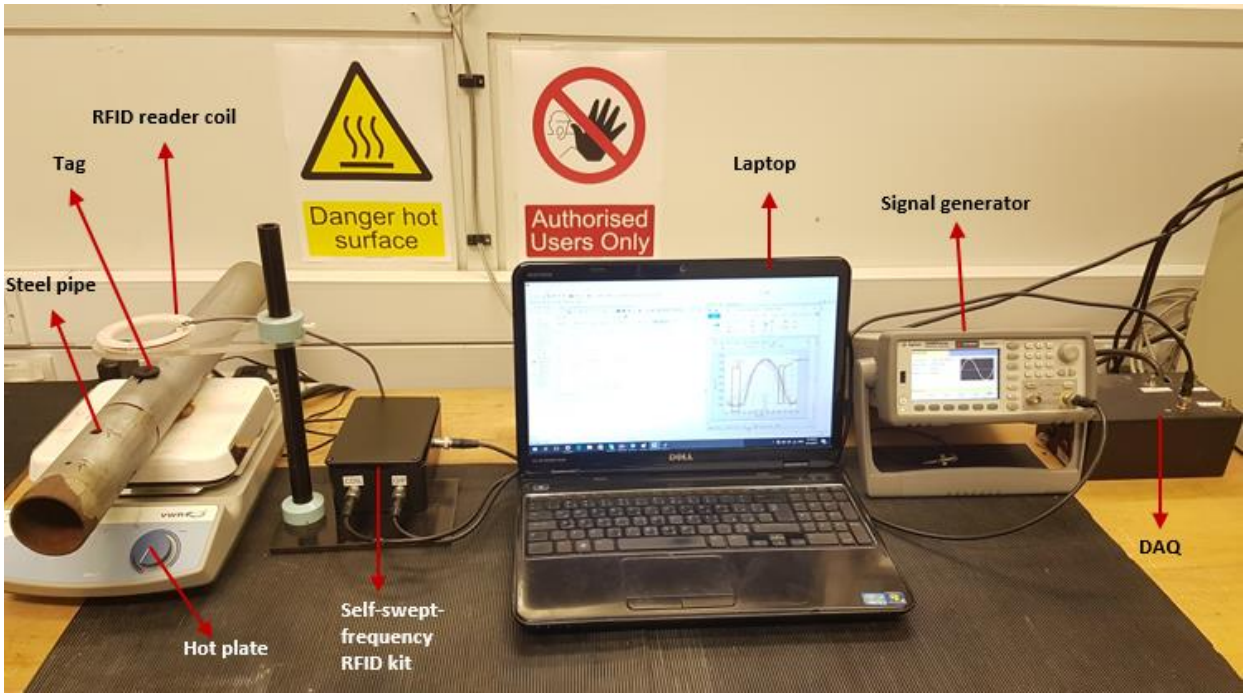

Figure 6.11: RFID system configuration for steel pipeline crack detection at various temperature

The measurements were initially taken at the beginning of the heating cycle with the pipes at room temperature i.e. 25 °C. For equal heat distribution to all the defect positions, the pipe was slanted over the hot plate as shown in the Figure 6.11. Before any measurements could be taken, the section of aluminium foil covering the insulation layer had been removed since no response from the tag could be obtained through it. This is a hurdle for potential field application of the system. In order to tackle this problem, much higher power reader unit may need to be designed. In this experimental work, the output of the RFID reader was sampled at 1 MHz and 10,000 data points. The results on Figure 6.12 shows the RFID signal from the tag with (solid line) and without (dash line) the insulation. This is to see what influence the insulation material plays on the magnitude of the RFID signal. From the response it is evident that the signal response is reduced by at least 2 times under the insulation due to the change in the dielectric properties of the insulation layer. The resonance of the RFID signal response can be seen in Figure 6.13. The blue dashed line represents the signal response without insulation and the red solid line represents the response with insulation.

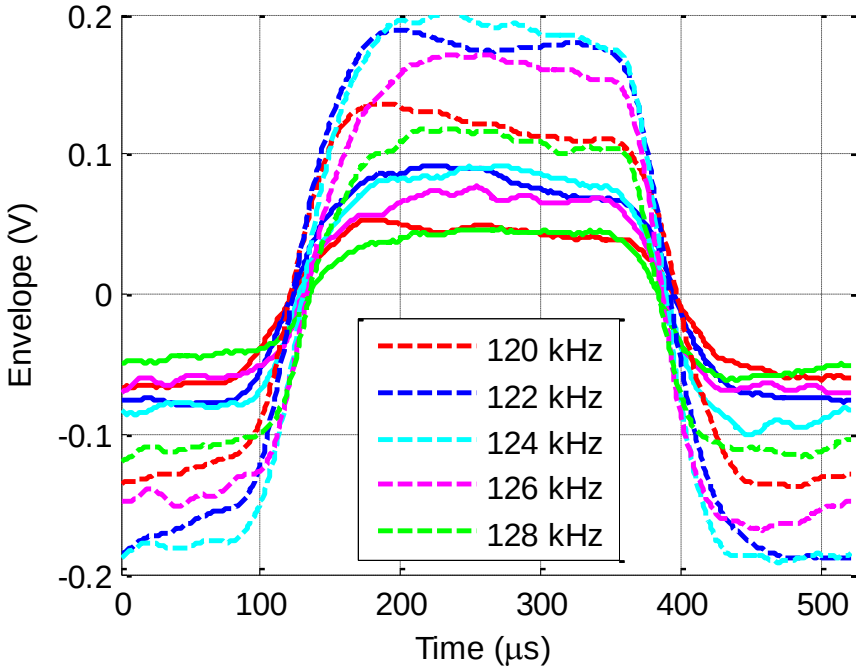

Figure 6.12: Envelope of the RFID signal with (solid line) and without (dash line) the insulation layer

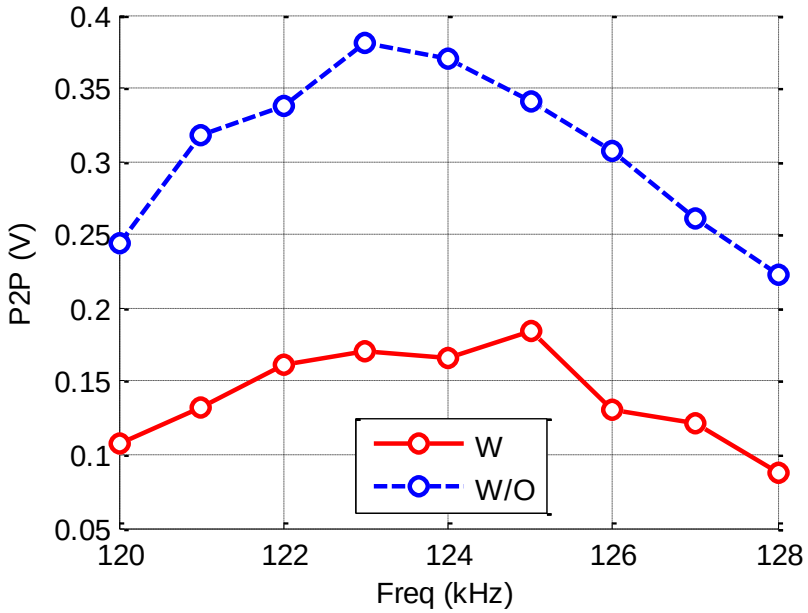

Figure 6.13: Resonant frequency response of the RFID signal with and without insulation

One of the observations were made during the experiment is that when the tag was placed on top of different cracks, the shape of the signal varied with varying frequency responses. Therefore, in this experimental work, the responses were taken from the near zero temperature coefficient i.e. 119 kHz. Due to the complex nature of the crack on the pipeline and the size of the tag, it was estimated that the responses would be difficult to differentiate and hence the response showed similar case. The temperature coefficient can be seen in Figure 6.14.

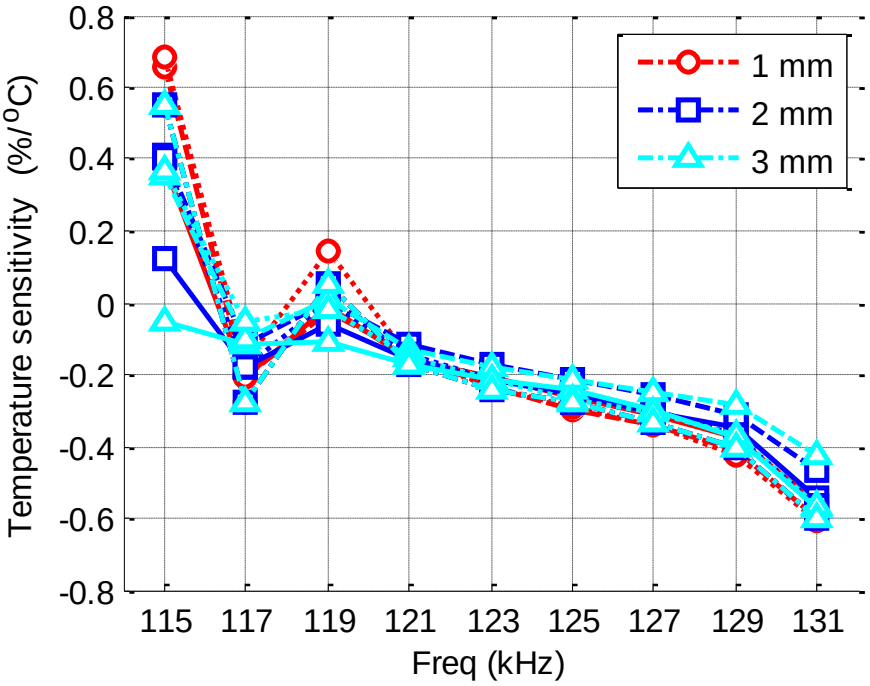

Figure 6.14: Temperature sensitivity under variation of frequencies for pipe sample

As can be seen from Figure 6.14, there is a decrease in the temperature sensitivity with the increase in temperature for different depths of defects. The results from the response can be seen in Figure 6.15.

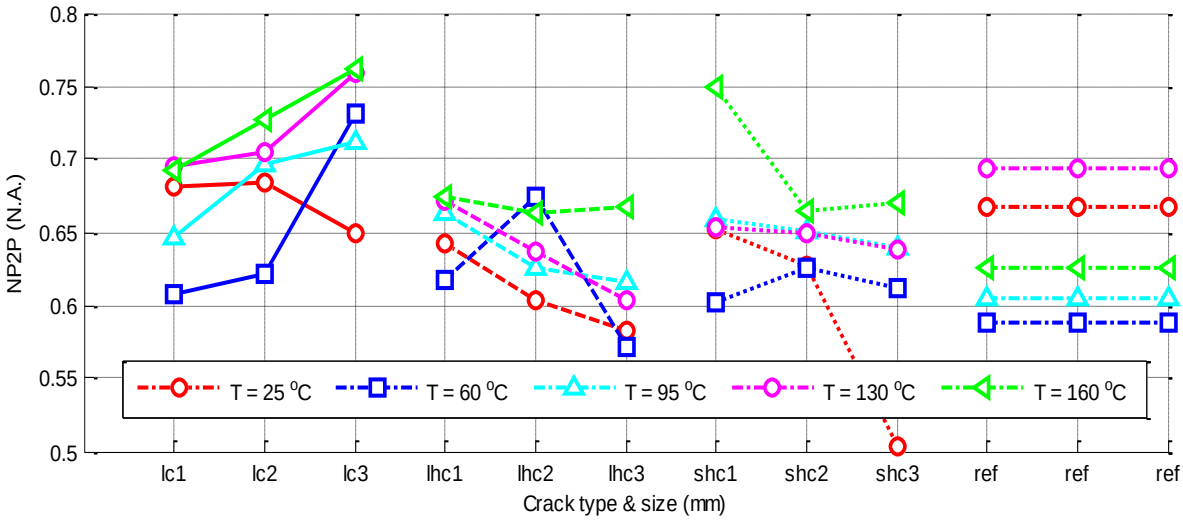

Figure 6.15: Results of the pipeline defect under insulation

It can be observed from the responses that even though the temperature was possibly minimised to some extent in comparison to the previous results obtained in Chapter 5 without insulation layer, it was still difficult to characterise the different defects. This can be explained as such

that since ‘lc’ represents long transverse cracks, therefore even under insulation layer, the three different depths were easily characterised. The response obtained from 25 ºC differs in comparison to others for the transverse crack which is simply thought to be an error caused by the minimised signal response obtained from the tag under insulation. Also the responses from ‘ref’ position where there were no defects show the stability for different measurements. However, the major concern is in the responses obtained for ‘lhc’ and ‘shc’ which are the long pit hole crack and small pit hole crack respectively. Their responses are not being characterised by the RFID tag and this is because the size of the holes were much lower than the size of the tag. Since the tag was 25mm while the cracks were 10mm and 5mm, therefore, the eddy current produced from the tag could not reach to the centre and were generated only around the edges of the holes. This experimental study can be further carried out using ferrite sheet to improve the sensitivity as well as operating through aluminium layer by concentrating flux towards the tag and underneath it.

6.3 Chapter Summary

In this chapter, the focus was given on two important aspects that closes the loop for the experimental studies. First section of the work focused on the mitigation of the influence of lift-off variation between the reader and the tag by utilizing the normalization technique. After normalization, the proposed fusion of features were carried out which subtracted the lower frequency response from the higher frequency response to extract the defect information. The responses show the influences of the communication distance is further reduced using this technique while both the sensitivity and the resolution of the LF RFID sensing system for defect characterisation are highly improved.

The next work focused on conducting a more realistic experimental study. For this section, a pipeline with calcium silicate insulation layer has been used which is of 50 mm. Artificial defects were made on the pipeline based on the BSI standards publication. Three different types of defects with different depths were monitoring under thick insulation at varying temperature. The swept frequency response has been taken in order to see the behaviour of the defects at each frequency points. Near zero temperature coefficient has been used to suppress temperature influence and determine the defect. Notably, the transverse cracks were possibly detected but due to a fixed shaped tag which is much larger than the other two defects, the small defects were not possible to characterise. Further experiments require to be carried out with different sized tags for varying defects shapes and sizes for wider applicability of the system.

Chapter 7. Conclusion and Further Work

In this final chapter the research is summarised and the conclusions are drawn on the potentials of the RFID sensing system as a non-destructive testing and evaluation technique. The potential outlooks on the future research are outlined in terms of improving the system sensitivity and robustness.

7.1 Research Conclusions

Challenges associated with the existing NDT&E technique generate scopes for novel approaches to tackle the limitations posed by CUI and defect monitoring in harsh environmental conditions. One such major challenge is the sequestered pipe surfaces covered under insulation or paint layer. From the literature review it was found that the techniques to overcome the large standoff distance required high powered systems such as PEC which have low sensitivity or even through the use of guided waves. On the other hand, the latter technique requires accessibility of the pipe surface through small inspection holes. In this research, the potential of passive LF RFID sensing systems for monitoring of corrosion under thick paint layer and defect monitoring in harsh environmental conditions have been experimentally demonstrated.

Passive sensing is a dynamic and developing research field. Various examples have been mentioned in the literature exploring the usage of RFID sensing for numerous applications starting from physical and chemical changes such as strain, displacement, moisture, gas and temperature. The attractive attributes such as the low cost, tolerance to harsh environmental conditions, ease of incorporation in to other automated systems and its passive operation are amongst the other enormous factors enticing researchers all over the world to further explore this technology for sensing. Maximum number of researches related to passive RFID system involved the modification of the tags in terms of designing them through the use of silver pastes and inks along with reactive thin films with sacrificial elements attached to the tags. These methods undoubtedly provide good attractive approaches towards the challenges but fail to ensure rugged performance in harsh environmental conditions such as high temperature. Apart from this, these methods not only increase the costs but also limits the long term applicability of the tags. The proposed method overcomes these challenges by using the tag coil's interaction with the metal as the sensing mechanism. This research has therefore been conducted without any further modification of the tag, allowing greater usability of the commercial off-the-shelf tags.

The research work started by understanding the fundamental operating principles described in Chapter 3, in particular, the eddy current distribution and magnetic diffusion behaviour in the

presence of conductive substrate and their related effects, mainly the fact that RFID reader and tag operate best at particular resonance. The main work focused on the design and development of the LF RFID sensing system and the implementation of the prototype. In free space, the resonant frequency of the tag is same as that of the operating frequency of the reader. In close proximity to the metallic object, the inductive coupling between the tag and metal causes a shift in the resonance. This shift minimises the amount of power absorbed by the tag and therefore the loading effect it has on the reader coil. As there is a change in the metallic object due to the development of corrosion or cracks, there will be a change in the electrical conductivity and magnetic permeability which will result in the tag's resonant frequency to shift towards the free space value. The hardware section firstly included the selection of the best commercially available LF RFID tags for the particular applicability in the high temperature conditions. Main focus was given in the fabrication of the reader unit which is completely custom built 9 cm diameter reader coil. Test results have shown the capability of the reader to energise and read tags from a distance of up to 50 mm which is sufficient for the insulation type used in this study.

Major work of the thesis are detailed in Chapter 4, where an experimental study has been carried out using carefully designed samples that demonstrates the systems detection capabilities. The qualitative nature of the study, tested the systems capabilities to distinguish between different surface conditions and corrosion levels under paint coating and also without coating. The quantitative analysis allowed the best feature selection i.e. transient feature which contains multiple frequency responses of the RFID signal for robust corrosion characterisation. First set of samples involved the surface preparation samples with different corrosion levels. The results showed that the RFID system not only differentiated between the corroded and non-corroded samples but were also able to distinguish between the different surface roughness due to corrosion. The second set of samples used is a set of paint coated and uncoated steel samples which has corrosion patches in the centre of the plate of 3×3 cm. The samples have been exposed to the atmosphere for different level of corrosion to build up on them i.e. 1, 3, 6, 10 and 12 months. Seven features (three from the pulse response and four from the differential of the pulse signal) are summarised, validated and compared to characterise corrosion. Best two features have been selected i.e. *Max(A)* feature to characterize permeability change and *PVmax(δA/δt)* to characterize conductivity variation and further prove the robustness of the system. Both these features have been compared and transient responses have proven to be significantly more sensitive and robust with corrosion progression compared to conventional static features. The results demonstrated the RFID systems ability in the characterisation of all the different corrosion levels. The final study in chapter 4, demonstrated the increased

sensitivity of the RFID system using ferrite sheet attached to the tag through FEA analysis and experimental studies. The variables in that experiment were the presence (or absence) of ferrite sheet attached to the tag for both uncoated and coated samples for corrosion characterisation. Approximately around 10 - 45% increase in sensitivity has been estimated using ferrite sheet without changing the distance between the RFID reader and the tag.

The usability of RFID system in high temperature conditions for detecting defects is experimentally explored in chapter 5. At high temperatures, the metal resistivity increases with an increase in temperature whereas in case of semi-conductors such as IC in RFID, the resistivity of it decreases exponentially with an increase in temperature thus reducing the magnitude of the tag's response. In this study, new aluminium crack sample is used with a geometrical dimension of 210 mm × 50 mm × 12 mm and had machined slit defects of constant width of 3 mm with crack depths of 3 mm, 5 mm, 7 mm and 9 mm. Similar to the previous study in chapter 4, if only the single frequency was used for the feature extraction, the crack could somehow be detected but the effect of temperature and its influence will still persist which may result in ineffective crack detection and characterization. Therefore, in this study, the reader unit is further modified to generate a swept-frequency signal in a specific frequency range in order to measure the resonance frequency shifts caused by both the defect and the temperature variation. The temperature sensitivity is calculated in terms of temperature coefficients across the swept frequency. A new feature is proposed based on the responses obtained from the reader unit and was named 'Fusion of Peak-to-Peak' feature, where the summation from both sides of the resonant frequency point i.e. the lower frequency points and the higher frequency points is taken in order to minimise the effect of temperature while maintaining the sensitivity of defect characterisation. To further validate the performance of the system and the technique, inhomogeneity study using steel corrosion progression samples were carried out. The effect of inhomogeneity was monitored at different oscillating frequency for the corrosion progression samples. It was observed that using the fusion feature technique, the corrosion progression levels were effectively identified minimising the temperature variation. In the final study of chapter 5, reduction of thermal effect and improvement of system robustness have been carried out using ceramic substrate. The ceramic filled PTFE substrate material was attached to the RFID tag and the approach was modelled and simulated in COMSOL and then experimentally verified to make a fair comparison. Thermal sensitivity drop without the use of ceramic filled PTFE substrate material was approximately 10 mV/°C whereas with the ceramic filled substrate the temperature sensitivity drop was approximately 6 mV/°C. An improvement of 40% using the ceramic filled substrate showed the potential of this system

for further industrial applicability. Both these phenomena used to compensate the uncertainty caused by the temperature variation for defect characterization and the results show the potentiality of this approach using RFID system which bridges the gap between NDT&E and SHM.

In the final chapter, the effect of reading range variation is studied. The reading range is considered as the insulation layer here. Initially, the experiment was carried out at 3 different communication/reading distances: L1 = 20 mm, L2 = 30 mm, and L3 = 40 mm. The tests were carried out on the same aluminium crack samples used in chapter 5. The influence of the tags signal from different crack depths were suppressed using normalization method and further feature extraction of the time domain in the swept frequency range was carried out. It was observed that the normalized response in the frequency lower than the resonant point has a positive coefficient with the crack growth while on the other hand frequency higher than the resonant points has a negative coefficient. Therefore, a new feature fusion technique was applied in this case which subtracted the two coefficients and by doing this the influences of the communication distance was further reduced while both the sensitivity and the resolution of the LF RFID sensing system were highly improved. This technique is also applicable for any angular variation of the reader coil which makes it even more feasible for industrial use. Finally, to replicate an actual field test scenario, the steel pipeline sample with several defect types and depths in it have been tested with tags deployed under 50 mm insulation layer. The tests involved a coated 60 cm long sections of steel pipe with 6 cm diameter and 3 mm thickness. Three different defects were made on the sample and they are long crack of 30 mm length, pit crack of 10 mm diameter and 5 mm diameter. Different shaped defects were made to present the feasibility of the RFID sensing system. The effect of insulation layer has been minimised using the aforementioned extraction technique and thus robust defect characterisation has been carried out at varying temperature. However, the higher temperature survivability of the RFID tags is particularly a challenge on its own and requires novel solutions in order to expand the potential applicability of the RFID system.

7.2 Main contributions

In this thesis a thorough review of electromagnetic NDT&E techniques for defect detection and characterisation in petrochemical structures has been carried out. Also, since the commercially available RFID reader unit could not work in metal proximity, therefore, a custom reader unit was designed and implemented for allowing measurements up to 50 mm on mild steel samples. Their major benefits and their limitations are assessed.

Delineation of the effects of permeability and conductivity in RFID response signal have been investigated and justified. From the justification it was found that the electrical conductivity effect is largely associated with the rising edge and the magnetic permeability is associated with the stable phase of the transient response. These two EM properties provide a commendable prospective for multiple parameter measurement.

- This finding becomes valuable in RFID applications for displacement measurement along with SCC characterisation of the ferromagnetic materials and components with low and high relative permeability.
- This study also shows that the magnetic permeability of the RFID response could be enhanced by the usage of ferrite sheet for better sensitivity in terms of corrosion characterisation

The characteristics and behaviour of defect under harsh environmental condition i.e. high temperature have been studied. The study have been carried out under different testing conditions: incremental temperature, ferrous and non-ferrous materials, different surface conditions i.e. crack and corrosion behaviour. A modified reader amplification unit allowed for sweeping frequency to be captured in order to understand the resonance behaviour of the system and for the physical understanding of related parameters and defect influences. A novel method was proposed that was invariant to the parametric influences caused by the temperature variation. Also this proposed method allowed a direct mean of inspecting ferromagnetic and non-ferromagnetic materials. This proposed method mitigated the temperature influence and allowed for correct crack depth and corrosion progression characterisation. Also simulations show that the use of ceramic filled PTFE substrate can be useful to reduce the temperature influence while maintaining good sensitivity to defect monitoring.

- This approach is useful for multiple parameter quantification; measurement of coating thickness of the paint; surface material discontinuities and for accurate profiling of the geometry of crucial structural materials such as internal pipeline walls.
- Furthermore, in field application for SHM, sensing stability against environmental temperature change is critical. Therefore, ceramic sensor materials can be used with copper claddings to study sensing behaviour at varying temperature.

An experimental study showing the potential of the proposed method have been carried out for defect monitoring that is invariant to lift-off. The study retrospect the communication principle of magnetic resonant coupling for LF RFID sensing system. Influence of the communication distance between the reader and the tag is mitigated through two steps: sweeping frequency to

analyse the resonance behaviour and their variation under different measurement conditions such as the extraction of multiple features, feature selection and fusion for robust monitoring under varying measurement conditions i.e. through normalization of the selected time-domain feature of P2P. To replicate the field scenario, a steel pipeline with various defects have been used to characterise the defects under thick silicon insulation.

- The study signifies the potential of the RFID system for industrial applications where the sensing system can be permanently installed/co-designed within large scale infrastructures for continuously monitoring throughout their lifecycle.

7.3 Future work suggestions

The proposed work shows promising outcomes in detection of defects under harsh environmental conditions. Future work with the RFID system will be driven towards improvement of the system to tackle other challenges related to CUI including working in extreme temperature environments with pressure and moisture monitoring capability and metallic outer casing.

In this research, the effect of magnetic permeability and electrical conductivity have been studied in RFID signal response via experimental validation. However, the quantification of these parameters have not yet been addressed which is worth considering and exploring with RFID measurements so that the multiple parameter estimation (defect, temperature influence, communication range) achieved in this research work can be further extended to the estimation of the permeability and conductivity as well. In this manner, four parameters can be estimated from a single inspection area which may be realised through the correlation of RFID response to the reference conductivity and permeability standards.

Apart from this, future work can be directed towards the extension and optimization of the proposed multiple parameters estimation and separation of the RFID response signal to deal with other challenges associated with inaccuracies in the RFID response due to complex geometries such as varying pipe diameters and curvatures in conjunction with flanges, weld joints and irregular defects formation in critical materials in the oil and gas industry.

Another future aspect is in the research towards the high temperature survivability of the RFID tags which is a significant problem that limits wider applicability of the system. Majority petrochemical industries operate at temperatures far beyond the limit of current semiconductor technology. This may be dealt with the usage of silicon based microchips that can withstand higher temperature, however, less radical solution could be the use of chip-less tags which are

not new but still in the initial implementation phase. A chip-less RFID tag can be made on flexible substrate using conducting inks and printing technologies. This would expand usability of RFID to a wider range of applications as chip-less RFID can be printed on stretchable substrates such as the use of thermal resistance ceramic substrate which would enable RFID to not only fit on any surface but also work in high temperature conditions for wider NDT&E applications and SHM.

Also, the inability of RFID system to monitor large areas rather than only point monitoring cuts down its potential field of application. This problem could be resolved by the use of polyethylene material with conductive ink printed antenna design on it as a solution for mass production of the tags and formation of sensor arrays would could be applied for a wider coverage. Along with this, passive RFID based monitoring network can be formed by the combination of RFID tag with SAW (surface acoustic wave). These cost efficient and lower power consumption approaches, will open revolutionary solution for intelligent SHM of railways, nuclear power plants and aerospace applications.

A continuing research on new features for signal processing is essential because under varying conditions different defects may look similar when using simple feature extraction methods analysed. Time-frequency distribution is an auspicious tool to study the complexity of the RFID response signals for overall 3-D mapping of the complex structures. Hence, analysis like Short-Term Fourier Transform (STFT), wavelet decomposition and Wigner-Ville distribution may be explored.

Apart from the improvement in the realisation of the WPT system with regards to higher Q-factor that is obtained in this research in terms of adjusting reading distance between the reader and the coil, however, another aspect would be looking into automatic impedance matching (self-tuning) that would compensate for the effects of the changing targets which are close to the antenna and therefore achieving a higher reading performance.

Over all these, the world is in the era of IoTs therefore focus is required on the implementation of the passive RFID sensing system. Hence, in addition to the highlighted forefront, future trend will focus on the robust antenna sensing design (i.e. sensitivity, quality factor enhancement, automatic impedance matching), low-cost printing system and applications.

References

[1] BBC, *http://news.bbc.co.uk/1/hi/scotland/glasgow_and_west/8495807.stm*, 2009.

[2] BBC, "http://www.bbc.co.uk/news/world-asia-china-25050300," 2013.

[3] CNN, "http://edition.cnn.com/2017/08/06/us/ohio-state-fair-ride-collapse/index.html," 2017.

[4] V. G. M. Annamdas and C. K. Soh, "Application of electromechanical impedance technique for engineering structures: review and future issues," *Journal of Intelligent material systems and structures*, vol. 21, pp. 41-59, 2010.

[5] P. Priyada, M. Margret, R. Ramar, Shivaramu, M. Menaka, L. Thilagam, *et al.*, "Intercomparison of gamma scattering, gammatography, and radiography techniques for mild steel nonuniform corrosion detection," *Review of scientific instruments*, vol. 82, p. 035115, 2011.

[6] P. Huthwaite, R. Ribichini, P. Cawley, and M. J. S. Lowe, "Mode selection for corrosion detection in pipes and vessels via guided wave tomography," *IEEE transactions on ultrasonics, ferroelectrics, and frequency control*, vol. 60, pp. 1165-1177, 2013.

[7] J. Ou and H. Li, "Structural health monitoring in mainland China: review and future trends," *Structural Health Monitoring*, vol. 9, pp. 219-231, 2010.

[8] A. I. Sunny, G. Y. Tian, J. Zhang, and M. Pal, "Low frequency (LF) RFID sensors and selective transient feature extraction for corrosion characterisation," *Sensors and Actuators A: Physical*, vol. 241, pp. 34-43, 2016.

[9] A. Imam and G. Y. Tian, "Enhanced Sensitivity of Low Frequency (LF) RFID Sensor Signal for Structural Health Monitoring (SHM) in High Temperature Environment," in *Proc. 9th World Conf. Non Destruct. Test*, 2016, pp. 1-8.

[10] A. I. Sunny, G. Y. Tian, and M. Alamin, "RFID (Radio Frequency Identification) Sensor System for Detecting Corrosion Progression Using Transient Responses," *Presented at BINDT 2014, Manchester, UK*, 2014.

[11] C. Argent, "Macaw's pipeline defects. sl: Yellow Pencil Marketing, 2003," ISBN 0-9544295-0-8.

[12] W. Zhu, R. François, C. S. Poon, and J.-G. Dai, "Influences of corrosion degree and corrosion morphology on the ductility of steel reinforcement," *Construction and Building Materials*, vol. 148, pp. 297-306, 2017.

[13] S. Ahmad, "Reinforcement corrosion in concrete structures, its monitoring and service life prediction—a review," *Cement and concrete composites*, vol. 25, pp. 459-471, 2003.

[14] Y. Yuan, Y. Ji, and S. P. Shah, "Comparison of two accelerated corrosion techniques for concrete structures," *ACI Structural Journal*, vol. 104, p. 344, 2007.

[15] M. Lettich, "Is There A Cure for Corrosion under Insulation," *Insulation Outlook Magazine*, 2005.

[16] S. Ramesh, B. Bhuvaneswari, G. S. Palani, D. M. Lal, and N. R. Iyer, "Effects on corrosion resistance of rebar subjected to deep cryogenic treatment," *Journal of Mechanical Science and Technology*, vol. 31, pp. 123-132, 2017.

[17] D. De la Fuente, I. Díaz, J. Simancas, B. Chico, and M. Morcillo, "Long-term atmospheric corrosion of mild steel," *Corrosion Science*, vol. 53, pp. 604-617, 2011.

[18] W. D. Callister and D. G. Rethwisch, *Materials science and engineering* vol. 5: John Wiley & Sons NY, 2011.

[19] M. Twomey, "Inspection techniques for detecting corrosion under insulation," *Materials evaluation*, vol. 55, 1997.

[20] R. K. Ginzel and W. A. Kanters, "Pipeline corrosion and cracking and the associated calibration considerations for same side sizing applications," *NDT. net*, vol. 7, pp. 1435-4934, 2002.

[21] P. Pillai, S. Venugopal, and V. Gopalan, "Crevice Corrosion of Aluminium and It's Prevention in Automobile Coolant Circuit," SAE Technical Paper 0148-7191, 2017.

[22] S. Caines, F. Khan, and J. Shirokoff, "Analysis of pitting corrosion on steel under insulation in marine environments," *Journal of Loss Prevention in the process Industries*, vol. 26, pp. 1466-1483, 2013.

[23] Y. Xie, S. Guo, A. Leong, J. Zhang, and Y. Zhu, "Corrosion behaviour of stainless steel exposed to highly concentrated chloride solutions," *Corrosion Engineering, Science and Technology*, vol. 52, pp. 283-293, 2017.

[24] J. Bhandari, F. Khan, R. Abbassi, V. Garaniya, and R. Ojeda, "Reliability assessment of offshore asset under pitting corrosion using Bayesian Network," in *Corrosion 2016*, 2016, pp. 1-15.

[25] R. A. Cottis, "Stress corrosion cracking: Guides to good practice in corrosion control," *The National Physical Laboratory, Tech. Rep*, 2000.

[26] R. C. Newman, P. Marcus, and J. Oudar, "Corrosion mechanisms in theory and practice," *New York, NY: Marcel Dekker*, p. 331, 1995.

[27] R. H. Scott, P. Banerji, S. Chikermane, S. Srinivasan, P. A. M. Basheer, F. Surre, *et al.*, "Commissioning and evaluation of a fiber-optic sensor system for bridge monitoring," *IEEE Sensors Journal*, vol. 13, pp. 2555-2562, 2013.

[28] R. Francis, "Bimetallic corrosion: Guides to good practice in corrosion control," *Teddington, Middlesex: National Physical Laboratory. Retrieved July*, vol. 14, p. 2008, 2000.

[29] F. De Vogelaere, "Corrosion under insulation," *Process Safety Progress,* vol. 28, pp. 30-35, 2009.

[30] M. Halliday, "Preventing corrosion under insulation-new generation solutions for an age old problem," *Journal of protective coatings & linings,* vol. 24, 2007.

[31] E. J. Opila, "High temperature materials corrosion challenges for energy conversion technologies," *The Electrochemical Society Interface,* vol. 22, pp. 69-73, 2013.

[32] H. Wiggenhauser and H. W. Reinhardt, "NDT in civil engineering: Experience and results of the for 384 research group," in *AIP Conference Proceedings*, 2010, pp. 47-54.

[33] R. Arndt and F. Jalinoos, "NDE for corrosion detection in reinforced concrete structures—A benchmark approach," *Proceedings of Non-destructive Testing in Civil Engineering,* 2009.

[34] J. Rhazi, O. Dous, and S. Laurens, "A new application of the GPR technique to reinforced concrete bridge decks," in *Proceeding of the 4th Middle East NDT conference and Exhibition, Manama, Kingdom of Bahrain*, 2007, pp. 2-5.

[35] C. Guo and T. Yang, "Aero-engine interior damage recognition based on texture features of borescope image [J]," *Chinese Journal of Scientific Instrument*, vol. 8, p. 028, 2008.

[36] M. Lozev, R. Smith, and B. Grimmett, "Evaluation of methods for detecting and monitoring of corrosion damage in risers," *Journal of pressure vessel technology*, vol. 127, pp. 244-254, 2005.

[37] D. O'Flynn, C. Crews, N. Fox, B. P. Allen, M. Sammons, and R. D. Speller, "X-ray backscatter sensing of defects in carbon fibre composite materials," in *SPIE Commercial+ Scientific Sensing and Imaging*, 2017, pp. 102120R-102120R-8.

[38] L. Bai, B. Gao, G. Y. Tian, W. L. Woo, and Y. Cheng, "Spatial and time patterns extraction of eddy current pulsed thermography using blind source separation," *IEEE sensors Journal*, vol. 13, pp. 2094-2101, 2013.

[39] A. Yin, B. Gao, G. Yun Tian, W. L. Woo, and K. Li, "Physical interpretation and separation of eddy current pulsed thermography," *Journal of Applied Physics,* vol. 113, p. 064101, 2013.

[40] Y. He, G. Y. Tian, M. Pan, D. Chen, and H. Zhang, "An investigation into eddy current pulsed thermography for detection of corrosion blister," *Corrosion Science,* vol. 78, pp. 1-6, 2014.

[41] C. Xu, X. Gong, W. Zhang, and G. Chen, "An Investigation on Eddy Current Pulsed Thermography to Detect Surface Cracks on the Tungsten Carbide Matrix of Polycrystalline Diamond Compact Bit," *Applied Sciences*, vol. 7, p. 429, 2017.

[42] D. Huang, K. Li, G. Y. Tian, A. I. Sunny, X. Chen, C. Tang, *et al.*, "Thermal pattern reconstruction of surface condition on freeform-surface using eddy current pulsed thermography," *Sensors and Actuators A: Physical*, vol. 251, pp. 248-257, 2016.

[43] J. Peng, K. Zhang, K. Yang, Z. He, Y. Zhang, C. Peng, *et al.*, "The early stage wheel fatigue crack detection using eddy current pulsed thermography," in *AIP Conference Proceedings*, 2017, p. 100010.

[44] R. Vedalakshmi, L. Balamurugan, V. Saraswathy, S. H. Kim, and K. Y. Ann, "Reliability of Galvanostatic Pulse Technique in assessing the corrosion rate of rebar in concrete structures: laboratory vs field studies," *KSCE Journal of Civil Engineering*, vol. 14, pp. 867-877, 2010.

[45] J. J. Shi, W. Sun, and G. Q. Geng, "Steel corrosion in simulated concrete pore solutions using a galvanostatic pulse method," *J. Univ. Sci. Technol. Beijing*, vol. 33, pp. 727-733, 2011.

[46] J. X. Xu, Y. L. Cao, L. H. Jiang, Y. B. Song, and W. Feng, "Error Estimation of Linear Polarization Resistance Measurement Caused by IR Drop for Reinforcement Corrosion in Concrete," in *Materials Science Forum*, 2016, pp. 14-19.

[47] Y. W. Liu, Z. Y. Wang, G. W. Cao, Y. Cao, and Y. Huo, "Study on corrosion behavior of zinc exposed in coastal-industrial atmospheric environment," *Materials Chemistry and Physics*, 2017.

[48] S. U. N. Shuangqing, Q. Zheng, L. I. Chunling, W. Xiumin, and H. U. Songqing, "Effect of Corrosion Products on Long-term Atmospheric Corrosion of Pure Aluminum 8A06," *Journal of Chinese Society for Corrosion and protection*, vol. 37, pp. 110-116, 2017.

[49] G. Salvago, G. Bollini, and P. L. Cavalotti, "Electrochemical Evaluation of Localized Corrosion Probaility in Stainless Steel," in *Materials science forum*, 1998, pp. 933-954.

[50] J. Zhang, B. W. Drinkwater, and P. D. Wilcox, "Defect characterization using an ultrasonic array to measure the scattering coefficient matrix," *IEEE transactions on ultrasonics, ferroelectrics, and frequency control*, vol. 55, 2008.

[51] G. Dobmann, O. A. Barbian, and H. Willems, "State of the art of in-line nondestructive weld inspection of pipelines by ultrasonics," *Russian Journal of Nondestructive Testing*, vol. 43, pp. 755-761, 2007.

[52] A. C. Cobb, J. E. Michaels, and T. E. Michaels, "An automated time–frequency approach for ultrasonic monitoring of fastener hole cracks," *NDT & E International,* vol. 40, pp. 525-536, 2007.

[53] L. Satyarnarayan, J. Chandrasekaran, B. Maxfield, and K. Balasubramaniam, "Circumferential higher order guided wave modes for the detection and sizing of cracks and pinholes in pipe support regions," *NDT & E International,* vol. 41, pp. 32-43, 2008.

[54] J. Blitz and G. Simpson, *Ultrasonic methods of non-destructive testing* vol. 2: Springer Science & Business Media, 1995.

[55] K. S. Kumar and K. Balasubramaniam, "Simulations and Experiments for the Detection of Flow-Assisted Corrosion in Pipes," *Journal of Pressure Vessel Technology,* vol. 137, p. 061409, 2015.

[56] D. Cerniglia and A. Pantano, "Experimental and numerical method for nondestructive ultrasonic defect detection," *Nondestructive Testing: Methods, Analyses and Applications,* pp. 63-94, 2011.

[57] B. Park, H. Sohn, P. Malinowski, and W. Ostachowicz, "Delamination localization in wind turbine blades based on adaptive time-of-flight analysis of noncontact laser ultrasonic signals," *Nondestructive Testing and Evaluation,* vol. 32, pp. 1-20, 2017.

[58] F. Hernandez-Valle, A. R. Clough, and R. S. Edwards, "Stress corrosion cracking detection using non-contact ultrasonic techniques," *Corrosion Science,* vol. 78, pp. 335-342, 2014.

[59] Y. Sun, S. Liu, R. Li, Z. Ye, Y. Kang, and S. Chen, "A new magnetic flux leakage sensor based on open magnetizing method and its on-line automated structural health monitoring methodology," *Structural Health Monitoring,* vol. 14, pp. 583-603, 2015.

[60] H. G. Ramos and A. L. Ribeiro, "Present and future impact of magnetic sensors in NDE," *Procedia Engineering,* vol. 86, pp. 406-419, 2014.

[61] A. Sophian, G. Y. Tian, and S. Zairi, "Pulsed magnetic flux leakage techniques for crack detection and characterisation," *Sensors and Actuators A: Physical,* vol. 125, pp. 186-191, 2006.

[62] M. R. Kandroodi, B. N. Araabi, M. M. Bassiri, and M. N. Ahmadabadi, "Estimation of Depth and Length of Defects From Magnetic Flux Leakage Measurements: Verification With Simulations, Experiments, and Pigging Data," *IEEE Transactions on Magnetics,* vol. 53, pp. 1-10, 2017.

[63] D. L. Atherton, "Magnetic inspection is key to ensuring safe pipelines," *NDT and E International,* vol. 1, p. 40, 1997.

[64] T. Azizzadeh and M. S. Safizadeh, "Three-Dimensional Finite Element and Experimental Simulation of magnetic flux leakage-type NDT for Detection of Pitting Corrosions."

[65] D. Kim, L. Udpa, and S. Udpa, "Remote field eddy current testing for detection of stress corrosion cracks in gas transmission pipelines," *Materials Letters,* vol. 58, pp. 2102-2104, 2004.

[66] Y. Wang, X. Wang, and K. Ding, "Width quantification of corrosive defect on pipeline based on pulsed magnetic flux leakage," *Journal of Test and Measurement Technology,* vol. 5, 2009.

[67] H. Zhang, L. Liao, R. Zhao, J. Zhou, M. Yang, and R. Xia, "The non-destructive test of steel corrosion in reinforced concrete bridges using a micro-magnetic sensor," *Sensors,* vol. 16, p. 1439, 2016.

[68] Y. Lijian, L. Gang, Z. Guoguang, and G. Songwei, "Sensor development and application on the oil-gas pipeline magnetic flux leakage detection," in *Electronic Measurement & Instruments, 2009. ICEMI'09. 9th International Conference on*, 2009, pp. 2-876-2-878.

[69] Y. Sun, Y. Kang, and C. Qiu, "A permanent magnetic perturbation testing sensor," *Sensors and Actuators A: Physical,* vol. 155, pp. 226-232, 2009.

[70] H. Rowshandel, G. L. Nicholson, C. L. Davis, and C. Roberts, "A combined threshold and signature match method for the automatic detection of rail RCF cracks using an ACFM sensor," 6th IET Conference on Railway Condition Monitoring, pp. 3.1.1, 2014.

[71] M. J. Knight, F. P. Brennan, and W. D. Dover, "Effect of residual stress on ACFM crack measurements in drill collar threaded connections," *Ndt & E International,* vol. 37, pp. 337-343, 2004.

[72] M. Smith and R. Sutherby, "The detection of pipeline SCC flaws using the ACFM technique," *Insight-Non-Destructive Testing and Condition Monitoring,* vol. 47, pp. 765-768, 2005.

[73] D. Topp, "Quantitative in-service inspection using the alternating current field measurement(ACFM) method," in *NDTISS'99: International Symposium on Nondestructive Testing Contribution to the Infrastructure Safety Systems in the 21 st Century*, 1999, pp. 48-54.

[74] M. Smith and C. Laenen, "Inspection of nuclear storage tanks using remotely deployed ACFMT," *Insight-Non-Destructive Testing and Condition Monitoring,* vol. 49, pp. 17-20, 2007.

[75] S. Kharkovsky and R. Zoughi, "Microwave and millimeter wave nondestructive testing and evaluation-Overview and recent advances," *IEEE Instrumentation & Measurement Magazine,* vol. 10, pp. 26-38, 2007.

[76] J. Han and C. Nguyen, "Development of a tunable multiband UWB radar sensor and its applications to subsurface sensing," *IEEE Sensors Journal,* vol. 7, pp. 51-58, 2007.

[77] J. Park and C. Nguyen, "Development of a new millimeter-wave integrated-circuit sensor for surface and subsurface sensing," *IEEE Sensors Journal,* vol. 6, pp. 650-655, 2006.

[78] Z. Abbas, Y. K. Yeow, A. H. Shaari, K. Khalid, J. Hassan, and E. Saion, "Complex permittivity and moisture measurements of oil palm fruits using an open-ended coaxial sensor," *IEEE Sensors Journal,* vol. 5, pp. 1281-1287, 2005.

[79] C.-Y. Yeh and R. Zoughi, "A novel microwave method for detection of long surface cracks in metals," *IEEE Transactions on Instrumentation and Measurement,* vol. 43, pp. 719-725, 1994.

[80] D. Hughes, N. Wang, T. Case, K. Donnell, R. Zoughi, R. Austin, *et al.*, "Microwave nondestructive detection of corrosion under thin paint and primer in aluminum panels," *Subsurface Sensing Technologies and Applications,* vol. 2, pp. 435-471, 2001.

[81] F. Noorian and A. Sadr, "Computation of transient Eddy currents in EMATs using discrete Picard Method," in *Electrical Engineering (ICEE), 2010 18th Iranian Conference on*, 2010, pp. 727-731.

[82] S. Wang, P. Xin, L. Kang, and G. Zhai, "Research on influence of lorentz force mechanism on EMAT's transduction efficiency in steel plate," in *Industrial Electronics and Applications (ICIEA), 2010 the 5th IEEE Conference on*, 2010, pp. 196-201.

[83] S. Aliouane, M. Hassam, A. Badidi Bouda, and A. Benchaala, "Electromagnetic acoustic transducers (EMATs) design evaluation of their performances," in *Proceedings of the 15th World Conference on NDT (WCNDT 2000)*, 2000.

[84] O. Mesnil, "Sparse reconstruction and analysis of guided wavefields for damage detection and quantification," Georgia Institute of Technology, 2016.

[85] B. Park, H. Sohn, and P. Liu, "Accelerated noncontact laser ultrasonic scanning for damage detection using combined binary search and compressed sensing," *Mechanical Systems and Signal Processing,* vol. 92, pp. 315-333, 2017.

[86] N. Hosoya, R. Umino, A. Kanda, I. Kajiwara, and A. Yoshinaga, "Lamb wave generation using nanosecond laser ablation to detect damage," *Journal of Vibration and Control,* p. 1077546316687904, 2017.

[87] Wikipedia., ""Electromagnetic acoustic transducer," wikipedia.org. [Online]. Available: [https://en.wikipedia.org/wiki/Electromagnetic_acoustic_transducer]," 2017.

[88] S. Štarman and M. Václav, "Separation of signals acquired with EMAT in dual coil configuration."

[89] R. S. Edwards, A. Sophian, S. Dixon, G. Y. Tian, and X. Jian, "Dual EMAT and PEC non-contact probe: applications to defect testing," *NDT & E International,* vol. 39, pp. 45-52, 2006.

[90] I. Baillie, P. Griffith, X. Jian, and S. Dixon, "Implementing an ultrasonic inspection system to find surface and internal defects in hot, moving steel using EMATs," *Insight-Non-Destructive Testing and Condition Monitoring,* vol. 49, pp. 87-92, 2007.

[91] A. Idris, C. Edwards, and S. B. Palmer, "Acoustic wave measurements at elevated temperature using a pulsed laser generator and an electromagnetic acoustic transducer detector," *Nondestructive Testing and Evaluation,* vol. 11, pp. 195-213, 1994.

[92] K. Mirkhani, C. Chaggares, C. Masterson, M. Jastrzebski, T. Dusatko, A. Sinclair, *et al.*, "Optimal design of EMAT transmitters," *NDT & e International,* vol. 37, pp. 181-193, 2004.

[93] E. Bardal and J. M. Drugli, "Corrosion detection and diagnosis," *Materials science and engineering,* vol. 3, 2004.

[94] F. Gan, G. Tian, Z. Wan, J. Liao, and W. Li, "Investigation of pitting corrosion monitoring using field signature method," *Measurement,* vol. 82, pp. 46-54, 2016.

[95] A. Daaland, "Modelling of local corrosion attacks on a plate geometry for developing the FSM technology," *Insight,* vol. 38, pp. 872-875, 1996.

[96] R. D. Strommen, "Seven years of unique experience from subsea, deepwater pipeline internal corrosion monitoring," in *CORROSION 2002*, 2002.

[97] F. Gan, Z. Wan, Y. Li, J. Liao, and W. Li, "Improved formula for localized corrosion using field signature method," *Measurement,* vol. 63, pp. 137-142, 2015.

[98] B. Lebrun, Y. Jayet, and J.-C. Baboux, "Pulsed eddy current signal analysis: application to the experimental detection and characterization of deep flaws in highly conductive materials," *NDT & e international,* vol. 30, pp. 163-170, 1997.

[99] A. Sophian, G. Tian, and M. Fan, "Pulsed Eddy Current Non-destructive Testing and Evaluation: A Review," *Chinese Journal of Mechanical Engineering,* vol. 30, pp. 500-514, 2017.

[100] M. Fan, B. Cao, A. I. Sunny, W. Li, G. Tian, and B. Ye, "Pulsed eddy current thickness measurement using phase features immune to liftoff effect," *NDT & E International,* vol. 86, pp. 123-131, 2017.

[101] Y. Li, B. Yan, D. Li, Y. Li, and D. Zhou, "Gradient-field pulsed eddy current probes for imaging of hidden corrosion in conductive structures," *Sensors and Actuators A: Physical,* vol. 238, pp. 251-265, 2016.

[102] M. Alamin, G. Y. Tian, A. Andrews, and P. Jackson, "Principal component analysis of pulsed eddy current response from corrosion in mild steel," *IEEE Sensors Journal,* vol. 12, pp. 2548-2553, 2012.

[103] Z. Xu, X. Wu, J. Li, and Y. Kang, "Assessment of wall thinning in insulated ferromagnetic pipes using the time-to-peak of differential pulsed eddy-current testing signals," *NDT & E International,* vol. 51, pp. 24-29, 2012.

[104] G. Y. Tian and A. Sophian, "Defect classification using a new feature for pulsed eddy current sensors," *Ndt & E International,* vol. 38, pp. 77-82, 2005.

[105] X. Chen, D. Hou, L. Zhao, P. Huang, and G. Zhang, "Study on defect classification in multi-layer structures based on Fisher linear discriminate analysis by using pulsed eddy current technique," *NDT & E International,* vol. 67, pp. 46-54, 2014.

[106] A. Sophian, G. Y. Tian, D. Taylor, and J. Rudlin, "A feature extraction technique based on principal component analysis for pulsed eddy current NDT," *NDT & e International,* vol. 36, pp. 37-41, 2003.

[107] P. F. Horan, P. R. Underhill, and T. W. Krause, "Real time pulsed eddy current detection of cracks in F/A-18 inner wing spar using discriminant separation of modified principal components analysis scores," *IEEE Sensors Journal,* vol. 14, pp. 171-177, 2014.

[108] X. Qiu, P. Zhang, J. Wei, X. Cui, C. Wei, and L. Liu, "Defect classification by pulsed eddy current technique in con-casting slabs based on spectrum analysis and wavelet decomposition," *Sensors and Actuators A: Physical,* vol. 203, pp. 272-281, 2013.

[109] M. Pan, Y. He, G. Tian, D. Chen, and F. Luo, "Defect characterisation using pulsed eddy current thermography under transmission mode and NDT applications," *NDT & E International,* vol. 52, pp. 28-36, 2012.

[110] C. A. Stott, P. R. Underhill, V. K. Babbar, and T. W. Krause, "Pulsed eddy current detection of cracks in multilayer aluminum lap joints," *IEEE Sensors Journal,* vol. 15, pp. 956-962, 2015.

[111] J. A. Buck, P. R. Underhill, S. G. Mokros, J. E. Morelli, V. K. Babbar, B. Lepine, *et al.*, "Pulsed eddy current inspection of support structures in steam generators," *IEEE Sensors Journal,* vol. 15, pp. 4305-4312, 2015.

[112] R. F. Abrantes, L. S. Rosado, M. Piedade, and P. M. Ramos, "Pulsed eddy currents testing using a planar matrix probe," *Measurement,* vol. 77, pp. 351-361, 2016.

[113] Y. He, M. Pan, F. Luo, and G. Tian, "Pulsed eddy current imaging and frequency spectrum analysis for hidden defect nondestructive testing and evaluation," *Ndt & E International,* vol. 44, pp. 344-352, 2011.

[114] G. Yang, A. Tamburrino, L. Udpa, S. S. Udpa, Z. Zeng, Y. Deng, *et al.*, "Pulsed eddy-current based giant magnetoresistive system for the inspection of aircraft structures," *IEEE transactions on magnetics,* vol. 46, pp. 910-917, 2010.

[115] G. Y. Tian, A. Sophian, D. Taylor, and J. Rudlin, "Wavelet-based PCA defect classification and quantification for pulsed eddy current NDT," *IEE Proceedings-Science, Measurement and Technology,* vol. 152, pp. 141-148, 2005.

[116] C. S. Angani, H. G. Ramos, A. L. Ribeiro, T. J. Rocha, and P. Baskaran, "Lift-off point of intersection feature in transient eddy-current oscillations method to detect thickness variation in stainless steel," *IEEE Transactions on Magnetics,* vol. 52, pp. 1-8, 2016.

[117] Z. Liu, P. Ramuhalli, S. Safizadeh, and D. S. Forsyth, "Combining multiple nondestructive inspection images with a generalized additive model," *Measurement Science and Technology,* vol. 19, p. 085701, 2008.

[118] G. Y. Tian, Y. Li, and C. Mandache, "Study of lift-off invariance for pulsed eddy-current signals," *IEEE transactions on magnetics,* vol. 45, pp. 184-191, 2009.

[119] J. Li, X. Wu, Q. Zhang, and P. Sun, "Measurement of lift-off using the relative variation of magnetic flux in pulsed eddy current testing," *NDT & E International,* vol. 75, pp. 57-64, 2015.

[120] H.-C. Yang and C.-C. Tai, "Pulsed eddy-current measurement of a conducting coating on a magnetic metal plate," *Measurement science and technology,* vol. 13, p. 1259, 2002.

[121] M. A. Robert, "Pulsed eddy current in corrosion detection," *NDT-net,* vol. 7, 2002.

[122] E. L. S. Sheet, "http://www.eddyfi.com/wpcontent/

uploads/2016/09/specifications-sheet-lyft.pdf.," *http://www.eddyfi.com/wpcontent/*

uploads/2016/09/specifications-sheet-lyft.pdf., 2016.

[123] S. Xie, Z. Chen, T. Takagi, and T. Uchimoto, "Quantitative non-destructive evaluation of wall thinning defect in double-layer pipe of nuclear power plants using pulsed ECT method," *NDT & E International,* vol. 75, pp. 87-95, 2015.

[124] D. G. Park, C. S. Angani, G. D. Kim, C. G. Kim, and Y. M. Cheong, "Evaluation of pulsed eddy current response and detection of the thickness variation in the stainless steel," *ieee transactions on magnetics*, vol. 45, pp. 3893-3896, 2009.

[125] X. Chen and Y. Lei, "Electrical conductivity measurement of ferromagnetic metallic materials using pulsed eddy current method," *NDT & E International*, vol. 75, pp. 33-38, 2015.

[126] I. D. Adewale and G. Y. Tian, "Decoupling the influence of permeability and conductivity in pulsed eddy-current measurements," *IEEE Transactions on Magnetics*, vol. 49, pp. 1119-1127, 2013.

[127] S. Giguère and S. J. M. Dubois, "Pulsed eddy current: finding corrosion independently of transducer lift-off," in *AIP Conference Proceedings*, 2000, pp. 449-456.

[128] S. Giguere, B. A. Lepine, and J. M. S. Dubois, "Pulsed eddy current technology: Characterizing material loss with gap and lift-off variations," *Journal of Research in Nondestructive Evaluation*, vol. 13, pp. 119-129, 2001.

[129] G. G. Diamond, D. A. Hutchins, T. H. Gan, P. Purnell, and K. K. Leong, "Single-sided capacitive imaging for NDT," *Insight-Non-Destructive Testing and Condition Monitoring*, vol. 48, pp. 724-730, 2006.

[130] Z. Zhao, S. Fan, and D. Zheng, "Non-destructive testing of solid wood plate using variable permittivity plate capacitor," in *Instrumentation and Control Technology (ISICT), 2012 8th IEEE International Symposium on*, 2012, pp. 153-156.

[131] X. Dérobert, J. Iaquinta, G. Klysz, and J.-P. Balayssac, "Use of capacitive and GPR techniques for the non-destructive evaluation of cover concrete," *NDT & E International*, vol. 41, pp. 44-52, 2008.

[132] D. Sharma, S. Goyal, R. Khanna, and A. Mukherjee, "Non-destructive testing of materials using capacitive sensing technique," *MIT International Journal of Electronics and Communication Engineering*, vol. 1, pp. 73-77, 2011.

[133] X. Yin, D. A. Hutchins, G. Chen, and W. Li, "Detecting surface features on conducting specimens through an insulation layer using a capacitive imaging technique," *NDT & E International*, vol. 52, pp. 157-166, 2012.

[134] X. Li, A. S. Zyuzin, and A. V. Mamishev, "Measuring moisture content in cookies using dielectric spectroscopy," in *Electrical Insulation and Dielectric Phenomena, 2003. Annual Report. Conference on*, 2003, pp. 459-462.

[135] K. Sundara-Rajan, L. Byrd, and A. V. Mamishev, "Moisture content estimation in paper pulp using fringing field impedance spectroscopy," *IEEE Sensors Journal*, vol. 4, pp. 378-383, 2004.

[136] R. A. Potyrailo, A. Burns, C. Surman, D. J. Lee, and E. McGinniss, "Multivariable passive RFID vapor sensors: roll-to-roll fabrication on a flexible substrate," *Analyst*, vol. 137, pp. 2777-2781, 2012.

[137] R. Lodato and G. Marrocco, "Close Integration of a UHF-RFID transponder into a limb prosthesis for tracking and sensing," *IEEE Sensors Journal*, vol. 16, pp. 1806-1813, 2016.

[138] J. Zhang, G. Y. Tian, A. M. J. Marindra, A. I. Sunny, and A. B. Zhao, "A review of passive RFID tag antenna-based sensors and systems for structural health monitoring applications," *Sensors*, vol. 17, p. 265, 2017.

[139] X. Yi, C. Cho, B. Cook, Y. Wang, M. Tentzeris, and R. T. Leon, "Frequency doubling antenna sensor for wireless strain and crack sensing," ed: Google Patents, 2016.

[140] C. Occhiuzzi, C. Paggi, and G. Marrocco, "Passive RFID strain-sensor based on meander-line antennas," *IEEE Transactions on Antennas and Propagation*, vol. 59, pp. 4836-4840, 2011.

[141] M. Hasani, A. Vena, L. Sydänheimo, M. M. Tentzeris, and L. Ukkonen, "A novel enhanced-performance flexible RFID-enabled embroidered wireless integrated module for sensing applications," *IEEE Transactions on Components, Packaging and Manufacturing Technology*, vol. 5, pp. 1244-1252, 2015.

[142] M. J. Cazeca, J. Mead, J. Chen, and R. Nagarajan, "Passive wireless displacement sensor based on RFID technology," *Sensors and Actuators A: Physical*, vol. 190, pp. 197-202, 2013.

[143] C. Paggi, C. Occhiuzzi, and G. Marrocco, "Sub-millimeter displacement sensing by passive UHF RFID antennas," *IEEE Transactions on Antennas and Propagation*, vol. 62, pp. 905-912, 2014.

[144] D. Alonso, Q. Zhang, Y. Gao, and D. Valderas, "UHF passive RFID-based sensor-less system to detect humidity for irrigation monitoring," *Microwave and Optical Technology Letters*, vol. 59, pp. 1709-1715, 2017.

[145] M. Borgese, F. Dicandia, F. Costa, S. Genovesi, and G. Manara, "An Inkjet Printed Chipless RFID Sensor for Wireless Humidity Monitoring," *IEEE Sensors Journal*, 2017.

[146] A. Vena, E. Perret, D. Kaddour, and T. Baron, "Toward a Reliable Chipless RFID Humidity Sensor Tag Based on Silicon Nanowires," *IEEE Transactions on Microwave Theory and Techniques*, vol. 64, pp. 2977-2985, 2016.

[147] A. A. Kutty, T. Björninen, L. Sydänheimo, and L. Ukkonen, "A novel carbon nanotube loaded passive UHF RFID sensor tag with built-in reference for wireless gas sensing," in *Microwave Symposium (IMS), 2016 IEEE MTT-S International*, 2016, pp. 1-4.

[148] R. A. Potyrailo and C. Surman, "A passive radio-frequency identification (RFID) gas sensor with self-correction against fluctuations of ambient temperature," *Sensors and Actuators B: Chemical*, vol. 185, pp. 587-593, 2013.

[149] I. Jauregi, H. Solar, A. Beriain, I. Zalbide, A. Jimenez, I. Galarraga, *et al.*, "UHF RFID temperature sensor assisted with body-heat dissipation energy harvesting," *IEEE Sensors Journal*, vol. 17, pp. 1471-1478, 2016.

[150] S. Amendola, G. Bovesecchi, A. Palombi, P. Coppa, and G. Marrocco, "Design, Calibration and experimentation of an epidermal RFID sensor for remote temperature monitoring," *IEEE Sensors Journal*, vol. 16, pp. 7250-7257, 2016.

[151] M. R. G. Karkani, M. Kamarei, and A. F. Ahmady, "A low-power smart temperature sensor for passive UHF RFID tags and Sensor nets," in *Telecommunications (IST), 2016 8th International Symposium on*, 2016, pp. 12-17.

[152] A. Kang, C. Zhang, X. Ji, T. Han, R. Li, and X. Li, "SAW-RFID enabled temperature sensor," *Sensors and Actuators A: Physical*, vol. 201, pp. 105-113, 2013.

[153] J. Virtanen, L. Ukkonen, T. Bjorninen, A. Z. Elsherbeni, and L. Sydänheimo, "Inkjet-printed humidity sensor for passive UHF RFID systems," *IEEE Transactions on Instrumentation and Measurement*, vol. 60, pp. 2768-2777, 2011.

[154] E. M. Amin, J. K. Saha, and N. C. Karmakar, "Smart sensing materials for low-cost chipless RFID sensor," *IEEE Sensors Journal*, vol. 14, pp. 2198-2207, 2014.

[155] C. Occhiuzzi, A. Rida, G. Marrocco, and M. Tentzeris, "RFID passive gas sensor integrating carbon nanotubes," *IEEE Transactions on Microwave Theory and Techniques*, vol. 59, pp. 2674-2684, 2011.

[156] D. Girbau, Á. Ramos, A. Lazaro, S. Rima, and R. Villarino, "Passive wireless temperature sensor based on time-coded UWB chipless RFID tags," *IEEE Transactions on Microwave Theory and Techniques*, vol. 60, pp. 3623-3632, 2012.

[157] J. J. Martínez-Martínez, F. J. Herraiz-Martínez, and G. Galindo-Romera, "Design and Characterization of a Passive Temperature Sensor Based on a Printed MIW Delay Line," *IEEE Sensors Journal*, vol. 16, pp. 7884-7891, 2016.

[158] M. Buettner, R. Prasad, A. Sample, D. Yeager, B. Greenstein, J. R. Smith, *et al.*, "RFID sensor networks with the Intel WISP," in *Proceedings of the 6th ACM conference on Embedded network sensor systems*, 2008, pp. 393-394.

[159] P. Kalansuriya, R. Bhattacharyya, and S. Sarma, "RFID tag antenna-based sensing for pervasive surface crack detection," *IEEE Sensors Journal,* vol. 13, pp. 1564-1570, 2013.

[160] I. Mohammad, V. Gowda, H. Zhai, and H. Huang, "Detecting crack orientation using patch antenna sensors," *Measurement Science and Technology,* vol. 23, p. 015102, 2011.

[161] P. Kalansuriya, R. Bhattacharyya, S. Sarma, and N. Karmakar, "Towards chipless RFID-based sensing for pervasive surface crack detection," in *RFID-Technologies and Applications (RFID-TA), 2012 IEEE International Conference on*, 2012, pp. 46-51.

[162] X. Xu and H. Huang, "Multiplexing passive wireless antenna sensors for multi-site crack detection andmonitoring," *Smart Materials and Structures,* vol. 21, p. 015004, 2011.

[163] S. Caizzone, E. DiGiampaolo, and G. Marrocco, "Wireless crack monitoring by stationary phase measurements from coupled RFID tags," *IEEE Transactions on Antennas and Propagation,* vol. 62, pp. 6412-6419, 2014.

[164] S. Caizzone and E. DiGiampaolo, "Wireless passive RFID crack width sensor for structural health monitoring," *IEEE Sensors Journal,* vol. 15, pp. 6767-6774, 2015.

[165] X. Yi, C. Cho, J. Cooper, Y. Wang, M. M. Tentzeris, and R. T. Leon, "Passive wireless antenna sensor for strain and crack sensing—Electromagnetic modeling, simulation, and testing," *Smart Materials and Structures,* vol. 22, p. 085009, 2013.

[166] K. Yagi, N. Sato, Y. Sato, K. Tamakawa, D. Minkov, and T. Shoji, "Detection and evaluation of the depth of surface cracks in conductive materials by using a loop antenna," *Applied Physics A: Materials Science & Processing,* vol. 77, pp. 461-468, 2003.

[167] Y. Gotoh, H. Hirano, M. Nakano, K. Fujiwara, and N. Takahashi, "Electromagnetic nondestructive testing of rust region in steel," *IEEE transactions on magnetics,* vol. 41, pp. 3616-3618, 2005.

[168] M. Alamin, G. Y. Tian, A. Andrews, and P. Jackson, "Corrosion detection using low-frequency RFID technology," *Insight-Non-Destructive Testing and Condition Monitoring,* vol. 54, pp. 72-75, 2012.

[169] H. Zhang, R. Yang, Y. He, G. Y. Tian, L. Xu, and R. Wu, "Identification and characterisation of steel corrosion using passive high frequency RFID sensors," *Measurement,* vol. 92, pp. 421-427, 2016.

[170] J. Zhang and G. Y. Tian, "UHF RFID tag antenna-based sensing for corrosion detection & characterization using principal component analysis," *IEEE Transactions on Antennas and Propagation,* vol. 64, pp. 4405-4414, 2016.

[171] R. Khalifeh, M. S. Yasri, B. Lescop, F. Gallée, E. Diler, D. Thierry, *et al.*, "Development of wireless and passive corrosion sensors for material degradation monitoring in coastal zones and immersed environment," *IEEE Journal of Oceanic Engineering*, vol. 41, pp. 776-782, 2016.

[172] H. Zhang, G. Y. Tian, A. Simm, and M. Alamin, "Electromagnetic methods for corrosion under paint coating measurement," in *Proc. SPIE*, 2013, pp. 875919-1-875919-10.

[173] J. Kim, Z. Wang, and W. S. Kim, "Stretchable RFID for wireless strain sensing with silver nano ink," *IEEE Sensors Journal*, vol. 14, pp. 4395-4401, 2014.

[174] W. Leon-Salas, S. Kanneganti, and C. Halmen, "Development of a smart RFID-based corrosion sensor," in *Sensors, 2011 IEEE*, 2011, pp. 534-537.

[175] M. M. Andringa, D. P. Neikirk, N. P. Dickerson, and S. L. Wood, "Unpowered wireless corrosion sensor for steel reinforced concrete," in *Sensors, 2005 IEEE*, 2005, p. 4 pp.

[176] M. Gustafsson and B. L. G. Jonsson, "Antenna Q and stored energy expressed in the fields, currents, and input impedance," *IEEE Transactions on Antennas and Propagation*, vol. 63, pp. 240-249, 2015.

[177] C. Occhiuzzi and G. Marrocco, "Constrained-design of passive UHF RFID sensor antennas," *IEEE Transactions on Antennas and Propagation*, vol. 61, pp. 2972-2980, 2013.

[178] K. Domdouzis, B. Kumar, and C. Anumba, "Radio-Frequency Identification (RFID) applications: A brief introduction," *Advanced Engineering Informatics*, vol. 21, pp. 350-355, 2007.

[179] B. Konsynski and H. A. Smith, "Developments in practice x: Radio frequency identification (rfid)-an internet for physical objects," *Communications of the Association for Information Systems*, vol. 12, p. 19, 2003.

[180] S. Hoyt, D. St John, D. Wilson, and L. Bushnell, "A tree tour with radio frequency identification (RFID) and a personal digital assistant (PDA)," in *Industrial Electronics Society, 2003. IECON'03. The 29th Annual Conference of the IEEE*, 2003, pp. 2035-2040.

[181] A. P. Sohrab, Y. Huang, M. Kod, M. Hussein, and P. Carter, "Label-type 3D RFID tag mountable on metallic and non-metallic objects," in *Antennas & Propagation Conference (LAPC), 2016 Loughborough*, 2016, pp. 1-3.

[182] K. Arora, H. Mallinson, A. Kulkarni, J. Brusey, and D. McFarlane, "The practical feasibility of using RFID in a metal environment," in *Wireless Communications and Networking Conference, 2007. WCNC 2007. IEEE*, 2007, pp. 1679-1683.

[183] D. D. Deavours, "Improving the near-metal performance of UHF RFID tags," in *RFID, 2010 IEEE International Conference on*, 2010, pp. 187-194.

[184] A. Hamani, M. C. E. Yagoub, T.-P. Vuong, and R. Touhami, "A Novel Broadband Antenna Design for UHF RFID Tags on Metallic Surface Environments," *IEEE Antennas and Wireless Propagation Letters,* vol. 16, pp. 91-94, 2017.

[185] S. Zuffanelli, G. Zamora, F. Paredes, P. Aguila, F. Martin, and J. Bonache, "On-metal UHF-RFID passive tags based on complementary split-ring resonators," *IET Microwaves, Antennas & Propagation,* vol. 11, pp. 1040-1044, 2017.

[186] P. C. Arribas, P. Sanchez, and C. Aroca, "RFID in Metal Environments: An Overview on Low (LF) and Ultra-Low (ULF) Frequency Systemsled," in *Radio frequency identification fundamentals and applications design methods and solutions*, ed: InTech, 2010.

[187] K. Finkenzeller, *RFID handbook: fundamentals and applications in contactless smart cards, radio frequency identification and near-field communication*: John Wiley & Sons, 2010.

[188] J. Kim, H.-C. Son, K.-H. Kim, and Y.-J. Park, "Efficiency analysis of magnetic resonance wireless power transfer with intermediate resonant coil," *IEEE Antennas and Wireless Propagation Letters,* vol. 10, pp. 389-392, 2011.

[189] K. Sasaki, S. Sugiura, and H. Iizuka, "Distance adaptation method for magnetic resonance coupling between variable capacitor-loaded parallel-wire coils," *IEEE Transactions on Microwave Theory and Techniques*, vol. 62, pp. 892-900, 2014.

[190] D. H. S. Cheng, "The reflected impedance of a circular coil in the proximity of a semi-infinite medium," *IEEE Transactions on Instrumentation and Measurement,* vol. 14, pp. 107-116, 1965.

[191] C. V. Dodd and W. E. Deeds, "Analytical Solutions to Eddy-Current Probe-Coil Problems," *Journal of applied physics,* vol. 39, pp. 2829-2838, 1968.

[192] N. Harfield and J. R. Bowler, "Theory of thin-skin eddy-current interaction with surface cracks," *Journal of applied physics,* vol. 82, pp. 4590-4603, 1997.

[193] R. J. Ditchburn, S. K. Burke, and M. Posada, "Eddy-current nondestructive inspection with thin spiral coils: Long cracks in steel," *Journal of Nondestructive Evaluation,* vol. 22, pp. 63-77, 2003.

[194] Q.-A. Huang, L. Dong, and L.-F. Wang, "LC Passive Wireless Sensors Toward a Wireless Sensing Platform: Status, Prospects, and Challenges," *Journal of Microelectromechanical Systems,* vol. 25, pp. 822-841, 2016.

[195] S. Assawaworrarit, X. Yu, and S. Fan, "Robust wireless power transfer using a nonlinear parity–time-symmetric circuit," *Nature*, vol. 546, pp. 387-390, 2017.

[196] Atmel, ""ATA5577 Datasheet", [Online: Available: http://www.atmel.com]," 2017.

[197] H. V. Tag, ""HID Volcano Tag Datasheet", [Online: Available: http://www.therfidshop.com/index.php?cPath=70_75_204_205_157&osCsid=297264aa89f698087ec2517e3fabd1ba]," 2017.

[198] H. Global, ""RFID Tag Comparison", [Online: Available: https://www.hidglobal.com/sites/default/files/resource_files/hid-idt-tag-products-ct-en.pdf]," 2017.

[199] G. Net, ""Reader and Writer module", [Online: Available: http://www.gis-net.de/rfid/english/125khz/ts_rw38plus.htm],"

2017.

[200] A. K. RamRakhyani, S. Mirabbasi, and M. Chiao, "Design and optimization of resonance-based efficient wireless power delivery systems for biomedical implants," *IEEE Transactions on Biomedical Circuits and Systems*, vol. 5, pp. 48-63, 2011.

[201] W. Fu, B. Zhang, and D. Qiu, "Study on frequency-tracking wireless power transfer system by resonant coupling," in *Power Electronics and Motion Control Conference, 2009. IPEMC'09. IEEE 6th International*, 2009, pp. 2658-2663.

[202] W.-S. Lee, W.-I. Son, K.-S. Oh, and J.-W. Yu, "Contactless energy transfer systems using antiparallel resonant loops," *IEEE Transactions on Industrial Electronics*, vol. 60, pp. 350-359, 2013.

[203] C.-J. Chen, T.-H. Chu, C.-L. Lin, and Z.-C. Jou, "A study of loosely coupled coils for wireless power transfer," *IEEE Transactions on Circuits and Systems II: Express Briefs*, vol. 57, pp. 536-540, 2010.

[204] T. P. Duong and J.-W. Lee, "Experimental results of high-efficiency resonant coupling wireless power transfer using a variable coupling method," *IEEE Microwave and Wireless Components Letters*, vol. 21, pp. 442-444, 2011.

[205] Y. He, F. Luo, M. Pan, X. Hu, J. Gao, and B. Liu, "Defect classification based on rectangular pulsed eddy current sensor in different directions," *Sensors and Actuators A: Physical*, vol. 157, pp. 26-31, 2010.

[206] D. Zhou, G. Y. Tian, B. Zhang, M. Morozov, and H. Wang, "Optimal features combination for pulsed eddy current NDT," *Nondestructive Testing and Evaluation*, vol. 25, pp. 133-143, 2010.

[207] M. Morozov, G. Y. Tian, and P. J. Withers, "Noncontact evaluation of the dependency of electrical conductivity on stress for various Al alloys as a function of plastic deformation and annealing," *Journal of applied physics*, vol. 108, p. 024909, 2010.

[208] G. Y. Tian, A. Sophian, D. Taylor, and J. Rudlin, "Multiple sensors on pulsed eddy-current detection for 3-D subsurface crack assessment," *IEEE Sensors Journal*, vol. 5, pp. 90-96, 2005.

[209] M. Morozov, G. Y. Tian, and P. J. Withers, "The pulsed eddy current response to applied loading of various aluminium alloys," *NDT & E International*, vol. 43, pp. 493-500, 2010.

[210] Y. He, G. Tian, H. Zhang, M. Alamin, A. Simm, and P. Jackson, "Steel corrosion characterization using pulsed eddy current systems," *IEEE Sensors Journal*, vol. 12, pp. 2113-2120, 2012.

[211] A. Tran, M. Bolic, and M. C. E. Yagoub, "Magnetic-field coupling characteristics of ferrite-coil antennas for low-frequency RFID applications," *Int. J. Comput. Sci. Issues*, vol. 7, pp. 7-11, 2010.

[212] C. Stergiou, E. Eleftheriou, and V. Zaspalis, "Enhancement of the near-field UHF RFID with ferrite substrates," *IEEE Transactions on Magnetics*, vol. 48, pp. 1497-1500, 2012.

[213] C. Multiphysics, "An RFID System [Online: Available: https://www.comsol.com/model/an-rfid-system-1264]," 2017.

[214] A. Bid, A. Bora, and A. K. Raychaudhuri, "Temperature dependence of the resistance of metallic nanowires of diameter⩾ 15 nm: Applicability of Bloch-Grüneisen theorem," *Physical Review B*, vol. 74, p. 035426, 2006.

[215] D. K. Schroder, *Semiconductor material and device characterization*: John Wiley & Sons, 2006.

[216] J. R. Bowler and N. Harfield, "Thin-skin eddy-current interaction with semielliptical and epicyclic cracks," *IEEE transactions on magnetics*, vol. 36, pp. 281-291, 2000.

[217] J. R. Bowler and N. Harfield, "Evaluation of probe impedance due to thin-skin eddy-current interaction with surface cracks," *IEEE Transactions on Magnetics*, vol. 34, pp. 515-523, 1998.

[218] K. G. Ong, C. A. Grimes, C. L. Robbins, and R. S. Singh, "Design and application of a wireless, passive, resonant-circuit environmental monitoring sensor," *Sensors and Actuators A: Physical*, vol. 93, pp. 33-43, 2001.

[219] G. Y. Tian, Z. X. Zhao, and R. W. Baines, "The research of inhomogeneity in eddy current sensors," *Sensors and Actuators A: physical*, vol. 69, pp. 148-151, 1998.

[220] R. Corporation, "RT/duroid® 6202

High Frequency Laminates [Online: Available: http://www.rogerscorp.com/documents/610/acs/RT-duroid-6202-Laminate-Data-Sheet.pdf]," 2017.

[221] T. Chen, G. Y. Tian, A. Sophian, and P. W. Que, "Feature extraction and selection for defect classification of pulsed eddy current NDT," *Ndt & E International*, vol. 41, pp. 467-476, 2008.

[222] A. Metwally and S. Mahmoud, "Mutual coupling between loops on layered earth using images," *IEEE transactions on antennas and propagation*, vol. 32, pp. 574-579, 1984.

[223] M. R. Nabavi and S. N. Nihtianov, "Design strategies for eddy-current displacement sensor systems: Review and recommendations," *IEEE Sensors Journal*, vol. 12, pp. 3346-3355, 2012.

[224] A. A. Howling, P. Guittienne, R. Jacquier, and I. Furno, "Complex image method for RF antenna-plasma inductive coupling calculation in planar geometry. Part I: basic concepts," *Plasma Sources Science and Technology*, vol. 24, p. 065014, 2015.